



Architectures for radio over fiber transmission of high-quality video and data signals

Lebedev, Alexander

Publication date:
2013

Document Version
Publisher's PDF, also known as Version of record

[Link back to DTU Orbit](#)

Citation (APA):
Lebedev, A. (2013). *Architectures for radio over fiber transmission of high-quality video and data signals*. Technical University of Denmark.

General rights

Copyright and moral rights for the publications made accessible in the public portal are retained by the authors and/or other copyright owners and it is a condition of accessing publications that users recognise and abide by the legal requirements associated with these rights.

- Users may download and print one copy of any publication from the public portal for the purpose of private study or research.
- You may not further distribute the material or use it for any profit-making activity or commercial gain
- You may freely distribute the URL identifying the publication in the public portal

If you believe that this document breaches copyright please contact us providing details, and we will remove access to the work immediately and investigate your claim.

Architectures for radio over fiber transmission of high-quality video and data signals

Ph.D. Thesis

by Alexander Lebedev

Main supervisor: *Søren Forchhammer*

Co-supervisor: *I. Tafur Monroy*

Co-supervisor: *J. J. Vegas Olmos*

Department of Photonics Engineering

Technical University of Denmark

DK-2800, Kgs. Lyngby, Denmark

August 31, 2013

“There are these two young fish swimming along and they happen to meet an older fish swimming the other way, who nods at them and says “Morning, boys. How’s the water?” And the two young fish swim on for a bit, and then eventually one of them looks over at the other and goes “What the hell is water?”

David Foster Wallace

Abstract

In this Ph.D. project, design and performance evaluation of mm-wave radio over fiber links for diverse applications including video transmission are conducted. Major objective of this Thesis is to study performance of video and data signals transmitted in radio over fiber (RoF) setups with a constraint on complexity.

For wireless personal area networks distribution, we explore the notion of joint optimization of physical layer parameters of a fiber-wireless link (optical power levels, wireless transmission distance) and the codec parameters (quantization, error-resilience tools) based on the peak signal-to-noise ratio as an objective video quality metric for compressed video transmission. Furthermore, we experimentally demonstrate uncompressed 1080i high-definition video distribution in V-band (50–75 GHz) and W-band (75–110 GHz) fiber-wireless links achieving 3 m of wireless transmission in both cases. For the W-band, experimental assessment of passive and active approaches for implementation of base stations is included, and the channel coding use is assessed.

Use of millimeter-wave signals in metropolitan mobile backhaul is also considered in this Thesis. We propose a setup enabling efficient wired/wireless backhaul of picocell networks. Gigabit signal transmission is realized in combined fiber-wireless-fiber link enabling simultaneous backhaul of dense metropolitan and suburban areas.

In this Thesis, we propose a technique to combat periodic chromatic dispersion-induced radio frequency (RF) power fading in a simple intensity

modulation-direct detection mm-wave RoF link through introduction of a degree of frequency tunability at the RoF transmitter.

We study advanced RoF infrastructures to better suit video transmission. To enable efficient dynamic multicast/broadcast of video services, we have proposed and evaluated an approach of increasing the functionality of the optical remote node by including the wireless channel replication and allocation. Another approach for multicast of RF signals - delivering multiple simultaneously upconverted lightwaves from the central office to designated BSs is evaluated for diverse lightwave generation and data modulation techniques.

Mm-wave RoF links employing various lightwave generation techniques are experimentally demonstrated for diversified fiber infrastructure including standard single mode fiber, multimode fiber and dispersion shifted fiber in order to estimate the feasibility of mm-wave wireless video services' delivery through fiber infrastructure with different nonlinear impairments and dispersion.

Abstrakt

Dette Ph.D. projekt omhandler design og performance evaluering af mm-wave "radio over fiber" links for diverse applikationer, inklusiv video transmission. Hovedfokus er lagt på studie af performance af video og data signaler transmitteret over RoF opsætninger med begrænsninger i kompleksiteten.

For distribution i "wireless personal area networks" undersøger vi gensidig optimering af parametre i det fysiske lag af en fiber-wireless forbindelse (optiske effekt niveauer, trådløs transmissionslængde) og koder/dekoder parametre (kvantisering, fejl-beskyttelses værktøjer) baseret på "peak signal-to-noise ratio" som et objektivt mål for kvaliteten af komprimeret video transmission. Desuden demonstrerer vi eksperimentelt ukomprimeret 1080i high-definition video distribution i V-band (50–75 GHz) og W-band (75–110 GHz) fiber-wireless forbindelser, hvor vi i begge tilfælde opnår trådløs transmission over 3 meter. For W-band inkluderes den eksperimentelle evaluering brug af passive og aktive metoder til implementering af basis stationer, ligeledes evalueres brugen af kanal-kodning.

Afhandlngen omhandler også brugen af millimeter-wave signaler i "metropolitan mobile backhaul". Vi foreslår et set-up som giver effektiv "wired/wireless backhaul" i picocell netværk. Trådløs gigabit transmission realiseres i kombinerede fiber-wireless-fiber forbindelser som muliggør effektiv "backhaul" i tæt bymæssig bebyggelse.

Vi foreslår en ny løsning for "RF power fading" forårsaget af periodisk kromatisk dispersion i et simpelt "intensity modulation-direct detection" mm-wave RoF system ved hjælp af delvis frekvens justering i RoF senderen.

Vi studerede avanceret RoF infra-struktur for bedre tilpasning til video transmission. For effektiv dynamisk multicast/broadcast af video tjenester har vi foreslået og evalueret en metode til optimering af den optiske "remote node"s evne til at håndtere replikation og allokering af de trådløse kanaler. En anden metode til multicast af RF signaler – der leverer flere opkonverterede "lightwaves" fra "central office" til basis station bliver evalueret for diverse "lightwave" generering og modulations-teknikker.

Mm-wave RoF forbindelser med diverse "lightwave" genererings teknikker er realiseret eksperimentelt for "diversified" fiber infrastruktur, inklusiv single mode fibre, multimode fibre og "dispersion shifted" fiber, men henblik på at estimere muligheden for at levere mm-wave trådløse video tjenester over fiber infrastruktur med forskellige ikke-linære fejkilder og dispersion.

Acknowledgments

I'd like to thank my supervisors, colleagues in the groups, officemates, and all the wonderful people in Fotonik and DTU. It was a joy and a privilege to work with you.

I would also like to thank my parents and my sister for knowing that I always can do more.

Contents

Abstract.....	v
Abstrakt.....	vii
Acknowledgments	ix
List of publications.....	xiii
List of abbreviations	xv
List of figures.....	xvii
List of tables.....	xviii
1. Introduction	1
1.1 Motivation.....	1
1.2 MM-wave fiber-wireless networks.....	2
1.3 Lightwave generation and baseband data modulation.....	4
1.4 Photomixing	6
1.5 Techniques of RF modulation of the lightwave	7
1.6 RF downconversion.....	9
1.7 Optical fiber transmission impairments.....	11
1.7.1 RF signal power fading.....	11
1.7.2 Bit walk-off	13
1.8 Noise in mm-wave RoF links	14
1.9 Wireless channel.....	15
1.9.1 Overview of the applications and standards	15
1.9.2 60 GHz wireless channel modeling	16
1.10 Source and channel coding in mm-wave fiber-wireless setups.....	21
1.10.1 Uncompressed real-time HD video transmission.....	21
1.10.2 Compressed HD video transmission	21
1.10.3 Channel coding	24

2. Overview of state-of-the-art work.....	25
3. Description of the papers.....	27
3.1. Overview of the papers included in the Thesis	27
3.2. Detailed description of the papers	28
4. Conclusions.....	33
5. Future work	35
Bibliography	37
Paper 1	45
Paper 2	57
Paper 3	63
Paper 4	79
Paper 5	91
Paper 6	107
Paper 7	113
Paper 8	123
Paper 9	133

List of publications

This Thesis is based on the following peer-reviewed journal and conference publications. We note that 2 papers have been submitted for peer-review, but not yet published.

[Paper 1]

Alexander Lebedev, Tien-Thang Pham, Marta Beltrán, Xianbin Yu, Anna Ukhanova, Roberto Llorente, Idelfonso Tafur Monroy, "Optimization of high-definition video coding and hybrid fiber-wireless transmission in the 60-GHz band," *Opt. Express.*, vol. 19, no. 26, pp. 895-904, 2011.

[Paper 2]

Tien-Thang Pham, Alexander Lebedev, Marta Beltran, Xianbin Yu, Roberto Llorente, and Idelfonso Tafur Monroy, "Combined Single-mode/Multimode Fiber Link supporting Simplified In-building 60-GHz Gigabit Wireless Access," *Opt. Fiber Technol.*, vol. 18, no. 4, pp. 226-229, 2012.

[Paper 3]

Alexander Lebedev, J. J. Vegas Olmos, Xiaodan Pang, Søren Forchhammer, Idelfonso Tafur Monroy, "Demonstration and Comparison Study for V- and W-band Real-Time HD Video Delivery in Diverse Fiber-Wireless Infrastructure," *Fiber Integr. Opt.*, vol. 32, no. 2, pp. 93-104, 2013.

[Paper 4]

Alexander Lebedev, Juan Jose Vegas Olmos, Miguel Iglesias, Søren Forchhammer, Idelfonso Tafur Monroy, "A novel method for combating dispersion induced power fading in dispersion compensating fiber," *Opt. Express*, vol. 21, no. 11, pp. 13617-13625, 2013.

[Paper 5]

Alexander Lebedev, Xiaodan Pang, J. J. Vegas Olmos, Marta Beltran, Roberto Llorente, Søren Forchhammer, Idelfonso Tafur Monroy, "Feasibility study and experimental verification of simplified fiber-supported 60-GHz picocell mobile backhaul links," *IEEE Photon. J.*, vol. 5, no. 4, pp. 7200913, 2013.

[Paper 6]

Alexander Lebedev, Xiaodan Pang, J. J. Vegas Olmos, Søren Forchhammer, Idelfonso Tafur Monroy, "Simultaneous 60 GHz RoF Transmission of Lightwaves Emitted by ECL, DFB, and VCSEL," *IEEE Photon. Technol. Lett.*, submitted.

[Paper 7]

Alexander Lebedev, Xiaodan Pang, J. J. Vegas Olmos, Søren Forchhammer, Idelfonso Tafur Monroy, "Gigabit close-proximity wireless connections supported by 60-GHz RoF links with low carrier suppression," *Opt. Express*, vol. 21, no. 21, pp. 24574-24581.

[Paper 8]

Alexander Lebedev, J. J. Vegas Olmos, Xiaodan Pang, Søren Forchhammer, Idelfonso Tafur Monroy, "Low-complexity source and channel coding for mm-wave hybrid fiber-wireless links," *Opt. Commun.*, submitted.

[Paper 9]

Alexander Lebedev, Xiaodan Pang, Juan Jose Vegas Olmos, Søren Forchhammer, Idelfonso Tafur Monroy, "Tunable photonic RF generator for dynamic allocation and multicast of 1.25-Gbps channels in the 60-GHz unlicensed band," in *Proceedings of International Microwave Symposium (IMS 2013)*, paper THPP-2, 2013.

List of abbreviations

AVC	advanced video coding
ASE	amplified spontaneous emission
ASK	amplitude shift keying
BS	base stations
BER	bit error rate
BCH	Bose-Chaudhuri-Hocquenghem
C/N	carrier-to-noise
DC	direct current
DML	directly modulated lasers
DFB	distributed feedback
DSB	double sideband
DSB-SC	double sideband with suppressed carrier
E/O	electrical-to-optical
EAM	electro absorption modulator
EDFA	erbium doped fiber amplifiers
ECC	error correction codes
ECL	external cavity lasers
FBG	fiber Bragg grating
FMO	flexible macroblock ordering
FEC	forward error correction
HD	high definition
HDMI	high-definition multimedia interface
IM/DD	intensity modulation / direct detection
LAN	local area network
LOS	line-of-sight
LO	local oscillator

LDPC	low-density parity-check code
MZM	Mach-Zehnder modulator
MAC	medium access control
MMF	multimode fiber
NAL	network abstraction layer
NLOS	non-line-of-sight
OCS	optical carrier suppression
OSSB	optical single sideband
O/E	optical-to-electrical
PER	packet error rate
PSNR	peak signal-to-noise ratio
PD	photodiode
PIC	photonic integrated circuits
POF	polymer optical fibers
QP	quantization parameter
RF	radio frequency
RoF	radio over fiber
RS	Reed-Solomon
RIN	relative intensity noise
SNR	signal-to-noise ratio
SSMF	standard single mode fiber
UVLC	universal variable length coding
VCSEL	vertical cavity surface emitting lasers
VoIP	voice over Internet protocol

List of figures

Figure 1. Techniques of fiber-wireless networking .	3
Figure 2. Schematic diagram of main functional blocks of radio over fiber system and communication system diagram according to Shannon.....	4
Figure 3. Experimentally measured PI curves for the C-band DFB-EAM and the C-band VCSEL.	5
Figure 4. Schematic diagram for photonic RF generation by dual-laser remote heterodyning.....	8
Figure 5. Schematic diagram for IM/DD RoF system.....	8
Figure 6. Schematic diagram for OCS RoF system.....	9
Figure 7. BER as a function of SNR for synchronous and envelope detection schemes.....	10
Figure 8. Optical spectrum of the RoF DSB signal	11
Figure 9. CD-induced RF C/N penalty.....	12
Figure 10. Optical spectra of the OCS/DSB-SC signal and the original lightwave carrier signal.....	13
Figure 11. Maximum attainable fiber link length as a function of the carrier frequency in OCS setups.	14
Figure 12. Noise contributions in RoF links.....	14
Figure 13. Rainfall attenuation as a function of frequency.	18
Figure 14. The 60-GHz wireless channel path loss in several indoor environments and the path loss for 60-GHz, 73.5-GHz and 83.5-GHz systems based on the Friis transmission equation.....	19

List of tables

Table 1. Overview of emerging 60-GHz wireless standards..... 15

Table 2. Parameters for wireless channel modeling. 19

Table 3. Bitrate requirements for real-time uncompressed transmission of video sequences. 21

1. Introduction

1.1 Motivation

The explosive growth of communication technology in recent years has brought the high-capacity wireless connectivity to end users. The rising Internet traffic volume is predicted to boost the requirements for wireless channel capacity in coming years with major applications such as data, file sharing, interactive high definition (HD) video, voice over internet protocol (VoIP) and gaming [1, 2]. Video traffic is predicted to increase at a very high annual growth rate taking up more than 70 percent of the overall traffic [1].

In the near future, users shall be able to receive the same services on their mobile/wireless access systems that they are currently receiving over wireline networks, including interactive real-time HD multimedia. Therefore, transcoding will no longer be necessary at the wired/wireless transmission interface and more computationally efficient video coding solutions can be introduced.

Photonic devices are currently undergoing the process of cost reduction along with enhancement of functionalities. Techniques that for a long time belonged to a domain of wireless communication research e. g. support of advanced modulation formats are now being adopted for optical fiber communication [3]. Recent progress in photonic integrated circuits (PICs)

enables integration of devices such as lasers, couplers, modulators, and detectors on the same chip [4]. PIC-based optical transmitters and receivers for fiber-wireless networks have already been implemented [5]. These developments allow us to envision that future optical transmitters will gradually adopt the functionalities of photonic radio frequency (RF) processing and uncover the potential of microwave photonics research.

In this Thesis, the broadband access network segment is studied. As access and metro networks migrate from the copper-based infrastructure for baseband data delivery to hybrid and all-fiber solutions, the RF transmission over optical fiber is becoming more feasible as the same pre-installed fiber-optic infrastructure can be used for both baseband and the RF signal delivery.

The capacity of fiber-wireless networks is limited by the wireless connection bandwidth bottleneck. The low spectrum availability in microwave range leads to higher interest in the bandwidth available in a millimeter-wave (mm-wave) range. V (50-75 GHz), E (60-90 GHz) and W (75-110 GHz) bands allow unlicensed transmission in 57-66 GHz region and transmission with low cost swift approval license in 71-76 and 81-86-GHz bands [6].

In this Thesis, access fiber networks are studied for simplified transport of Gigabit mm-wave RF signals supporting real-time HD video transmission.

1.2 MM-wave fiber-wireless networks

For mm-wave radio transmission, the simplicity and low cost of BSs is advantageous as utilization of mm-wave bands would require a higher count of base stations (BS)/access points/remote antenna units to provide a wireless coverage for a given area compared to transmission on microwave frequencies. With increased density of BSs, distributed antenna systems (DAS) architecture becomes advantageous [7]. In the DAS scenario, the central office (CO) contains most of the functionalities, and the BS should be simplified. Later in this work, we refer to wireless transmitters and receivers as the BS irrespective of the level of complexity assigned.

As an example of the DAS architecture, we study radio over fiber (RoF) technology where upconversion to the wireless carrier is performed at the CO, and the combination of RF and data signals is then delivered to the BS through the fiber. At the BS, the RF carrier is recovered simply by means of optical-to-electrical (O/E) conversion, and then radiated.

In RoF systems, RF amplification and filtering may be used at the BS, however, expensive mm-wave RF generation and mixing are avoided [8-13].

Centralized RF generation at the CO brings additional benefits of easier control and monitoring. Potentially, using the RoF technology, BSs can be built containing only passive electronic components [14]. Furthermore, RoF systems can be designed transparent to advanced modulation formats [15], and electrical/optical multiplexing of radio and data signals is allowed. The simple RoF architecture is shown in Fig. 1 (bottom).

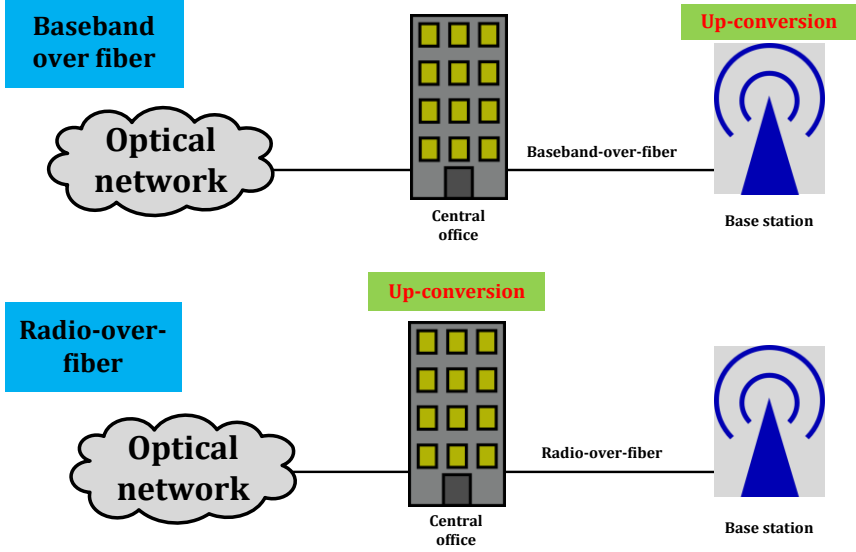


Figure 1. Techniques of fiber-wireless networking: baseband over fiber (top), radio over fiber (bottom).

As an alternative to the RoF technology, fiber-wireless systems can be designed in such a way that the upconversion to a wireless carrier is to take place at the BS. This architecture is commonly referred to as “baseband over fiber.” Baseband over fiber is a mature technique with low cost electrical-to-optical (E/O) and O/E modules available [14], it is depicted on Fig. 1 (top). Furthermore, a lower penalty is imposed on transmission performance by dispersion and nonlinearities in the fiber. However, in the scenarios where the density of BSs is increased, such as in mm-wave WPANs, the cost of the system may escalate.

Building blocks of the RoF communication system are depicted in Fig. 2. As shown in Fig. 2 (top), RoF transmission requires implementation of two modulation and two detection techniques and includes transmission through fiber-optical and wireless channels. We depict how the RoF systems correspond to a standard communication system scheme proposed by Shannon [16] in Fig. 2 (bottom). In the following sections, we present a high-level overview of the

processes taking place in each block. Optical and RF transmitters are designated as '2' and '3', optical and RF receivers are designated as '5' and '7'.

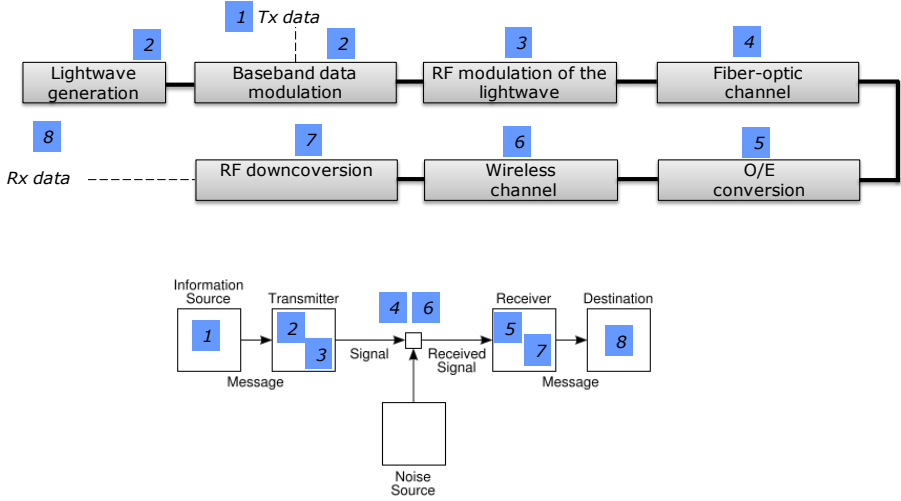


Figure 2. Schematic diagram of the main functional blocks of radio over fiber system (top), schematic diagram of a general communication system according to Shannon [16] (bottom).

1.3 Lightwave generation and baseband data modulation

In this section, techniques for lightwave generation and baseband data modulation are discussed. In the present Thesis, both external and direct modulation techniques are utilized for RoF links.

The direct modulation of a laser diode can simply be achieved by varying its driving current. Among laser devices for direct modulation, vertical cavity surface emitting lasers (VCSELs) have shown a remarkable promise for improving reliability, bringing cost reduction and enhanced scalability [17]. However, the modulation bandwidth is restricted by the laser diode's relaxation frequency [18]. Furthermore, high power output is not achievable when direct modulation is utilized, and the frequency chirp is present [19].

Resorting to the external modulation is commonly performed as means of overcoming drawbacks of direct modulation. In this case, a laser diode emits a continuous lightwave, and a change in light power (modulation) is imposed further on in the system. There are two widely used devices for external modulation: a Mach-Zehnder modulator (MZM) and an electro absorption modulator (EAM).

EAM's operation principles are based on the Franz-Keldysh effect as described in [19]. Using EAM modulators, high modulation bandwidth is achievable [19] and higher extinction ratio compared to directly modulated lasers (DML) can be attained, however chirp imposes a limitation (as also in the case of DMLs). The primary highlight of EAM technique, from our perspective, lies in possibility of the easy integration of DFBs and EAMs leading to simplified network setup. The experimentally measured PI (output optical power as a function of the direct current (DC)) curves for the VCSEL and the DFB-EAM are presented in Fig. 3.

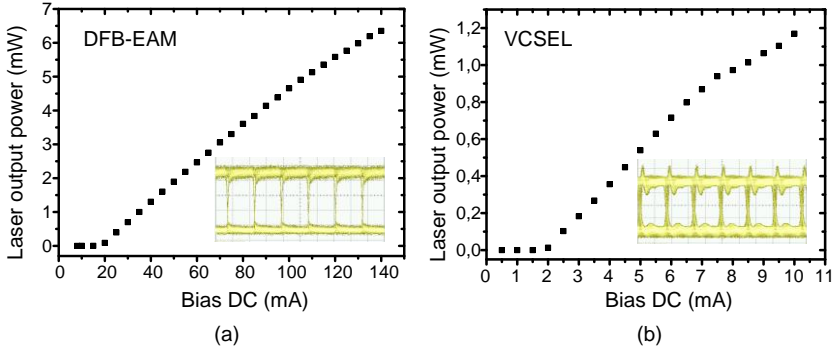


Figure 3. Experimentally measured PI curves for the C-band DFB-EAM (a) and the C-band VCSEL (b).

Frequency chirp is present in both VCSELs and integrated DFB-EAM modules. Chirp in DMLs appears because the injected current does not only modulate the optical gain and therefore the output power, but also modulates the refractive index of the gain medium and thus the optical frequency of the laser diode [19]. Chirp in the DFB-EAM is caused by the electrical crosstalk due to integration of the laser and modulator sections in the same chip of the DFB-EAM module [20].

Given the fact that we model the access fiber deployment, chirp will impose a negligible receiver sensitivity penalty for bitrates considered in this Thesis. As defined in [21], chirp-induced power penalty at the receiver is measured as a function of $|\beta_2|B^2L$, where $\beta_2 \approx -20 \text{ ps}^2/\text{km}$ is a group velocity dispersion parameter for standard single mode fiber (SSMF), $B=3 \text{ Gb/s}$ is a maximum bitrate used in this Thesis, and $L=20 \text{ km}$ is a fiber link length for access deployment. In our case, the value of $|\beta_2|B^2L$ is such that, according to [21], it brings a negligible receiver sensitivity penalty across the possible chirp values.

External optical modulation by using the MZM is based on the electro-optic effect [19, 21]. The MZM technique has a few drawbacks such as higher insertion loss compared to the EAM technique and high requirements for amplitude of the peak-to-peak voltage of the driving electrical data signal. However, MZMs exhibit excellent performance in terms of chirp making them suitable for long-haul high-speed transmission [19].

Techniques that we described in this section were investigated in this Thesis for access fiber transmission.

1.4 Photomixing

The photodiode (PD) is performing the function of O/E conversion at the BS. In RoF systems, the optical power is converted into the RF power through the process of photomixing. In this section, we proceed to describe the photomixing process as detailed in [22, 23]. Photocurrent on the output of the PD as a function of time and in proportion to the optical power on the input of the PD is governed by:

$$I_{PD}(t) = R \times P(t), \quad (1)$$

where P [W] is an incident optical power, R [A/W] is the responsivity of the PD.

In order to describe the O/E conversion for superposition of optical lightwaves / multiple spectral lines, phase information cannot be neglected. In the simplest case, the optical signal can be the sum of two optical fields. After launching 2 optical fields with the same polarization into the PD, the photocurrent on the PD output is obtained as expressed in:

$$\begin{aligned} I_{PD}(t) &= R \times |E_1 \cos(\omega_1 t + \varphi_1) + E_2 \cos(\omega_2 t + \varphi_2)|^2 = \\ &= R \times \left[\frac{1}{2} E_1^2 + \frac{1}{2} E_2^2 + \frac{1}{2} E_1^2 \cos 2(\omega_1 t + \varphi_1) + \frac{1}{2} E_2^2 \cos 2(\omega_2 t + \varphi_2) + \right. \\ &\quad \left. E_1 E_2 \cos[(\omega_1 - \omega_2)t + \varphi_1 - \varphi_2] + E_1 E_2 \cos[(\omega_1 + \omega_2)t + \varphi_1 + \varphi_2] \right] = \\ &= R \times \left(\frac{1}{2} E_1^2 + \frac{1}{2} E_2^2 + E_1 E_2 \cos[(\omega_1 - \omega_2)t + \varphi_1 - \varphi_2] \right), \end{aligned} \quad (2)$$

Eq. (2) is the fundamental equation governing optical heterodyning in the PD for two spectral components. The first two terms represent the DC component and the third term is the radio signal fluctuating at the frequency that is further radiated with antennas. Terms with cyclic frequencies equal to $2\omega_1$, $2\omega_2$ and $\omega_1 + \omega_2$ are omitted assuming that the cutoff frequency of the PD is much lower than the frequency of these terms.

The Eq. (2) can be extended for mixing of multiple spectral components at the PD. In particular, of interest is the result for mixing of three spectral lines as it is the case for photomixing of the double sideband (DSB) signal [23].

If the complex form of the optical field is used, assuming the same polarization of the optical fields, the photocurrent can be written as:

$$\begin{aligned}
 I_{PD}(t) &= R \times |E_1 \cos(\omega_1 t + \varphi_1) + E_2 \cos(\omega_2 t + \varphi_2) + E_3 \cos(\omega_3 t + \varphi_3)|^2 = \\
 &= R \times [E_1 e^{j[\omega_1 t + \varphi_1]} + E_2 e^{j[\omega_2 t + \varphi_2]} + E_3 e^{j[\omega_3 t + \varphi_3]}] \times \\
 &\times [E_1 e^{-j[\omega_1 t + \varphi_1]} + E_2 e^{-j[\omega_2 t + \varphi_2]} + E_3 e^{-j[\omega_3 t + \varphi_3]}], \tag{3}
 \end{aligned}$$

If we assume, as in case of intensity modulation, $E_1 = E_3 = E_{SB}$ are the sideband spectral components, and $\omega_3 - \omega_2 = \omega_{LO}$, $\omega_2 - \omega_1 = \omega_{LO}$, $E_2 = E_c$ is the optical field of the carrier, $\varphi_2 = 0$, then Eq. (3) can be transformed into:

$$\begin{aligned}
 I_{PD}(t) &= R \times \frac{1}{2} [E_c^2 + 2E_{SB}^2 + 4E_c E_{SB} \cos(\frac{\varphi_3 - \varphi_1}{2}) \cos(\omega_{LO} t + \frac{\varphi_1 + \varphi_3}{2}) + \\
 &+ 2E_{SB}^2 \cos 2(\omega_{LO} t + \frac{\varphi_1 + \varphi_3}{2})], \tag{4}
 \end{aligned}$$

Two things are important to note from Eq. (4). First, the component generated at the ω_{LO} is dependent upon the phase change between optical fields. Second, after photomixing of three components, the photocurrent oscillating at the double of the ω_{LO} is also generated. In the following sections, we will study both mixing of two and three spectral components at the PD.

1.5 Techniques of RF modulation of the lightwave

Techniques of the RoF signal generation (RF modulation of the lightwave) and fiber delivery that were used in this Thesis are presented in Fig. 4-6.

Figure 4 depicts the technique of photonic RF generation through heterodyning of two lightwaves uncorrelated in phase and frequency at the PD. At the CO, laser diodes are used generating the lightwaves which are offset at the frequency that is later used as a carrier frequency for radiation. A 3-dB coupler is employed subsequently to multiplex two lightwaves. The RF signal is generated through photomixing at the PD. This scheme has been extensively used for generation of microwave and mm-wave RoF signals [24].

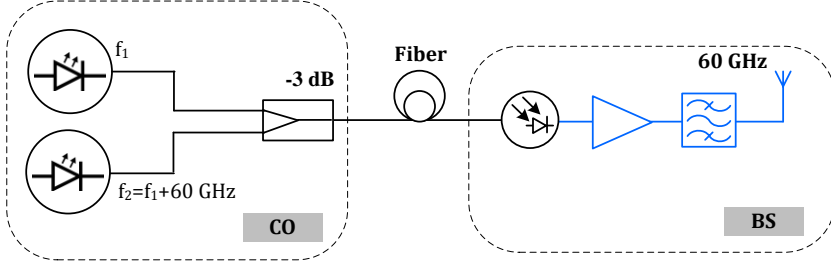


Figure 4. Schematic diagram for photonic RF generation by dual-laser remote heterodyning.

The advantage of the dual-laser remote heterodyning scheme is that it allows circumventing the use of the local oscillator (LO) generating the RF carrier at the CO. However, due to the fact that the lasers are uncorrelated, phase and frequency instability is expected [25].

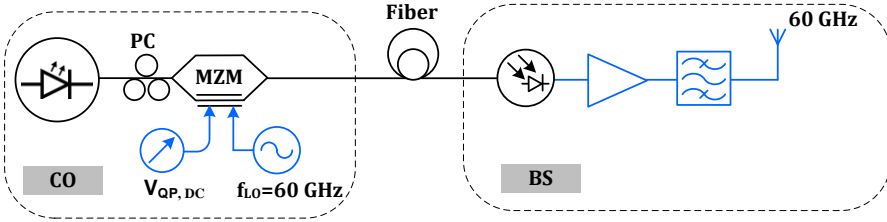


Figure 5. Schematic diagram for intensity modulation / direct detection (IM/DD) RoF scheme. PC: polarization controller.

The most straightforward technique for homodyne photonic RF signal generation at the BS is the direct modulation of the lightwave with the RF signal at the CO as exemplified in Fig. 5. In this scheme, the MZM is used as an amplitude modulator, therefore its bias is set to the linear operation region. In this case, the spectrum of the modulated signal consists of three components: the lightwave carrier and two sidebands offset at the frequency equal to the frequency of LO modulating the lightwave. When this technique is used for transfer of mm-wave wireless signals through the fiber, high frequency E/O RF components are required which increases the cost of the system considerably. Due to the fact that sidebands are correlated, high performance of the recovered at the BS RF signal in terms of the RF phase noise is expected at the BS [26].

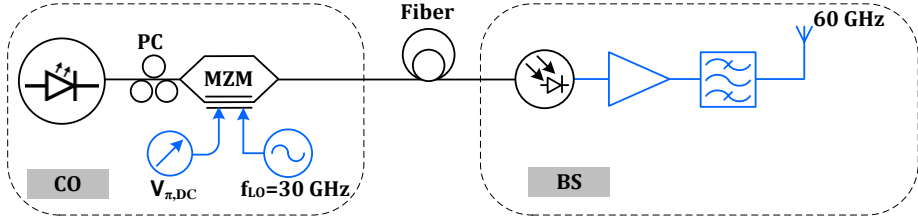


Figure 6. Schematic diagram for OCS RoF signal generation.

An attractive technique for photonic RF generation has been proposed in [27] as a modification of the simple intensity modulation method, showing that by biasing the MZM at the minimum transmission point, the optical carrier is suppressed and the value of the photonic generated RF at the BS is twice the RF originally fed into the MZM. This method is known as an optical carrier suppression (OCS) technique. The schematic diagram of the OCS RoF setup is depicted in Fig. 6. When this technique is utilized, higher optical power loss is imposed at the MZM, and usually an optical amplifier must be used before launching the RoF signal in the fiber.

Of the three techniques presented in this section, the first presented scheme might potentially become the most cost-efficient, especially if PICs are used [5], as low-cost distributed feedback (DFB) lasers could be employed, and the LO at the CO can be omitted. However, in this simple set-up, transmission of advanced spectrally-efficient modulation formats is challenging. Performance of the dual-laser remote heterodyning system may be enhanced by laser injection locking and optical phased locked loop at a price of increase in complexity [28, 29]. The IM/DD scheme requires the use of the mm-wave LO at the CO. The IM/DD scheme might become more practical with the progress in mm-wave RF generation, however it also entails the use of high-frequency E/O components. The OCS scheme allows alleviation of requirements for the LO at the CO compared to the IM/DD scheme, while preserving the sufficiently narrow linewidth of the generated RF.

Several other techniques are used such as optical single sideband (OSSB) modulation [30], frequency multiplication of higher order [31], and frequency comb [32], but they augment the complexity of the system, and therefore do not match the objective of our research.

1.6 RF downconversion

After the RF signal is downconverted from the optical carrier, radiated in the air and received, the baseband data are to be recovered. To downconvert the

data signal from the RF carrier into baseband, coherent and incoherent techniques apply.

Coherent (synchronous) detection technique employing the electrical LO and the mixer at the wireless receiver is commonly used allowing the detection of the amplitude and phase of the signal and therefore enabling advanced spectrally efficient modulation formats. The LO at the receiver is required to be synchronized with the transmitter LO in phase and frequency. Alternatively, the envelope detection technique is used when only the amplitude of the baseband data signal is recovered, and the use of the LO at the end-user terminal can be omitted [33].

Different statistics of voltage samples representing transmitted zeros and ones is expected in case of the envelope and synchronous RF detection. In the case of synchronous detection, voltage samples of the waveform representing the transmitted 'ones' and 'zeros' are expected to be distributed according to the Gaussian probability density function [34]. In the case of envelope detection, 'zeros' are expected to be Rayleigh-distributed, and 'ones' Rician-distributed [34]. Omitting the derivations detailed in [25, 34], the relationship between the signal-to-noise ratio (SNR) and the bit error rate (BER) for these two cases is described as:

$$BER_{synchronous} = \frac{1}{2} \operatorname{erfc} \left(\sqrt{\frac{E_b}{2N_0}} \right) \quad (5)$$

$$BER_{envelope} = \frac{1}{2} \exp \left(\frac{-E_b}{2N_0} \right) \quad (6)$$

where E_b is the energy per symbol, N_0 is the noise power spectral density, and erfc is a complementary error function.

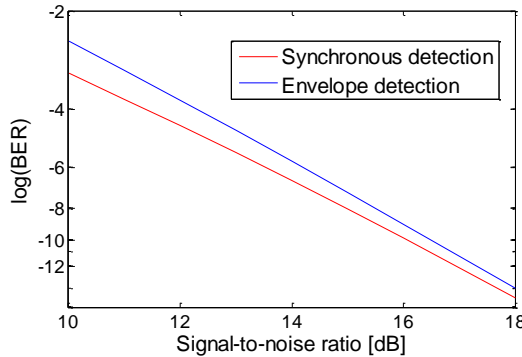


Figure 7. BER as a function of SNR for synchronous and envelope detection scheme.

As shown in Fig. 7, the sensitivity of synchronous detection-based receivers is higher, however, following the fact that we target the simplified system design, envelope detection technique is used more frequently than synchronous detection.

In this Thesis, we report on studying the statistics of the baseband waveform after envelope detection in the mm-wave fiber-wireless setup.

1.7 Optical fiber transmission impairments

In this section, an overview of signal impairments due to fiber transmission of mm-wave RF signals is presented.

1.7.1 RF signal power fading

Transmission of DSB RoF signals in dispersive fiber media leads to the appearance of the phase shift between the spectral lines that, after photomixing, leads to the RF carrier-to-noise (C/N) degradation as a function of both the fiber distance and the LO frequency. The experimentally measured optical spectrum of the DSB RoF signal is presented in Fig. 8.

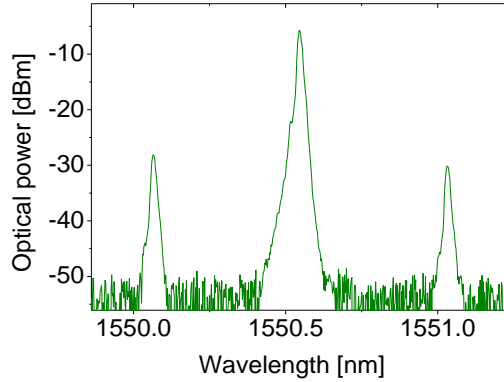


Figure 8. Optical spectrum of the DSB signal.

Analytical description of the chromatic dispersion (CD) induced RF power fading effect is given in [35, 36], and can also be noticed from Eq. (4). The transmission penalty can be calculated if the dispersion parameter, the fiber link length and the frequency of the LO at the optical transmitter are known.

Power of the recovered RF is varying as described in Eq. (7) [35, 36]:

$$P_{RF}(t) \approx I_{PD}^2(t) \approx \cos^2[\varphi(\omega_{LO})] \approx \cos^2\left[\pi c DL(f_{LO} / f_c)^2\right], \quad (7)$$

where c is a light velocity, $D=18$ ps/(nm×km) is the dispersion parameter for SSMF, L is the fiber length, f_{LO} is the cyclic frequency of the LO, $f_c=193.1$ THz is the frequency of the lightwave carrier.

Eq. (8) yields the value of RF C/N penalty in a logarithmic scale:

$$Penalty_{C/N} = 10 \log \left| \frac{X_{OUT}(f_{LO})_{fiber}}{X_{OUT}(f_{LO})_{nofiber}} \right|, \quad (8)$$

where $X_{OUT fiber}$ and $X_{OUT nofiber}$ are the RF signal power values recovered after photomixing with and without fiber transmission respectively.

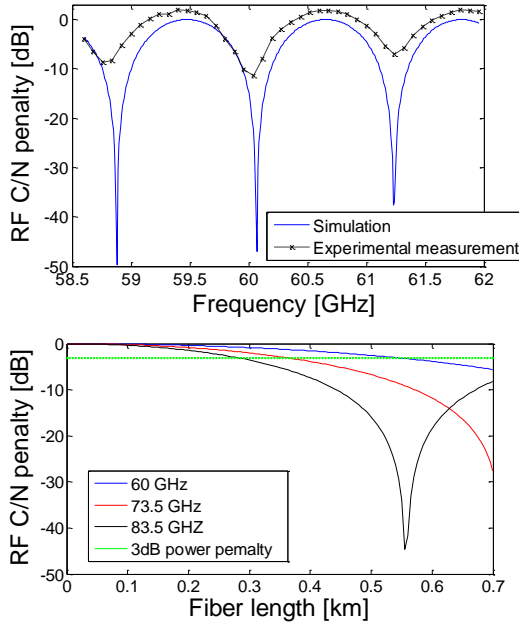


Figure 9. CD-induced RF C/N penalty as a function of (top) the RF carrier frequency for 48.8-km SSMF fiber length, and (bottom) fiber link length for 60-GHz, 73.5-GHz, and 83.5-GHz RoF systems.

In Fig. 9 (top), the results of numerical calculation of CD-induced RF power fading based on Eq. (7) and Eq. (8) for 48.8-km SSMF link as a function of the LO frequency are presented together with the experimentally measured data showing a close match. In Fig. 9 (bottom), the RF fading is compared for RF carriers in V and E bands. As presented in Fig. 9 (bottom), the first 3-dB penalty is expected at 280 m, 375 m and 560 m for 83.5-GHz, 73.5-GHz and 60-GHz systems respectively.

A number of techniques were proposed in order to combat the CD-induced RF power fading, such as employing transmitters with negative chirp [37], tunable compensation with Fiber Bragg Gratings (FBG) [38], and compensation through applying optimum electrical phase shift [39] and midway optical phase conjugation [40]. In this Thesis, we propose a technique to overcome the RF power fading by introducing a degree of frequency tunability of the LO.

1.7.2 Bit walk-off

When two sidebands are photomixed at the PD after fiber transmission, data pulses transmitted on lower and upper sidebands of the RoF signal are shifted in relation to each other in the time domain leading to the intersymbol interference after the photomixing. This effect is reported as the 'bit walk-off' [41-43].

The bit walk-off is present in the OCS RoF transmission case which is also sometimes referred to as double sideband with suppressed carrier (DSB-SC) modulation. The experimentally measured spectrum of the OCS RoF signal is presented in Fig. 10.

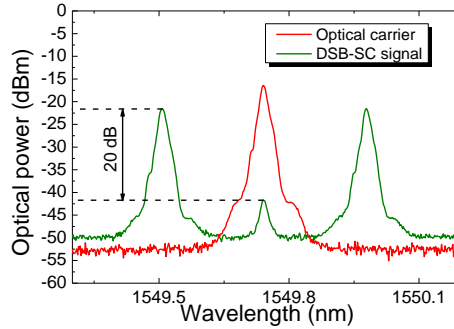


Figure 10. Optical spectra of the OCS/DSB-SC signal and the original lightwave carrier signal.

Assuming that the duty cycle is equal to 1 for non-return-to-zero (NRZ) signals, the bit walk-off evolution along the fiber length is governed according to [41-43]:

$$\Delta\tau = \frac{DL\lambda_c^2}{\Delta\lambda_{RF}}, \quad (9)$$

where $\Delta\lambda_{RF}$ is the wavelength distance between the sidebands, D is the dispersion parameter, L is the fiber length, and λ_c is the wavelength of the lightwave.

The limit on the bit walk-off as 0.7 of the pulse's time duration is set according to [42] in order to define the maximum feasible fiber transmission distance. The limiting distance is then given by:

$$L = \frac{\Delta\lambda_{\text{RF}}\Delta\tau \times 0.7}{D\lambda_c^2} \quad (10)$$

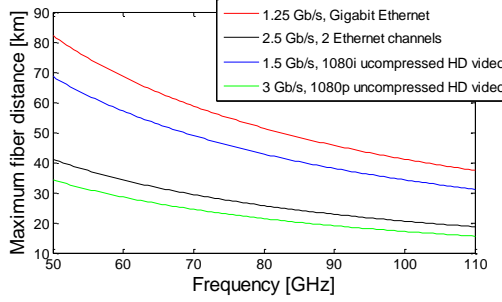


Figure 11. Maximum attainable fiber link length as a function of the carrier frequency.

In Fig. 11, the maximum feasible fiber transmission distance is depicted as a function of carrier frequency. It is evident from Fig. 11 that the application of the OCS technique in the case of mm-wave RF delivery is limited to the access fiber deployment.

1.8 Noise in mm-wave RoF links

Noise sources in RoF links are comprised of relative intensity noise (RIN) at the laser diode, the thermal (Johnson) noise, and the shot noise at the PD [44]. Additionally, the use of optical amplifiers in the link, such as erbium doped fiber amplifiers (EDFA), contributes the amplified spontaneous emission (ASE) noise.

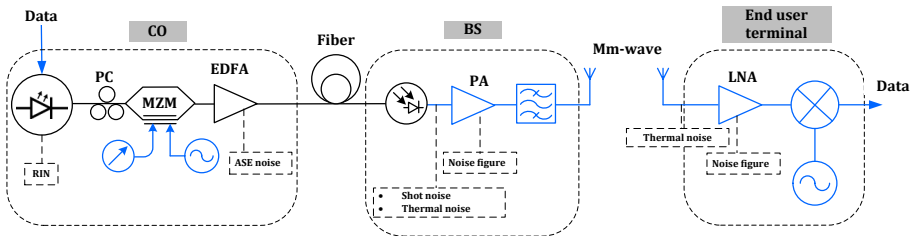


Figure 12. Noise contributions in RoF links.

It is important to note that, in the absence of ASE, the link performance is either limited by the shot noise, thermal noise or RIN depending on

specifications of the laser diode and the optical power into the PD. In Fig. 12, the critical points when the amplitude noise is imposed on the waveform are indicated. High values of RIN noise will impose the main limitation on the SNR of the system in the case of DFBs when the RIN noise spectral density is usually no better than -155 dB/Hz [44]. For external cavity lasers (ECL), RIN is typically less than -175 dB/Hz [44] which sets the limitation either by the thermal noise or the shot noise depending on the value of optical power into the PD [44].

For low powers incident to the PD, the system noise floor is defined by the thermal noise. At higher powers into the PD, the shot noise is dominant. However, in the shot-noise limitation region, SNR of the system is higher than the SNR in the thermal noise limited region [44].

1.9 Wireless channel

In the following subsections, emerging applications for utilization of the mm-wave wireless channel capacity are introduced, and limitations on transmission distance and end-user mobility are discussed.

1.9.1 Overview of the applications and standards

The 60 GHz wireless technology has already been widely adopted by industry for applications such as wireless Gigabit Ethernet bridges reaching distances up to 770 m sustaining 1.25 Gbps capacity [45-47] and high-definition multimedia interface (HDMI) cable replacement [48].

Table 1. Overview of the 60-GHz band wireless standards.

	IEEE 802.15.3C [55]	Wireless HD [48]	IEEE 802.11.ad [49]
Current Status	Released 2009	Released May, 2010	Absorbed by Wi-Fi alliance
Data rate	0.3 to 5775 Mbps	Up to >7 Gbps	Up to 7 Gbps
Target application	Cable replacement, video on demand, high-speed Internet access.	Uncompressed video transmission, data networking.	Wi-Fi compatible operation, multi-Gbps Wi-Fi
Channel coding	RS, LDPC	RS	Not specified
Multiband	No	No	Yes
Distance	Up to 10 m	At least 10 m	Beyond 10 m
Video coding	Not considered	Used.	Not considered.
Modulation format	BPSK, QPSK, 8-PSK, 16-QAM, OFDM	OFDM(QPSK, 16-QAM, 64-QAM)	OFDM(QPSK, 16-QAM, 64-QAM)

There are ongoing research and industrial developments in application of the 60-GHz technology for wireless personal area networks (WPANs) [49], data

center interconnects [50-52] and mobile backhaul links [53, 54]. In the Table 1, the overview of the recent and ongoing standardization activities is given.

The standards consider diverse channel coding i. e. (Reed-Solomon (RS) codes and low-density parity-check code (LDPC)). In the present Thesis, we report on the use of RS coding.

The primary difference of our research compared to the work described in the standards is in the modulation formats employed. In our work, binary amplitude shift keying (ASK) is used as we consider it a best fit for simplified RoF networks since given the abundant bandwidth (up to 9 GHz), low spectral efficiency is allowed.

1.9.2 60 GHz wireless channel modeling

In this section, large scale path loss modeling is performed accounting for the change in the average RF power as a function of the transmitter-receiver distance separation. Shadowing signifying average power variations over a few tens of wavelengths and the fast fading causing rapid changing in the envelope of the signal over a distance less than 10 wavelengths are omitted [56-58]. However, a good estimate of the coverage area can be facilitated by the large scale path loss modeling (usually referred to as the “path loss”) only [56-59].

The free space path loss as a function of distance including the shadowing margin is given by Eq. (11):

$$PL_{FS}(d) = \overline{PL}_{FS}(d) + X_{\sigma}, \quad (11)$$

where $\overline{PL}_{FS}(d)$ is the average path loss and X_{σ} is the shadowing fading [57-59]. $\overline{PL}_{FS}(d)$ can be expressed by a following equation:

$$\overline{PL}_{FS}(d) = PL_{FS}(d_0) + 10n\log_{10}\left(\frac{d}{d_0}\right) + \sum_{q=1}^Q X_q, \text{ for } d > d_0, \quad (12)$$

where d_0 and n denote the reference distance and the path loss exponent respectively, and d is the distance between the wireless transmitter and receiver [57-59]. The term X_q accounts for the additional attenuation due to specific obstruction by objects [58]. The reference distance is usually equal to 1 m unless otherwise specified. The path loss exponent is derived empirically for the particular environment of RF propagation, and can be used for both line-of-sight (LOS) and non-line-of-sight (NLOS) scenarios [58]. In the subsequent modelling, only first two terms from Eq. (12) are taken into account for the sake of keeping the model as deterministic and as general as possible.

The free space path loss can be calculated by the following formula (Friis transmission equation):

$$PL_{FS}(d) = 20 \log_{10} \left(\frac{4\pi d}{\lambda} \right) - G_{tx} - G_{rx}, \quad (13)$$

where λ is the central wavelength of the RF signal, and G_{tx} and G_{rx} are gain of transmitting and receiving antennas respectively. Eq. (13) yields the path loss values equivalent to the values obtained from Eq. (12) if the path loss exponent equal to 2 is assumed, and omnidirectional antennas are used. The Friis transmission equation is only applicable for the distances exceeding the Fraunhofer distance that is calculated according to Eq. (14):

$$d_f = \frac{2D^2}{\lambda}, \quad (14)$$

where D is the largest dimension of the antenna and λ is a wavelength of the radio signal. For a commercially available lens horn antenna of 42 dBi gain with a diameter of 0.25 m, the Fraunhofer distance is equal to 25 m, thus a higher gain horn antennas cannot be used indoors both because of their size and extended Fraunhofer distance.

It is also worth noting that with increase in antenna gain, the wireless link loses its 'mobility' characteristics since lower coverage is provided, and high-gain horn antennas are therefore usually used in fixed point-to-point wireless communication setting.

In outdoor scenarios, antennas are usually mounted on a roof, a communication pole, a wall etc., the LOS visibility between the transmitter and the receiver is required, and high-gain antennas are used.

The attenuation of mm-wave RF signals in the air is also caused by absorption on molecules of oxygen and water vapour. Gaseous attenuation (including both water vapour and oxygen-related absorption) peaks at the 60 GHz frequency reaching the value of approximately 15 dB/km due to the absorption peak on oxygen molecules, however, across the E-band, combined attenuation on molecules of oxygen and water vapour is measured to be about 0.4 dB/km [60].

An important performance criterion for outdoors wireless communication is stability of the link under the weather influence. In this work, we analyse the influence of rain on transmission performance. An estimate of the rain attenuation is given by:

$$\gamma_R = kR^\alpha, \quad (15)$$

where γ_R [dB/km] is the specific rain attenuation and R [mm/hour] is the rain rate parameter differentiating the intensity of a rainfall. The coefficients k and α are frequency dependent, a set of values of k and α is given in Recommendation P.838-2 [61]. Rain types are separated as a 'drizzle: 0.25 mm/hour', a 'light rain: 2.5 mm/hour', a 'heavy rain: 25 mm/hour', and a 'tropical rain: 100 mm/hour' [6]. Figure 13 presents the analytical results based on the recommendation P.838-2.

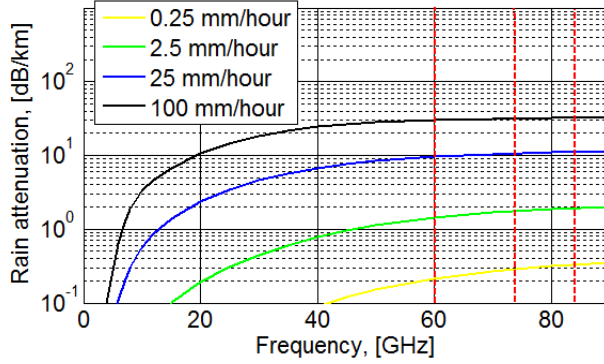


Figure 13. Rainfall attenuation as a function of frequency.

The overall air transmission path loss, including the free space path loss, rain attenuation, and attenuation due to gaseous absorption, is governed by:

$$PL = PL_{FS} [dB] + (\gamma_{gas} [\frac{dB}{km}] + \gamma_{rain} [\frac{dB}{km}]) \times d_{[km]} \quad (16)$$

In the Table 2, we present a set of values for the path loss exponent derived for specific environments in [62-65]. The path loss curves based on these parameters and assuming the use of omnidirectional antennas are depicted in Fig. 14. As shown in Fig. 14, path loss values for the LOS 60-GHz wireless signal air propagation are located around and below the path loss values obtained using the free space path loss formula. Contrariwise, reported in [64-65] NLOS path loss values tend to exceed the values obtained using the free space path loss formula.

Table 2. Parameters for wireless channel modelling.

Center frequency	Environment	Scenario	Path loss exponent	Reference distance	Reference
60GHz	Laboratory	LOS	1.8	1.5 m	[62]
60 GHz	Hallway	LOS	2.17	1 m	[64]
60 GHz	Corridor	LOS	1.64	1 m	[64]
60 GHz	Indoor	NLOS	2.5	1 m	[65]
60 GHz	Hall	NLOS	3.01	1 m	[64]

Indoor propagation is oftentimes affected by reflections from the walls, the furniture, and the moving objects. The effect of multipath propagation is reported to either improve the channel performance or deteriorate it depending on the particular environment, and the performance depicted in Fig. 14 (top) may therefore be subject to significant variations.

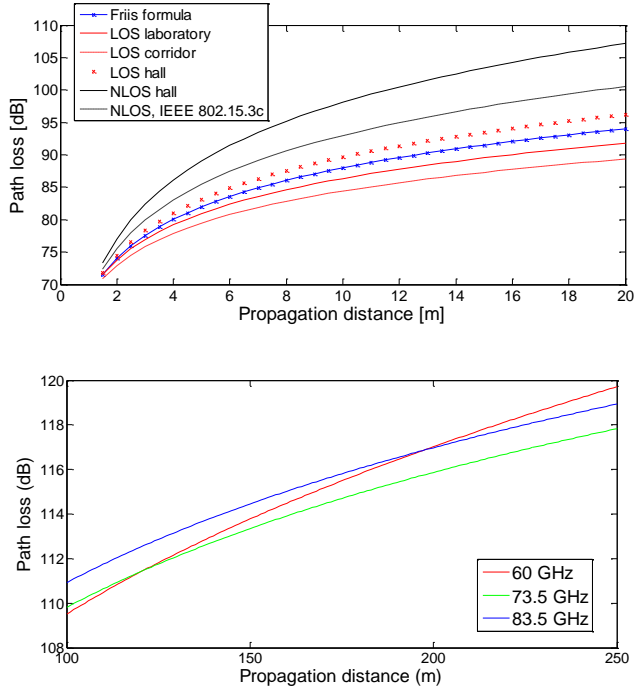


Figure 14. The 60-GHz wireless channel path loss in several indoor environments (top) and the path loss for 60-GHz, 73.5-GHz and 83.5-GHz systems based on Eq. (13) (bottom).

As we show in Fig. 14 (bottom), the outdoor 60 GHz systems show the path loss behaviour distinct to E-band transmission due to increased gaseous absorption. The frequencies are chosen at the center of unlicensed (57-66 GHz) and light licensing (71-76 GHz and 81-86 GHz) mm-wave bands. The thorough comparison between these wireless carriers for outdoor communication is conducted in our published **Paper [5]**.

Practically, the higher path loss in mm-wave bands can be compensated by using antennas with higher gain (up to 42 dBi gain antennas are commercially available). Received power in the wireless link with antenna gain can be calculated as in Eq. (17):

$$P_{rx} = P_{tx} - PL_{FS} - (\gamma_{gas} + \gamma_{rain}) \times d + G_{tx} + G_{rx} \quad (17)$$

However, when highly directional antennas are used, antenna blockage and misalignment may impose a significant drop of received power. When the LOS path is obstructed, lower gain antennas might be preferred in order that the wireless power arriving from the reflections can still be collected.

The wireless link budget, assuming that the signal is detected immediately after the receiving antenna, is defined by the noise floor imposed by the Johnson's noise, channel bandwidth, required SNR at the receiver and the transmitter power. The wireless link power budget margin available for wireless transmission, excluding the shadowing path loss, implementation loss etc., may be defined by:

$$\beta = P_{tx} - 10\log_{10}(1000 \times kt) - 10\log_{10}(B) - SNR \quad (18)$$

where k is a Boltzmann's constant, t [K] is a room temperature, and B is the channel bandwidth. To improve the wireless link budget, two more techniques can be applied. First, using higher gain/additional amplifiers is an option, however the noise figure of additional amplifiers would reduce the SNR of the signal, and the equation 18 should be adjusted accordingly. Second, launching higher power into the PD corresponds to the increase in the RF power before radiation. Furthermore, increasing the optical power into the PD, the SNR of the system might be improved as the noise floor will then be defined by the shot noise [44].

1.10 Source and channel coding in mm-wave fiber-wireless setups

In this section, we discuss how the mm-wave wireless channel capacity can be utilized for real-time HD video transmission. Both compressed and uncompressed HD video transmission systems are considered.

1.10.1 *Uncompressed real-time HD video transmission*

Commonly, even though video arrives to the household in compressed format, it is provided in an uncompressed format at the output of consumer devices such as DVD, Blue-ray players, and Set-top boxes. As a result, uncompressed video streaming has become an application of choice for utilization of the 60-GHz wireless channel. Using the 60-GHz wireless technology, essentially, the HDMI cable replacement is provided e. g. in [48].

Bitrate requirements for real-time uncompressed transmission of 1080p (1080 lines, progressive scan) HD video sequences with different frame rates and color subsampling methods are presented in Table 3.

Table 3. Bitrate requirements for real-time uncompressed HD video transmission.

Frame width	Frame height	Frame rate	Color depth	Sampling method	Bitrate, Gb/s
1920	1080	50	8	4:4:4	2.488
1920	1080	60	8	4:4:4	2.986
1920	1080	50	8	4:2:0	1.244
1920	1080	60	8	4:2:0	1.493

It is critical that wireless home networks make the uncompressed real-time uncompressed HD video transmission an integral part of their functionality which imposes the bandwidth requirements that can only be met by using the mm-wave technology.

1.10.2 *Compressed HD video transmission*

The indoor mm-wave transmission channels are highly prone to severe drops in SNR in the case of the LOS path blockage, and thus in order to maintain the seamless wireless connectivity, transmission systems must adapt their transmitting power or bitrate. Considering this, video coding can provide a significant advantage over uncompressed video by its possibility of much more flexible adaptation to dynamic channel conditions in terms of bitrate. For uncompressed video transmission, the bitrate control is limited as a fixed

number of bitrates is available depending on the resolution, frame rate and color subsampling method.

In terms of cross-layer optimization, typically, the higher layer optimizes parameters for the next lower layer. This cross-layer optimization approach has been deployed in most existing systems, where the application dictates the medium access control (MAC) protocol parameters and strategies, while the MAC selects the optimal physical layer modulation scheme [66].

Conversely, in our investigated video set-ups, the best effort is applied so that the lower layer isolates higher layers from bit errors.

Two primary objectives of optimization of the RoF system for video transmission can be identified: fiber/air distance extension and power consumption minimization. When the distance between the wireless transmitter and receiver is being increased, at a starting point, compression artifacts dominate the perceived video distortion. As distance increases and SNR in turn decreases, the video distortion due to channel-induced errors (packet loss) becomes dominant, and the quantization parameter (QP) should be adjusted accordingly.

To address the low-delay requirement, Intra-coding mode only and frame slicing are employed in the video coding experiments. The use of Intra coding and intra-frame slicing allows avoiding bitrate fluctuations and therefore buffering delays.

Our goal for optimization is to achieve the best received video quality for a given link budget without a severe constraint on bandwidth as in conventional links. There are different tools enabling this optimization. With regards to the role of the quantizer in the optimization, the smaller the QP, the smaller the source-related distortion but the larger the channel-related distortion it may entail (for the same level of channel protection) [66].

With introduction of H.264/advanced video coding (AVC) standard [67], simple and computationally efficient video compression solutions became available together with the improved algorithms for combating the channel impairments at the decoder.

With the ongoing rapid developments in the display technology, codec implementations based on current and upcoming video coding standards shall address following challenges:

- Provide control over “complexity versus coding efficiency” trade-off.

- Provide low-complexity low-delay coding of interactive HD video services.
- Enable new resolutions, including 4k×2k and 8k×4k resolutions.
- Provide the efficient encoding for video sequences using 4:4:4 subsampling.

In regards to source-coding enabled impairments compensation, H.264/AVC defines several mechanisms that allow error concealment at a decoder such as avoiding temporal error propagation with Intra-only (frame-by-frame) coding, intra-frame slicing, flexible macroblock ordering (FMO) inside of the slice, and data-partitioned slicing [67, 68]. Frame slicing leads to decreasing the average length of H.264/AVC network abstraction layer (NAL) units (video packets); lower packet size is reported in [68] to reduce the packet error rate (PER) and in turn improve the PSNR of the impaired video. The encoder is further simplified by using only universal variable length coding (UVLC) for H.264/AVC entropy coding.

Uncompressed real-time transmission of 1080p 60 frames per second 4:4:4 video signal requires 3-Gbps channel bandwidth (Table 3). The main lobe of the uncompressed 1080p video signal using binary amplitude shift keying (ASK) signaling will occupy 6 GHz of spectrum in RF domain. However, with a moderate compression ratio of 20, the real-time bitrate of the signal can be reduced to 150 Mbps. Uncompressed 1080p HD test video sequences were used for video coding experiments. The sequences were originally shot in 4:2:0 YUV 1080p format. We upsampled them to 4:4:4 YUV format to model the highest quality and the most bitrate demanding case.

We use the peak signal-to-noise ratio (PSNR) as an objective quality metric for video, which is defined in Eq. 19 and Eq. 20:

$$MSE = \frac{1}{N} \sum_{i=1}^N (x_i - y_i)^2, \quad (19)$$

$$PSNR = 10 \log_{10} \left(\frac{L^2}{MSE} \right), \quad (20)$$

where MSE stands for a mean squared error, N is the number of pixels in the image, and x_i and y_i are the i -th pixels in the original and the distorted signals, respectively. L is the dynamic range of pixel values. For an 8 bits/color signal, L is equal to 255. PSNR is evaluated for the luminance component of the transmitted video signal.

1.10.3 Channel coding

In this section, we discuss the choice of parameters for channel coding and provide the analytical description of error correction codes' (ECC) performance. Packetization is required in both channel and source coding, video packet size is chosen first, and the closest packet sizes capable to cover the video packet are chosen for Bose-Chaudhuri-Hocquenghem (BCH) and RS coding. An analytical solution for ECC performance is governed according to Eq. (21) [69]:

$$p_{pd} = \sum_{i=t+1}^n (i/n) \times (n, k) \times p^i \times (1-p)^{n-i}, \quad (21)$$

where k is a message length, n is a block length, t is an error-correction capability of the code, p is a BER before decoding, and p_{pd} is a post-decoding BER.

In this Thesis, the performance of BCH codes is compared to the performance of RS codes. For analytical estimation of RS codes' performance, we have applied approximation for the relation between the symbol-error rate and the bit error rate given by Eq. (22) and Eq. (23):

$$p_s = 1 - (1 - p_b)^m, \quad (22)$$

$$p_b = 1 - (1 - p_s)^{1/m}, \quad (23)$$

where p_s is a symbol error rate, p_b is a bit error rate, and m is a symbol length in bits.

2. Overview of state-of-the-art work

In this section, we present an overview of the work on mm-wave fiber-wireless transmission techniques posing similar objectives as our research. Particular interest is on the techniques considering advanced functionalities for simplified RoF networks such as transmission of multiband electrical signals, diversification of fiber infrastructure, multihop transmission, and the application-focused link design.

The recent progress in mm-wave electronic components' design has led to the appearance of commercially available 60-GHz up- and down-conversion modules [70, 71]. This development is accompanied by the introduction of highly linear high power 60 GHz analog photoreceivers [72] and compact E-band (60-90 GHz) wireless transmitters [73] combining progress in optoelectronic and mm-wave components design and further strengthening the potential for commercial deployment of mm-wave RoF links.

Integration of fiber and wireless transmission has been extensively studied [74, 75] also targeting of the design of duplex links [76]. Most of the physical layer system design papers focus on optical multiplexing, particularly on integration of coarse wavelength division multiplexing / dense wavelength division multiplexing systems with mm-wave wireless services.

Alternatively to optical baseband and RoF multiplexing in the optical domain, electrical multiplexing of the baseband and RF channels was studied recently. Guillory et al. consider both hybrid and electrical-only multiplexing of baseband and wireless channels in [77]. Diverse schemes for electrical

multiplexing of baseband data before fiber transmission have been studied [77, 78].

Multi-hop transmission setups including either a few fiber or a few wireless spans have been demonstrated. In case of fiber-wireless-fiber architecture, the mobile backhaul transmission can be suggested as a target [79]. Fiber tunnel transmission (wireless-fiber-wireless) has shown that two 60-GHz terminals separated by 300 m of multimode fiber (MMF) can communicate seamlessly [80].

Diversification of the fiber infrastructure by using polymer optical fibers (POF) was investigated recently. In particular, the architecture combining the POF transmission media in home network / local area network (LAN) with access fiber infrastructure wired by SSMF was studied [69].

In order to enable energy-efficient 60-GHz RoF communication, passive wireless transmitters were examined in [81].

WDM RoF systems delivering the simultaneous generation of multiple RF signals using a single E/O conversion module at the CO have been studied in [82-85].

A number of ECC solutions was proposed for mm-wave wireless systems [80-84]. Low-density parity check codes, RS codes, TURBO codes and convolutional codes were reported. In paper [86], the channel coding study for both omnidirectional antennas and antennas with high directivity is presented where in both cases a LOS condition is given, in paper [87] the study for the NLOS mm-wave transmission is presented. Paper [88] reports on channel coding for a model that includes the phase noise and nonlinear effects.

Telecommunication services such as broadband compressed and uncompressed HD video transmission in the combined 60-GHz fiber-wireless setups have been recently reported [89-91].

Subdividing the RoF setups by the wireless carrier frequency, larger amount of ongoing work is performed in mm-wave bands given the promise of large capacities.

Our work in this Thesis has significantly extended the list of application-focused fiber-wireless systems for access segment.

3. Description of the papers

In this chapter, position of our work among the state-of-the-art research is outlined on the architectural basis with case studies including wireless home networks, backhaul networks, and close-proximity wireless connectivity.

3.1. Overview of the papers included in the Thesis

First, our work on RoF delivery to the wireless home area networks was addressed in papers [1-3, 8]. Paper [1], presents the case for joint source-channel optimization in fiber-supported 60-GHz WPAN networks where the potential for fiber and wireless transmission extension has been shown through the use of source coding. This concept is later extended to the W-band wireless transmission in Paper [8] assisted with channel coding. Another work for this architecture addresses the fiber transmission in detail providing a solution for combined SSMF/MMF transmission (Paper [2]). We show that the bandwidth-length product of mm-wave RoF MMF links is suitable for gigabit data transmission. Our final work for fiber-supported mm-wave WPAN deals with the real-time uncompressed 1080i (1080 lines, interlaced) HD video transmission (Paper [3]). Passive and active solutions have been studied for W-band wireless transmitter implementation in order to ensure the future-proof energy efficiency.

Employing simplified setups leads to higher pronouncement of impairments. Our work on DSB RoF transmission in Paper [4] contributes a novel solution to combat the fading imposed on RF transport in simplified

fiber-wireless systems. Previous research would in certain cases require the change in fiber infrastructure, when our proposed method is suitable for implementation in pre-installed fiber networks.

Paper [5] addresses the issue of backhaul data delivery where a novel architecture including 2 fiber spans bridged by wireless transmission is studied in order to provide backhaul simultaneously for dense metropolitan and suburban areas.

Paper [6] and Paper [9] address the architectures for video broadcast/multicast. In Paper [6], the solution for simultaneous RoF upconversion of multiple lightwaves with a single RF oscillator at the CO is investigated. By using diverse lightwave generation techniques, service quality differentiation for the end users might be performed. Paper [9] investigates the architecture where RN functionalities are enhanced to include the dynamic capacity allocation and wireless data multicast.

Ultra-short range applications are studied in Paper [7], where advanced physical layer design of the link yields the use of low-end components for mm-wave E/O conversion nevertheless achieving excellent transmission performance.

We note that the main difference of our work from conventional approach is that we optimize the system performance under a constraint on complexity and feasibility for a specific application when the common approach aims at providing the highest bitrate to the end-user.

3.2. Detailed description of the papers

Below is the detailed description of the contribution of each paper based on their abstract and conclusion.

[Paper 1] This paper addresses the problem of distribution of HD video in fiber-wireless networks. We explore the notion of joint optimization of physical layer parameters of the RoF link (power levels, distance) and the codec parameters (quantization, error-resilience tools) based on the BER/PSNR as objective video quality metrics. The physical layer architecture with the low complexity envelope detection solution for RF downconversion is investigated. We present both experimental studies and simulation of high-quality compressed HD video transmission over a 60-GHz fiber-wireless link.

It should be noted that the combined noise figure of amplifiers in Eq. (3) may be calculated more precisely if Friis formula for noise is used.

[Paper 2] We propose and experimentally demonstrate a simple, cost-effective gigabit fiber-wireless system operating in the 60-GHz band for WPAN. Simplicity is achieved by utilizing direct modulation and envelope detection. Error-free transmission of 2-Gbps data in the 60-GHz band over a hybrid channel including 10-km SSMF/1-km MMF and 6.5-m air transmission is successfully achieved proving that the sufficient bandwidth-length product is available for mm-wave RoF signal transmission in MMF [92].

[Paper 3] We experimentally demonstrate uncompressed HD video distribution in V- and W-band fiber-wireless links achieving 3 meters of wireless transmission in both cases. We experimentally emulate access architecture by deploying single/multimode fibers. For W-band, we report on experimental assessment of passive and active approaches for implementation of the BS. The BER performance of the optical and wireless channels is reported. Based on the measured experimental results, we can conclude that V- and W-band dual-laser RF generation fiber-wireless systems can be regarded as viable candidates to provide fiber support in high-frequency WPAN particularly for uncompressed real-time 1080i (1080 lines, interlaced scanning) HD video delivery.

We note that in Fig. 7 of the Paper 3 the performance is different from our expectations. B2B transmission shows lower performance than transmission through 22.8-km SSMF, which, given the low penalty (~ 0.3 dB), is best explained as a random measurement error.

[Paper 4] We experimentally demonstrate a 60-GHz DSB RoF synchronous detection link capable of transmitting 3-Gbps data at 10^{-9} BER level. We studied CD induced RF degradation for DCF experimentally and theoretically. The experimental results indicate more rapid degradation of RF carrier after photomixing in case of DCF deployment, which agrees well with simulation and analytical solution. Theoretical results presented in this paper indicate that increase in the absolute value of the dispersion parameter when we employ DCF increases periodicity of CD induced RF degradation along the fiber length and along the frequency values of the electrical oscillator. Based on experimental results and analytical calculation, we then proposed the algorithm for frequency tuning of the electrical oscillator that uses an advantage of the wide 60-GHz bandwidth, and yields faster tuning optimization for DCF compared to SSMF.

[Paper 5] We propose and experimentally demonstrate a fiber-wireless transmission system for optimized delivery of 60-GHz RF signals through picocell mobile backhaul connections. Advantages of 60-GHz links for

utilization in short range mobile backhaul are identified through feasibility analysis in comparison with an alternative E-band technology. The system is simplified and tailored for OOK data signals delivery by employing a single module for lightwave generation and modulation combined with simplified RF downconversion technique by envelope detection. The power budget margin that is required to extend the wireless transmission distance from 4 m to a few hundred meters has been taken into account in the setup design, and the techniques to extend the wireless distance are analyzed. BER performance below the 7% overhead FEC limit is reached for 1.25-Gbps data transmission through up to 4 m wireless distance and up to 20 km of SSMF interfacing both 60-GHz BSs. 73-dB-Hz^{2/3} SFDR is reported when the EDFA is included as a part of an optical transmitter. Phase noise performance indicates high potential of the system for transmission of advanced modulation formats.

[Paper 6] Simultaneous 60-GHz RoF modulation and fiber transmission of lightwaves produced by the DFB, the ECL, and the C-band VCSEL laser devices is demonstrated. 1.25-Gbps data signals are transmitted on each of the lightwaves attaining a BER performance below 10^{-9} level. Carrier suppression of 20 dB is achieved simultaneously for all three lightwaves placed in a wide wavelength range. By investigating the lightwaves with diverse performance in terms of chirp and optical power, we can control directly at the CO the quality of service assigned for multiple end-users.

[Paper 7] We present an experimental investigation of the 60-GHz optical carrier suppressed radio over fiber systems with less than 5 dB carrier suppression. As a case study, the 60-GHz RoF signal is generated using a 12.5-Gb/s commercially available Mach-Zehnder modulator biased at its minimum point. We report on error-free transmission over 20 km of standard single mode fiber and 1 m of wireless distance. Furthermore, the efficiency of photonic RF generation depending on the value of carrier suppression is reported. Presence of the optical carrier and low separation between the carrier and sidebands lead to four wave mixing, however no error floor due to nonlinearities at 16-dBm optical power was reported.

We argue that transport of RoF signals with low carrier suppression combined with low-complexity techniques of lightwave generation, baseband data modulation, and RF downconversion might be a promising enabling technology for fiber support of close-proximity wireless terminals.

[Paper 8] We report on performance of channel and source coding as applied for an experimentally-realized hybrid fiber-wireless W-band link. BCH and RS pre- and post-decoding BER performance is assessed for 20-km fiber

transmission and a wireless propagation distance of 3 meters. We report on noise statistics for the envelope detection of mm-wave RF generated through photomixing of two unlocked lasers.

We argue that light video compression and low-complexity channel coding for the W-band fiber-wireless link enable multiple channel 1080p wireless HD video transmission. The experimental results for BCH-protected transmission match the results of the analytical calculation. Finally, we analyze performance of light compression techniques for a few 1080p HD video sequences.

[Paper 9] We propose an approach for dynamic channel allocation and multicast data delivery inside the 60-GHz unlicensed band. Channels, conveying 1.25-Gbps signals, are allocated by tuning the frequency sweep of an ECL either in the optical remote node (RN) or in the CO. At the RN, we perform the replication of the original channel suitable for closely spaced multicast applications such as HD video delivery where RN serves as a photonic RF generator for both channel allocation and multicast. Experimental demonstration is presented with BER performance below 10^{-9} for original and replicated channels after transmission through 22.8 km of SSMF. Higher receiver sensitivity may be achieved with OCS technique, but larger fiber transmission penalty is imposed as compared to remote heterodyning of uncorrelated lasers.

4. Conclusions

In this Ph.D. project, design and performance evaluation of simplified mm-wave RoF links suitable for HD video transmission were treated.

For WPAN distribution, we explored the notion of joint optimization of physical layer parameters of a fiber-wireless link and the codec parameters based on the PSNR as the objective video quality metric for compressed video transmission. Furthermore, uncompressed real-time HD video delivery and channel coding in mm-wave WPANs were examined.

Use of mm-wave signals for metropolitan and suburban mobile backhaul was studied in this Thesis. We proposed a setup for gigabit wireless transmission in the fiber-wireless-fiber link arguing that, despite the higher oxygen absorption, 60 GHz links can be used for the short range mobile backhaul.

In this Thesis, we proposed a novel solution to combat the periodic CD-induced RF power fading in a simple IM/DD mm-wave RoF links through introduction of a degree of frequency tunability at the RoF transmitter. Performance of the method was evaluated for SSMF and DCF transmission media. We have shown that, even though DCF fibers will impose the 3 dB penalty at a shorter distance than SSMF fiber, their performance can be easier optimized by using the frequency tuning of the LO at the transmitter.

We studied advanced RoF infrastructures in order to enable compressed/uncompressed real-time HD video transmission. To enable efficient dynamic multicast/broadcast of video services, we have proposed and evaluated an approach of increasing functionality of the optical RN. Dynamic

channel allocation and replication of channels at the RN were experimentally demonstrated by simply adding a tunable laser at the RN.

In order to decrease the count of expensive mm-wave LO modules at the CO, delivery of multiple upconverted lightwaves generated by a single E/O module was evaluated using diverse lightwave generation and data modulation techniques including VCSEL, ECL and DFB techniques. The three techniques have shown comparable performance under constraints of available power budget, chirp and the bit walk-off in OCS setups for access fiber-wireless network segment.

In this Thesis, mm-wave RoF links with diverse lightwave generation techniques were experimentally realized for diversified fiber infrastructure including SSMF, MMF and DSF and the estimate of the feasibility of delivering mm-wave wireless video services through fiber infrastructure under a constraint of different nonlinear impairments and dispersion is given.

5. Future work

In this section the directions for future development of simplified mm-wave RoF links for video distribution are outlined.

We believe that using low-directivity antennas supported by the fiber infrastructure is a promising approach capable of bringing together the flexibility of wireless technology and the capacity of fiber links. However, the thorough optical/wireless link budget planning should be performed including empirical studies for diverse wireless environments.

Another interesting solution to overcome the LOS obstruction is to handle blockages by relaying the signal to intermediate nodes available in the LOS visibility. When the LOS path between two nodes is blocked, the route around it should be built, using available intermediate LOS links [93]. However, this approach requires the use of a few access points per room, which may increase the system cost significantly, particularly considering that every access point might require fiber support.

Another attractive direction is to combine mm-wave fiber-wireless systems with conventional Wi-Fi WPAN / wireless local area networks (WLAN) systems. Under optimal propagation conditions, the user can exploit the resources of the mm-wave system. As the mm-wave channel conditions deteriorate, the connection is switched to the Wi-Fi bands. In this way, the Wi-Fi bands serve as a fallback option for mm-wave cells [94]. As Wi-Fi coverage is broader than mm-wave coverage, one Wi-Fi access point may support several mm-wave cells.

Bidirectional fiber-wireless transmission is also of interest, in particular, in combination with advanced modulation formats. Crosstalk in fiber-wireless channels for a variety of environments remains to be quantified.

Bibliography

- [1] Cisco white paper, "Cisco Visual Networking Index: Global Mobile Data Traffic Forecast Update, 2012-2017," (Cisco, 2012). http://www.cisco.com/en/US/solutions/collateral/ns341/ns525/ns537/ns705/ns827/white_paper_c11-520862.pdf.
- [2] Ericsson white paper, "Traffic and market data report," (Ericsson, 2011). <http://hugin.info/1061/R/1561267/483187.pdf>.
- [3] D. van den Borne, "Robust Optical Transmission Systems: Modulation and Equalization," Ph.D. dissertation, Eindhoven University of Technology, (2008).
- [4] T. Berceci, and P. R. Herczfeld, "Microwave Photonics—A Historical Perspective," *IEEE Trans. Microw. Theory Tech.*, vol. 58, no. 11, 2010.
- [5] M. J. Fice, E. Rouvalis, F. van Dijk, A. Accard, F. Lelarge, C. C. Renaud, G. Carpintero, and A. J. Seeds, "146-GHz millimeter-wave radio-over-fiber photonic wireless transmission system," *Opt. Express*, vol. 20, no. 2, pp. 1769-1774, 2012.
- [6] J. Wells, "Multi-gigabit microwave and millimeter-wave wireless communications," (Artech house, 2010).
- [7] Ericsson white paper, "Heterogeneous networks," (Ericsson, 2012). <http://www.ericsson.com/res/docs/whitepapers/WP-Heterogeneous-Networks.pdf>.
- [8] M. C. Parker, S. D. Walker, R. Llorente, M. Morant, M. Beltrán, I. Möllers, D. Jäger, C. Vázquez, D. Montero, I. Librán, S. Mikroulis, S. Karabetsos, A. Bogris, "Radio-over-fibre technologies arising from the building the future optical network in Europe (BONE) project," *IET Optoelectron.*, vol. 4, no. 6, pp. 247-259, 2010.
- [9] C. Lim, A. Nirmalathas, M. Bakaul, P. Gamage, K.-L. Lee, Y. Yang, D. Novak, R. Waterhouse, "Fiber-Wireless Networks and Subsystem Technologies," *J. Lightw. Technol.*, vol. 28, no. 4, pp. 390-405, 2010.
- [10] R. Herschel, C. G. Schaeffer, "Architectures for Multiband MultiGbps Radio-over-Fiber Systems," in *Proc. of 12th ITG Conference on Photonic Networks*, Leipzig, Germany, 2011, paper 24.
- [11] A. Stohr, S. Babel, P. Cannard, B. Charbonnier, F. van Dijk, S. Fedderwitz, D. Moodie, L. Pavlovic, L. Ponnampalam, C. Renaud, D. Rogers, V. Rymanov, A. Seeds, A. Steffan, A. Umbach, and M. Weiss, "Millimeter-wave photonic components for broadband wireless systems," *IEEE Trans. Microw. Theory Tech.*, vol. 58, no. 11, pp. 3071-3082, 2010.
- [12] J. Capmany and D. Novak, "Microwave photonics combines two worlds," *Nature Photon.*, vol. 1, no. 6, pp. 319-332, 2007.
- [13] L. Kazovsky, W.-T. Shaw, D. Gutierrez, N. Cheng, and S.-W. Wong, "Next-generation optical access networks," *J. Lightw. Technol.*, vol. 25, no. 11, pp. 3428-3442, 2007.
- [14] S. Iezekiel, *Microwave photonics: devices and applications*. John Wiley & Sons, New York, 2004.

- [15] A. Caballero, D. Zibar, R. Sambaraju, J. Martí, and I. T. Monroy, "High-Capacity 60 GHz and 75–110 GHz Band Links Employing All-Optical OFDM Generation and Digital Coherent Detection," *J. Lighw. Technol.*, vol. 30, no. 1, pp. 147-155, 2012.
- [16] C. E. Shannon, "A mathematical theory of communication," *Bell System Technical Journal*, vol. 27, pp. 379-423; pp. 623-656, 1948.
- [17] H. Li and K. Iga, *Vertical-Cavity Surface-Emitting Laser Devices*. (Springer, 2003).
- [18] W. Hofmann, M. Müller, P. Wolf, A. Mutig, T. Gründl, G. Böhm, D. Bimberg, M.-C. Amann, "40 Gbit/s modulation of 1550 nm VCSEL," *Electron. Lett.*, vol. 47, no. 4, pp. 270–271, 2011.
- [19] D. K. Mynbaev, L. L. Scheiner, *Fiber-Optic Communications Technology*. Prentice Hall, 2000.
- [20] I. Garcés, A. Villafranca, and J. Lasobras, "Characterization of the chirp behavior of integrated laser modulators (ILM) by measurements of its optical spectrum," in *Proc. SPIE 6997 69971S-2*.
- [21] G. P. Agrawal, *Lightwave technology: communication systems*. Wiley, 2005.
- [22] Mario Weiß, "60 GHz photonic millimeter-wave communication systems", Ph.D. dissertation, University of Duisburg-Essen, (2010).
- [23] G. Hilt, "Optical transmission and upconversion of microwave signals in radio-over-fiber telecommunication Systems," Ph.D. dissertation, Grenoble Institute of Technology, (1999).
- [24] X. Pang, A. Caballero, A. Dogadaev, V. Arlunno, L. Deng, R. Borkowski, J.S. Pedersen, D. Zibar, X. Yu, and I. Tafur Monroy, "25 Gbit/s QPSK Hybrid Fiber-Wireless Transmission in the W-Band (75–110 GHz) With Remote Antenna Unit for In-Building Wireless Networks," *IEEE Photon. J.*, vol. 4, no. 3, pp. 691-698, 2012.
- [25] I. G. Insua, "Optical generation of mm-wave signals for use in broadband radio over fiber systems," Ph.D. dissertation, Dresden University of Technology, (2010).
- [26] G. Qi, J. Yao, J. Seregelyi, and S. Paquet, "Phase-noise analysis of optically generated millimeter-wave signals with external optical modulation techniques", *J. Lighw. Technol.*, vol. 24, no. 12, pp. 4861–4875, 2006.
- [27] J. J. O'Reilly, P. M. Lane, R. Heidemann, and R. Hofstetter, "Optical generation of very narrow linewidth millimeter wave signals," *Electron. Lett.*, vol. 28, no. 25, pp. 2309–2311, 1992.
- [28] A. Bordonalli, C. Walton and A. Seeds, "High-performance phase locking of wide linewidth semiconductor lasers by combined use of optical injection locking and optical phase-lock loop", *J. Lighw. Technol.*, vol. 17, no.2, pp. 328-342, 1999.
- [29] C. Schaffer, F. H. Lubeck, R.-P. Braun, G. Grosskopf, F. Schmidt, M. Rohde, "Microwave multichannel system with a sideband injection locking scheme in the 60 GHz-band", in *Proceedings of International Topical Meeting on Microwave Photonics (MWP)*, paper P5, 1998.
- [30] M. Sieben, J. Conradi, and D. E. Dodds, "Optical single sideband transmission at 10 Gb/s using only electrical dispersion compensation," *J. Lighw. Technol.*, vol. 17, no. 10, pp. 1742–1749, 1999.

- [31] P.-T. Shih, C.-T. Lin, W.-J. Jiang, J. Chen, H.-S. Huang, Y.-H. Chen, P.-C. Peng, and S. Chi, "WDM up-conversion employing frequency quadrupling in optical modulator," *Opt. Express*, vol. 17, no. 3, pp. 1726-1733, 2009.
- [32] X. Pang, M. Beltrán, J. Sánchez, E. Pellicer, J.J. Vegas Olmos, R. Llorente, and I. Tafur Monroy, "DWDM Fiber-Wireless Access System with Centralized Optical Frequency Comb-based RF Carrier Generation," in *Proc. of Conference on Optical Fiber Communication, collocated with National Fiber Optic Engineers Conference*, (Optical Society of America, 2013), paper JTh2A.56.
- [33] Skyworks application note, "Mixer and detector diodes," (Skyworks, 2008).
- [34] S. B. Alexander, *Optical Communication Receiver Design*, (SPIE, 1997), Chapter 7.
- [35] H. Schmuck, "Comparison of optical millimetre-wave system concepts with regard to chromatic Dispersion," *Electron. Lett.*, vol. 32, no. 21, pp. 1848-1849, 1995.
- [36] U. Gliese, S. Norskov, and T.N. Nielsen, "Chromatic dispersion in fiber-optic microwave and millimeter wave links," *IEEE Trans. Microw. Theory*, vol. 44, no. 10, pp. 1716-1724, 1996.
- [37] A. Stohr, K. Kitayama, and T. Kuri, "Fiber-length extension in an optical 60-GHz transmission system using an EA-modulator with negative chirp," *IEEE Photon. Technol. Lett.*, vol. 11, no. 6, pp. 739-741, 1999.
- [38] H. Sun, M. C. Cardakli, K.-M. Feng, J.-X. Cai, H. Long, M.I. Hayee, and A.E. Willner, "Tunable RF-power fading compensation of multiple-channel double-sideband SCM transmission using a nonlinearly chirped FBG," *IEEE Photon. Technol. Lett.*, vol. 12, no. 5, pp. 546-548, 2000.
- [39] B. Hraimel, Zh. Xiupu, M. Mohamed, and W. Ke, "Precompensated Optical Double-Sideband Subcarrier Modulation Immune to Fiber Chromatic-Dispersion-Induced Radio Frequency Power Fading," *J. Opt. Commun. Netw.*, vol. 1, no. 4, pp. 331-342, 2009.
- [40] H. Sotobayashi, and K. Kitayama, "Cancellation of the signal fading for 60 GHz subcarrier multiplexed optical DSB signal transmission in nondispersion shifted fiber using midway optical phase conjugation," *J. Lighw. Technol.*, vol. 17, no. 12, pp. 2488-2497, 1999.
- [41] J. Ma, J. Yu, C. Yu, X. Xin, J. Zeng, and L. Chen, "Fiber Dispersion Influence on Transmission of the Optical Millimeter-Waves Generated Using LN-MZM Intensity Modulation," *J. Lightwave Technol.*, vol. 25, no. 11, pp. 3244-3256, 2007.
- [42] C. Lim, K.-L. Lee, A. Nirmalathas, D. Novak, and R. Waterhouse, "Impact of chromatic dispersion on 60 GHz radio-over-fiber transmission," in *Proc. of 21st Annual Meeting of the IEEE Lasers and Electro-Optics Society*, pp. 89-90, paper MJ5, 2008.
- [43] M. Zhou, J. Ma, C. Yu, X. Xin, H. Huang, L. Rao, Y. Zhan, and H. Liang, "Transmission performance of quadruple frequency optical millimeter-wave with single and dual carrier data modulations," in *Proc. of 2011 IEEE 13th International Conference on Communication Technology (ICCT)*, pp. 538-543, 2011.

- [44] C. H. Cox, *Analog Optical Links*. Cambridge University Press, New York, 2004.
- [45] Bridgewave whitepaper, "Gigabit wireless applications using 60 GHz radios," (Bridgewave, 2006).
- [46] Abbie Mathew, "Local Area Networking Using MillimetreWaves," (NewLANs, Inc., USA, 2005).
- [47] AIRLINX Communications, Inc. specification datasheet, "GigaLink® 6221/6421/6451," (AIRLINX Communications, Inc., 2013).
- [48] WirelessHD white paper, "WirelessHD Specification Version 1.1 Overview," (WirelessHD, 2010).
- [49] WiGig white paper, "Defining the future of multi-gigabit wireless communication," (WiGig alliance, July 2010).
- [50] K. Ramachadran, R. Kokku, R. Mahindra, and S. Rangarajan, "60 GHz data-center networking: wireless worry less?" *NEC Technical Report*, 2008.
- [51] S. Kandula, J. Padhye, P. Bahi, "Flyways to de-congest data center networks," *Eighth ACM Workshop on Hot Topics in Networks*, 2009.
- [52] K. Kawasaki, Y. Akiyama, K. Komori, M. Uno, H. Takeuchi, T. Itagaki, Y. Hino, Y. Kawasaki, K. Ito, and A. Hajimiri, "A millimeter-wave intra-connect solution," in *Proc. of IEEE International Solid-State Circuits Conference*, San Francisco, 2010, pp. 414–415.
- [53] Ceragon application note, "Wireless Backhaul Solutions for Small Cells," (Ceragon).
- [54] Sub10 Systems Limited white paper, "60GHz Metro Cell and Small Cell Backhauling for Service Providers," (Sub10 Systems Limited, 2011).
- [55] "IEEE Standard for Information technology - Telecommunications and information exchange between systems - Local and metropolitan area networks - Specific requirements. Part 15.3: Wireless Medium Access Control (MAC) and Physical Layer (PHY) Specifications for High Rate Wireless Personal Area Networks (WPANs) Amendment 2: Millimeter-wave-based Alternative Physical Layer Extension," IEEE Std 802.15.3c-2009 (Amendment to IEEE Std 802.15.3-2003) , pp. 1-187, Oct. 12 2009
- [56] J. Schonhther, "WP3-study "the 60 GHz channel and its modelling". Tech. Report IST-2001-32686 (2003).
- [57] Kao-Cheng Huang, David J. Edwards, Millimeter wave technology in wireless PAN, LAN, and MAN, (Wiley, 2008).
- [58] S.-K. Yong, *60 GHz technology for Gbps WLAN and WPAN: from theory to practice*. Wiley, 2011, Chap. 1.
- [59] S.-Q. Xiao, M.-T. Zhou, Y. Zhang, *Millimetre wave antennas for gigabit wireless communications: a practical guide to design and analysis in a system context*. CRC press, 2008.
- [60] ITU-R P.676-9 Recommendation (2012) Attenuation by atmospheric gases. ITU, Geneva, Switzerland.
- [61] ITU-R P.838-2 Recommendation (2003) Specific attenuation model for rain for use in prediction methods. ITU, Geneva, Switzerland.
- [62] N. Moriatis, and P. Constantinou "Indoor channel measurements and characterization at 60 GHz for wireless local area network applications," *IEEE T. Antenn. Propag.*, vol. 52, no. 12, pp. 3180–3189, 2004.

- [63] H. Radi, M. Fiacco, M. Parks, and S. Saunders, "Simultaneous indoor propagation measurements at 17 and 60 GHz for wireless local area networks," in *Proc. of the IEEE Vehicular Technology Conference*, pp. 510-514, 1998.
- [64] S. Geng, J. Kivinen, X. Zhao, and P. Vainikainen, "Millimeter-Wave Propagation Channel Characterization for Short-Range Wireless Communications," *IEEE T. Veh. Technol.*, vol. 58, no. 1, 2009.
- [65] IEEE 802.15-05-0493-27-003c, 'TG3c Selection Criteria', January 2007.
- [66] F. Zhai, A. K. Katsaggelos, Joint source-channel video transmission, (Morgan and Claypool publishers, 2007).
- [67] I. E. Richardson, The H.264 Advanced Video Compression Standard, (Wiley, 2010)
- [68] T. Stockhammer, M. Hannuksela, and T. Wiegand, "H.264/AVC in Wireless Environments," *IEEE Trans. Circuits Syst. Video Technol*, vol. 13, no. 7, July 2003.
- [69] G. C. Clark and J. B. Cain, Error-correction coding for digital communications. New York: Plenum Press, 1981.
- [70] Vubiq specification datasheet, "60 GHz receiver waveguide module," (Vubiq, 2013).
<http://www.vubiq.com/pdf/Data%20Sheet%20V60RXWG2%20rev1.3.pdf>
- [71] Siversima white paper, "MM-wave converter series for high capacity wireless transfer," (Siversima, 2010). <http://www.siversima.com/wp-content/uploads/2011/10/high-capacity-wireless-transfer-111010.pdf>.
- [72] S. Fedderwitz, C. Leonhardt, J. Honecker, P. Muller, A. Steffan, "A high linear and high power photoreceiver suitable for analog applications," in *Proc. of IEEE Photonics Conference (IPC)*, paper TuL3, pp. 308-309, 2012.
- [73] S. Babel, I. Flammia, A. Stohr, J. Montero-de-Paz, L. E. Garcia-Munoz, D. Segovia-Vargas, G. Carpintero, A. Lisauskas, O. Cojocari, "Compact transmitter and receiver modules for E-band wireless links," in *Proc. of Optical Fiber Communication Conference and Exposition*, paper OW3D.7, 2013.
- [74] Y.-T. Hsueh, C. Liu, S.-H. Fan, J. Yu, G.-K. Chang, "A novel full-duplex testbed demonstration of converged all-band 60-GHz radio-over-fiber access architecture," in *Proc. of Optical Fiber Communication Conference and Exposition (OFC/NFOEC)*, paper OTu2H.5, 2012.
- [75] T. Shao, F. Paresys, Y. Le Guennec, G. Maury, N. Corrao, and B. Cabon, "Simultaneous Transmission of Gigabit Wireline Signal and ECMA 387 mmW over Fiber Using a Single MZM in Multi-Band Modulation," in *Proc. of Microwave Photonics Conference*, pp.149-152, 2011.
- [76] F. Paresys, T. Shao, G. Maury, Y. Le Guennec, and B. Cabon, "Bidirectional Millimeter-Wave Radio-Over-Fiber System Based on Photodiode Mixing and Optical Heterodyning," *J. Opt. Commun. Netw.*, vol. 5, no. 1, pp. 74-80, 2013.
- [77] J. Guillory, F. Richard, P. Guignard, A. Pizzinat, S. Meyer, B. Charbonnier, L. Guillo, C. Algani, H. W. Li, E. Tanguy, "Towards a multiservice & multiformat

- optical Home Area Network," in *Proc. Of 14th ITG Conference on Electronic Media Technology (CEMT)*, 2011, pp. 1-6, 2011.
- [78] Y. Shi, M. Morant, C. Okonkwo, R. Llorente, E. Tangdiongga, A. M. J. Koonen, "Multistandard Wireless Transmission Over SSMF and Large-Core POF for Access and In-Home Networks," *IEEE Photon. Technol. Lett.*, vol. 24, no. 9, pp. 736-738, 2012.
- [79] T. P. McKenna, J. A. Nanzer, M. L. Dennis, T. R. Clark, "Fully fiber-remoted 80 GHz wireless communication with multi-subcarrier 16-QAM," in *Proc. of IEEE Photonics Conference (IPC)*, pp. 576-577, paper WS1, 2012.
- [80] J. Guillory, E. Tanguy, A. Pizzinat, B. Charbonnier, S. Meyer, H.-W. Li, C. Algani, "Radio over Fiber tunnel for 60 GHz wireless home network," in *Proceedings of Optical Fiber Communication Conference and Exposition (OFC/NFOEC)*, paper OWT6, 2011.
- [81] S. Babel, A. Perentos, S. Fedderwitz, B. Kunz, S. Iezekiel, A. Stöhr, "100 GHz Band Photonic Wireless System employing Passive RoF Transmitters," in *Proc. of International Symposium on Green Radio over Fibre & All Optical technologies for Wireless Access Networks, GROWAN 2011*, Paper C12, 2011.
- [82] H.-J. Kim, J.-I. Song, "Multi-channel photonic frequency upconverter using a single electro-absorption modulator for generating WDM RoF signals," in *Proc. of MTT-S International Microwave Symposium*, 2011, paper WEPL-2.
- [83] J. Yu, Z. Jia, L. Yi, Y. Su, G.-K. Chang, and T. Wang, "Optical millimeter-wave generation or up-conversion using external modulators", *IEEE Photon. Technol. Lett.*, vol. 18, no. 1, pp. 265-267, 2006.
- [84] K. Kojucharow, M. Sauer, H. Kaluzni, D. Sommer, F. Poegel, W. Nowak, A. Finger, and D. Ferling, "Simultaneous Electrooptical Upconversion, Remote Oscillator Generation, and Air Transmission of Multiple Optical WDM Channels for a 60-GHz High-Capacity Indoor System," *IEEE Trans. Microwave Theor. Tech.*, vol. 47, no. 12, pp. 2249-2256, 1999.
- [85] A. Nirmalathas, C. Lim, D. Novak, D. Castleford, R. Waterhouse, & G. Smith, "Millimeter-wave fiber-wireless access systems incorporating wavelength division multiplexing", in *Proc. of Asia-Pacific Microwave Conference*, pp. 625-629, 2000.
- [86] F. Poegel, S. Zeisberg, A. Finger, "Comparison of different coding schemes for high bit rate OFDM in a 60 GHz environment," in *Proc. of 4th International Symposium on Spread Spectrum Techniques and Applications*, pp. 122-125, 1996.
- [87] M. Marinkovic, M. Piz, C.-S. Choi, G. Panic, M. Ehrig, E. Grass, "Performance evaluation of channel coding for Gbps 60-GHz OFDM-based wireless communications," in *Proc. of IEEE 21st International Symposium on Personal Indoor and Mobile Radio Communications (PIMRC)*, pp. 994-998, 2010.
- [88] B. Gao, Z. Xiao, C. Zhang, L. Su, D. Jin, L. Zeng, "Performance comparison of channel coding for 60GHz SC-PHY and a multigigabit Viterbi decoder," in *Proc. of International Conference on Computational Problem-Solving (ICCP)*, pp. 714-718, 2011.
- [89] A. Chowdhury, H.-C. Chien, Y.-T. Hsueh, G.-K. Chang, "Advanced system technologies and field demonstration for in-building optical-wireless

- network with integrated broadband services," *J. Lightw. Technol.*, vol.27, no.12, pp. 1920-1927, 2009.
- [90] Z. Tang, S. Pan, "Transmission of 3-Gb/s uncompressed HD video in a optoelectronic-oscillator-based radio over fiber link," in *Proc. of IEEE 13th Topical Meeting on Silicon Monolithic Integrated Circuits in RF Systems (SiRF)*, Austin, TX, 2013, pp. 219-221.
 - [91] J. Guillory, A. Pizzinat, P. Guignard, F. Richard, B. Charbonnier, P. Chanclou, C. .Algani, "Simultaneous implementation of Gigabit Ethernet, RF TV and radio mm-wave in a multiformat Home Area Network," in *Proc. ECOC*, Geneve, 2011, paper We.7.C.3.
 - [92] T. T. Pham, "Data transmission techniques for short-range optical fiber and wireless communication links," Ph.D. dissertation, Technical University of Denmark, (2013).
 - [93] S. Singh, F. Ziliotto, U. Madhow, E. M. Belding and M. Rodwell, "Blockage and Directivity in 60 GHz Wireless Personal Area Networks: From Cross-Layer Model to Multihop MAC Design," *IEEE Journal on Selected Areas in Communication*, vol. 27, no. 8, 2009.
 - [94] P. Smulders, "Exploiting the 60 GHz Band for Local Wireless Multimedia Access: Prospects and Future Directions," *IEEE Communications Magazine*, vol. 40, no. 1, pp. 140-147, 2002.

[Paper 1]

Alexander Lebedev, Tien-Thang Pham, Marta Beltrán, Xianbin Yu, Anna Ukhanova, Roberto Llorente, Idelfonso Tafur Monroy, "Optimization of high-definition video coding and hybrid fiber-wireless transmission in the 60 GHz band," *Opt. Express.*, vol. 19, no. 26, pp. 895-904, 2011.

Optimization of high-definition video coding and hybrid fiber-wireless transmission in the 60 GHz band

Alexander Lebedev,^{1,2} Tien Thang Pham,¹ Marta Beltrán,² Xianbin Yu,¹
Anna Ukhanova,¹ Roberto Llorente,² Idelfonso Tafur Monroy,¹
and Søren Forchhammer¹

¹DTU Fotonik, Department of Photonics Engineering, Technical University of Denmark, 2800 Kgs. Lyngby, Denmark

²Valencia Nanophotonics Technology Center, Universidad Politécnica de Valencia, Camino de Vera s/n, 46022 Valencia, Spain

*alele@fotonik.dtu.dk

Abstract: The paper addresses the problem of distribution of high-definition video over fiber-wireless networks. The physical layer architecture with the low complexity envelope detection solution is investigated. We present both experimental studies and simulation of high quality high-definition compressed video transmission over 60 GHz fiber-wireless link. Using advanced video coding we satisfy low complexity and low delay constraints, meanwhile preserving the superb video quality after significantly extended wireless distance.

© 2011 Optical Society of America

OCIS codes: (060.2330) Fiber optics communications; (060.5625) Radio frequency photonics.

References and links

1. M. Beltrán, J. B. Jensen, X. Yu, R. Llorente, and I. T. Monroy, "Experimental performance comparison of 60 GHz DCM OFDM and impulse BPSK ultra-wideband with combined optical fibre and wireless transmission," in ECOC, 1465–1467 (2010).
2. Z. Jia, H.-C. Chien, Y.-T. Hsueh, A. Chowdhury, J. Yu, and G.-K. Chang, "Wireless HD services over optical access systems: Transmission, networking, and demonstration," in OFC, 1–5 (2009).
3. M. Weiß, "60 GHz photonic millimeter-wave communication systems," thesis (2010).
4. A. Belogolov, E. Belyaev, A. Sergeev, and A. Turlikov, "Video compression for wireless transmission: reducing the power consumption of the WPAN hi-speed systems," NEW2AN/ruSMART 2009, LNCS 5764, 313–322 (2009).
5. <http://iphone.hhi.de/suehring/tml/>.
6. T. Stockhammer, M. M. Hannuksela, and T. Wiegand, "H.264/AVC in wireless environments," IEEE Trans. Circuits Syst. Video Technol. **13**(7), 657–673 (2003).
7. I. E. Richardson, *The H.264 Advanced Video Compression Standard* (Wiley, 2010).
8. <http://www.vpiphotonics.com/>.
9. S.-K. Yong, *60 GHz Technology for Gbps WLAN and WPAN: From Theory to Practice* (Wiley, 2011), Chap. 2.
10. S. K. Yong and C.-C. Chong, "An overview of multigigabit wireless through millimeter wave technology: potentials and technical challenges," EURASIP J. Wireless Commun. Netw. **2007**(1), 078907 (2007).
11. K.-C. Huang and D. J. Edwards, *Millimetre Wave Antennas for Gigabit Wireless Communications: A Practical Guide to Design and Analysis in a System Context* (Wiley, 2008).

1. Introduction

The motivations for this work are three-fold. First, the unprecedented frequency range around 60 GHz (from 4 to 9 GHz within 57–66 GHz) has been regulated for unlicensed use in a number of countries around the world. Second motivation is the introduction of high quality video services such as high-definition (HD) video conferencing and distributed video gaming. These services define both the demand for increased data rates in the access networks and need for optimization of video compression schemes. Third, efficient convergence of wired and wireless technologies is required to enable the concept of "anytime anywhere" wireless

connectivity. Radio-over-fiber (RoF) is considered a promising example of such integration for optical networks [1].

Previous research in the area of 60 GHz RoF video transmission suggests the use of uncompressed video [2,3]. The main drawback of this approach is reduced flexibility in terms of bitrate: bitrates are fixed depending on resolution, number of bits per pixel, and frame rate of the video sequence. This therefore results in extremely complex adaptation of the HD video system to significant signal-to-noise ratio (SNR) drops caused by either severe shadowing in non-line-of-sight (NLOS) case or extremely high attenuation – problems that are typical for 60 GHz systems.

Source coding (compression) gives us desirable flexibility of bitrate but at the expense of introducing delay and increase of power consumption. However, there is a trade-off between the power needed to radiate larger bandwidth for uncompressed video and the power consumed for the computations of an encoder and a decoder for compressed video transmission. According to [4], low complexity compression can, in fact, bring about reduction in power consumption for a 60 GHz wireless video transmission system compared to the uncompressed case, while at the same time keeping delay under the acceptable limit.

In this work we explore the notion of joint optimization of physical layer parameters of a RoF link (power levels, distance) and the codec parameters (quantization, error-resilience tools) based on peak signal-to-noise ratio (PSNR) as an objective video quality metric. We experimentally demonstrate, first time to our knowledge, the combined optical access and wireless transmission of compressed HD video in the 60 GHz band employing simple envelope detection technique.

2. Experimental setup

The experimental setup of the 60 GHz optical-wireless RoF system is shown in Fig. 1. The binary sequence corresponding to compressed video file was uploaded in an arbitrary waveform generator (AWG). The non-return-to-zero (NRZ) electrical signal on the output of the AWG directly modulated a 1550 nm laser. After the baseband data modulation, frequency up-conversion to the 60 GHz band was performed by driving a Mach-Zehnder modulator (MZM) biased at the minimum transmission point with a 30 GHz sinusoidal signal. A polarization controller (PC) was used before the MZM to minimize its polarization-dependant losses. After the MZM, two sidebands with a frequency spacing of $2f_{LO}$ were generated according to the double sideband-suppressed carrier (DSB-SC) intensity modulation scheme (see Fig. 2). Optical carrier suppression of approximately 13.6 dB is achieved limited by the MZM extinction ratio. The generated sidebands have the same optical power and the locked phase. Subsequently, an Erbium doped fiber amplifier (EDFA) is employed to compensate the losses, and an optical band pass filter (OBPF) is used afterwards to mitigate the amplified spontaneous emission (ASE) noise produced by the EDFA. Then the signal is launched into a 20 km span of non-zero dispersion shifted fiber (NZDSF). We employ the NZDSF in order to minimize dispersion induced impairments. A variable optical attenuator (VOA) is employed to control the optical power impinging the photodiode (PD) in order to evaluate BER performance of the system as a function of the received optical power.

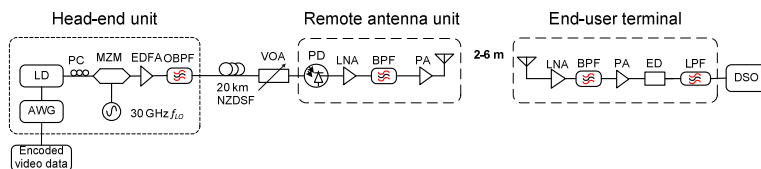


Fig. 1. Experimental 60 GHz optical-wireless RoF system with envelope detection, LD-laser diode, PC-polarization controller, MZM-Mach-Zehnder modulator, LO-local oscillator, EDFA-Erbium doped fiber amplifier, OBPF-optical band pass filter, PD-photodiode, LNA-low noise amplifier, BPF-band pass filter, ED- envelope detector, LPF-low pass filter, DSO-digital sampling oscilloscope.

After photodetection the 60 GHz signal was amplified (gain of amplifiers – 16 dB and 28.7 dB) and filtered (58.1-61.9 GHz) before feeding it to an antenna for up to 6 meters of wireless transmission. After receiving the signal with an antenna and following filtering (58.1-61.9 GHz) and amplification (gain of amplifiers – 16 dB and 28.7 dB) envelope detection was employed for down-conversion. The detected envelope is low-pass filtered and digitized by a digital sampling oscilloscope (DSO). Both the transmitting and receiving antennas used throughout the experiment are commercially available horn antennas with 20 dBi gain and 12° beam width. Bitrates that were transmitted over the fiber are low compared to similar research setups. This explains a good performance to a certain extent, but we emphasize that reduction of bitrate does not lead to a significant video quality deterioration.

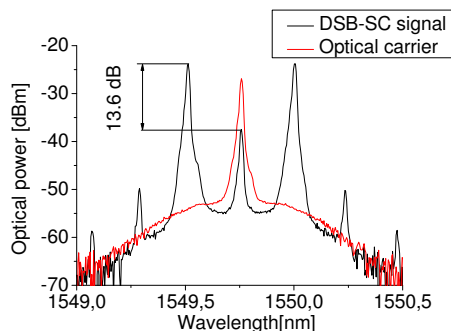


Fig. 2. Optical spectra on the input of the PD.

The encoding was performed using the Joint Model (JM) 17.0 reference software implementation of the H.264/Advanced Video Codec (AVC) [5]. It is a realistic scenario since H.264/AVC is one of the latest industrial video coding standards covering a wide range of applications, including, coding for transmission over wireless links and HDTV coding [6]. An Intra coding mode only and a frame slicing mechanism were employed to achieve the low delay requirement. Both mechanisms are improving the error-resilience as well [7]. Slicing was performed with the use of flexible macroblock ordering (FMO).

H.264 is not capable of coping with single-bit errors: its mechanisms of error-resilience on the encoding side and error concealment on the decoding side are adjusted to cope with packet loss when the packets affected by the errors are discarded such as usually occurs in networks. Packet error rate (PER) depends on the bit error rate (BER) and the size of the packet; in general, the noisier the transmission the shorter the length of the packet is desirable. Initially in the experiment we used the packet size equal to 2500 bytes, each packet containing a slice of the frame; afterwards we have been using packets of length of 3000 and 3500 bytes for

simulation. The uncompressed HD test video sequence ‘blue sky’ was used for encoding and transmission. The sequence was originally shot in 4:2:0 format 8 bits per color 1920×1080 pixels. However, in order to model the most bitrate demanding case upsampling to 4:4:4 format was performed (uncompressed bitrate – 3 Gbps for the frame rate of 60 frames per second).

We use PSNR as an objective quality metric for video, which is defined as:

$$MSE = \frac{1}{N} \sum_{i=1}^N (x_i - y_i)^2, \quad (1)$$

$$PSNR = 10 \log_{10} \left(\frac{L^2}{MSE} \right), \quad (2)$$

where MSE stands for mean squared error, N is the number of pixels in the image or video signal, and x_i and y_i are the i-th pixel values in the original and the distorted signals, respectively. L is the dynamic range of the pixel values. For an 8 bits/pixel signal, L is equal to 255. PSNR is evaluated for the luminance component of the transmitted video signal.

3. Composite fiber-wireless channel modeling for 60 GHz band

The difficulty of the modeling arises from the fact that we need to account for both the impairments induced by the wireless and the fiber-optic channels. We performed the modeling of the fiber-optic channel with VPI software [8]. The wireless channel model was implemented in Matlab and combined with VPI channel model afterwards. We combine below the description of the channel model with the excerpts from experimental measurements that allow us to simplify the model.

Noise processes in the optical part of the setup (such as amplified spontaneous emission (ASE) noise, Johnson noise, shot noise at the photodiode), attenuation and dispersion in the fiber are simulated in VPI software. We set the numerical values for these parameters according to the specifications of equipment we used in the experimental setup.

We performed the modeling of the wireless channel according to the physical parameters of the devices that have been used in the scheme and references on theoretical parameters taken from [9–11].

The path loss (attenuation) at 60 GHz is much more severe than the path loss at the frequencies that are currently employed for Wireless Personal Area Networks (WPAN). Theoretical description for this phenomenon is provided by Friis formula [9], according to which attenuation in the air is proportional to the frequency squared. It is known that the line-of-sight (LOS) attenuation of the 60 GHz wireless channel can be modeled with a log-normal model [11]. Parameters for this model have been defined through the extensive measurements presented in a number of publications. Summary on the parameters for different experimental environments can be found in [9]. We perform the modeling of the system without taking into account frequency dependency of the path loss. To the best of our knowledge, frequency dependent models for 60 GHz system have not yet been reported.

Influence of the noise on the signal can be modeled with the following formula [10,11]:

$$SNR = P_{tx} + G_T + G_R + G_{LNA_{tx} + PA_{tx}} + G_{LNA_{rx} + PA_{rx}} - PL - (10 \log_{10} (KTB) + NF_{LNA_{tx} + PA_{tx}} + NF_{LNA_{rx} + PA_{rx}}), \quad (3)$$

$$PL = PL(d_0) + 10n \log_{10} \left(\frac{d}{d_0} \right), \quad (4)$$

where P_{tx} in our case is the RF power on the output of the PD, G_T and G_R are the gain of transmitting and receiving antennas respectively, $G_{LNA_{tx} + PA_{tx}}$ and $G_{LNA_{rx} + PA_{rx}}$ are gains of

amplification cascades at transmitting and receiving parts of the scheme respectively, PL is the distance-dependent path loss (attenuation) in the air. The terms in brackets represent noise contributions. The first term represents the Johnson noise, second and third represents noise contributions from amplifiers. Parameters d_0 and d in Eq. (4) represent the reference distance (we used 1 m according to [9]) and the distance between a transmitter and a receiver respectively, n denotes path loss exponent.

The formula does not account for shadowing caused by LOS obstruction, but this resembles the experimental setting where we were working with the LOS scenario only.

Phase noise modeling for the channel was excluded after the experimental examination of the phase noise of the oscillator presented in Fig. 3. Figure 3 shows the high quality of the electrical oscillator for 3 cases: measuring the phase noise of LO, setup without fiber transmission up to a transmitting antenna (optical back-to-back) and after 20 km of NZDSF. Figure 3 also illustrates the fact that contribution from the system to the phase noise is insignificant. Moreover, it could be excluded from consideration, because after wireless transmission we finally recover with ED only the amplitude of the signal, and therefore discard information about phase or frequency.

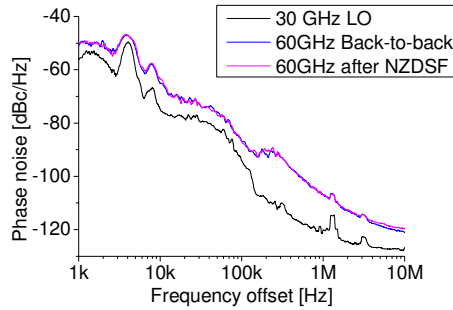


Fig. 3. Phase noise of RF subcarriers.

The model does not take into account the nonlinear effects that are reported for Power Amplifiers in [9]. Nevertheless we regard the model as feasible since the power after the PD is low, so we work in the linear region. Indeed, the power on the output of the PA at the transmitting side given the power at the photodiode of -10 dBm is around -6 dBm. Typically nonlinear effects are observed in the region above 0 dBm [9]. The RF-spectrum measured is depicted in Fig. 4. We refer to the power before the antenna, as the power before radiation P_{br} . Therefore the equation for wireless channel simulation based on Eq. (3) and Eq. (4) could be transformed into:

$$SNR = P_{br} + G_T + G_R + G_{LNA_{rx} + PA_{rx}} - PL(d_0) - 10n \log_{10} \left(\frac{d}{d_0} \right) - (10 \log_{10}(KTB) + NF_{LNA_{rx} + PA_{rx}} + NF_{LNA_{tx} + PA_{tx}}). \quad (5)$$

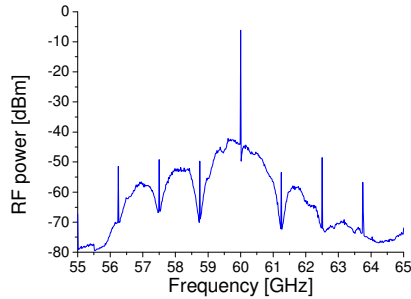


Fig. 4. RF spectrum measured before the antenna.

Typical parameters for the path loss at the reference distance and the path-loss exponent has been found in the references [9,10]. Values for the parameters that are used in modeling of the wireless channel are listed in the Table 1 below.

Table 1. System Parameters for Modeling

Parameter	Numerical value
Center frequency, GHz	60
Joint noise figure Tx amplifiers (LNA + PA), dB	$(6 + 7) = 13$
Joint noise figure Rx amplifiers (LNA + PA), dB	$(6 + 7) = 13$
Joint gain of Tx amplifiers (PA + LNA), dB	$(28.7 + 16) = 44.7$
Joint gain of Rx amplifiers (PA + LNA), dB	$(28.7 + 16) = 44.7$
Gain of the Tx antenna, dBi	20
Gain of the Rx antenna, dBi	20
Bit rate, Mbps	312.5/1250
Distance, m	2-6
Reference path loss at 1 meter, dB	57.5
Path loss exponent	1.77
Ambient temperature for Johnson noise modeling, K	298

We perform attenuation of the signal and addition of the Additive White Gaussian Noise (AWGN) in VPI, the noise power and attenuation to achieve SNR described in Eq. (5) are calculated in Matlab.

4. Results and discussion

Our goal for optimization is to achieve the best video delivery quality for a given link budget. With regards to the role of the quantization of transform coefficients of the coded video in the optimization, roughly speaking, the smaller the quantization parameter size, the smaller the source distortion (loss due to compression), but the larger the channel distortion it may cause. In the experiment we explored two cases. First, the chosen test video sequence ('blue sky' 4:4:4) was encoded with bitrate of 312.5 Mbps. Second, the tested video sequence was encoded in a high quality setting with the quantization parameter equal to 1, which gave us a compression ratio of 3.

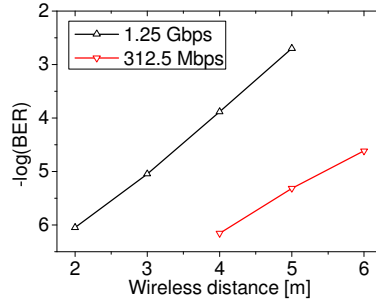


Fig. 5. BER as a function of the wireless distance.

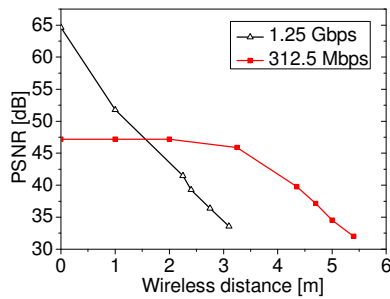


Fig. 6. PSNR as a function of the wireless distance.

On the Fig. 5 BER at the power level at the photodiode equal to -10 dBm as a function of the wireless distance is depicted. From the Fig. 5 we can see that in general the distortion induced by the wireless channel is severe in our system, but video coded with the use of higher quantization parameter has greater dynamic range of wireless distance, as shown in Fig. 6. The distance equal to 0 corresponds to the distortion introduced by the compression only. When we increase the wireless distance, in the beginning, the source distortion is dominant, and the use of lower quantization parameter is reasonable. Anyhow, we lose the advantage of lower distortion after around 2 m of transmission when video is evaluated based on the PSNR metric only. This shows the potential of optimization of the power budget of the system under the constraint of video quality. We obtain similar curves for changing optical power level at the photodiode at 5 m of wireless distance, as shown in Fig. 7 and Fig. 8. With the higher video compression we can work at lower optical power levels. At the same time, we should note that the video quality is high in both cases, and deterioration induced by the compression itself can be regarded as non-significant (PSNR of the video unimpaired by the channel is higher than 45 dB in both cases).

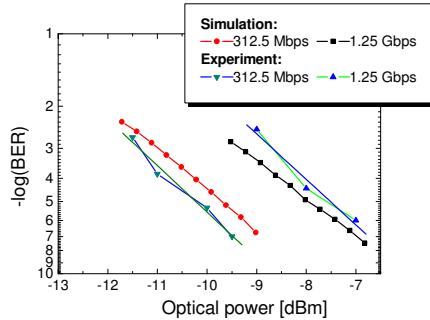


Fig. 7. BER as a function of the optical power at the photodiode.

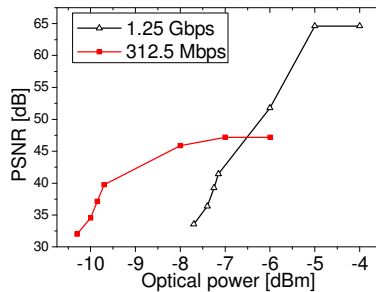


Fig. 8. PSNR as a function of the optical power at the photodiode.

Curves provided by simulation for 5 meters distance and dynamically changing optical power levels show close resemblance that verifies the correctness of the simplified wireless channel model employed. We do not provide simulation-based curves for PSNR, because our simulation is based on the analytical estimation of BERs with the use of VPI software, and we therefore do not have traces including erroneous bits to analyze video performance.

5. Video coding for 60 GHz radio-over-fiber

We employed video coding parameters in a simplified setting that is suitable for both conferencing applications and distributed video gaming. The main constraints for such type of an application are delay and energy consumption. As a part of simplified setting we were using Universal Variable Length Coding (UVLC) for entropy coding that is considered a lower complexity solution [7]. All coding experiments were performed in intra mode thus eliminating the need for long buffering time, and satisfying low delay requirement. The simulation below was performed with bit traces including erroneous bits.

H.264/AVC encoder employs the number of error-resilience tools: slicing of the frame, data partitioning, arbitrary slice ordering, and redundant coded slices [7]. Below we present simulation on two major tools providing error resilience: slices and Flexible Macroblock Ordering (FMO). On the decoder side, there are two error concealment tools used in JM 17.0 reference software implementation of H.264/AVC codec, one exploiting spatial information only, suitable for intra frames (the one used in the experiment and simulation), and one

exploiting temporal information. Details on the error concealment algorithms used can be found in [5].

First we performed the simulation with a different size of the packet (each containing one slice of the frame). Employing the smaller slices enables us to receive acceptable video quality in the regions with higher BER, and therefore extends distance for acceptable quality of video transmission. Indeed, enabling packets of shorter length reduces the amount of information lost when the packet is discarded, enabling decoder to reconstruct impaired parts of the picture better from unimpaired blocks of neighboring pixels. The simulation results are illustrated on Fig. 9.

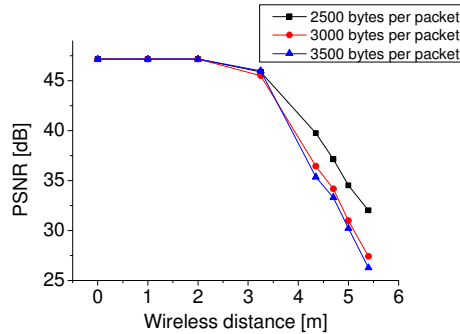


Fig. 9. PSNR as a function of the wireless distance for different packet sizes of the encoded video for the bitrate of 312.5 Mbps.

Below we also present the simulation results for enabling FMO in H.264 reference software [5]. H.264/AVC is the first standard defining this error-resilience tool [7]. In case if we do not use FMO, the images will be composed of a single slice groups with the macroblocks in a scan order. If we employ this algorithm, then when we lose a slice of the video frame, we can make better approximation with the neighboring blocks and therefore, presumably, can achieve gain in PSNR. Results of the simulation for the packet size of 3000 bytes are depicted in the Fig. 10. FMO shows up to 3 dB improvement of PSNR.

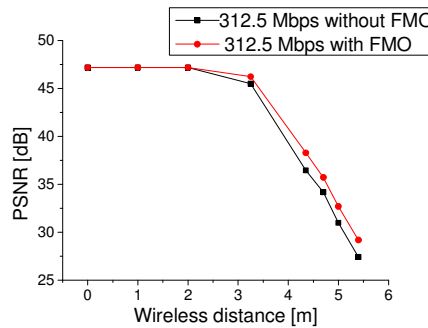


Fig. 10. PSNR performance as a function of the wireless distance for FMO effect estimation.

Coding simulations show the effect of employed source coding error-resilience mechanisms for a particular simplified setting of H.264/AVC and 60 GHz RoF setup as an example of physical layer architecture suitable for transmission high quality HD video

content. Employed tools of H.264/AVC show the greater robustness of video provided by advanced video coding against impairments induced by 60 GHz fiber-wireless channel.

6. Conclusions

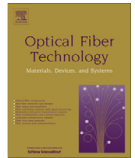
Our experiment and simulation demonstrates the trade-off between the distortion introduced by the source (lossy compression) and distortion introduced by channel for high quality HD video transmission over 60 GHz RoF fiber-wireless links. We have achieved significant extension of wireless distance employing low complexity physical layer solution for detection of RF modulated signal. Our work demonstrates the solutions for improving robustness and reach of simplified converged fiber-wireless RoF communication links provided by advanced video coding.

Acknowledgments

This work has been partly funded by the European Commission under FP7 ICT-249142 FIVER project and by the by the Spanish Ministry of Science and Innovation under the TEC2009-14250 ULTRADEF project.

[Paper 2]

Tien-Thang Pham, **Alexander Lebedev**, Marta Beltran, Xianbin Yu, Roberto Llorente, and Idelfonso Tafur Monroy "Combined Single-mode/Multimode Fiber Link supporting Simplified In-building 60-GHz Gigabit Wireless Access," *Opt. Fiber Technol.*, vol. 18, no. 4, pp. 226-229, 2012.



Combined single-mode/multimode fiber link supporting simplified in-building 60-GHz gigabit wireless access

Tien-Thang Pham^{a,*}, Alexander Lebedev^a, Marta Beltrán^b, Xianbin Yu^a, Roberto Llorente^b, Idefonso Tafur Monroy^a

^a DTU Fotonik-Department of Photonics Engineering, Technical University of Denmark, 2800 Kgs. Lyngby, Denmark

^b Valencia Nanophotonics Technology Center, Universidad Politécnica de Valencia, Camino de Vera s/n, 46022 Valencia, Spain

ARTICLE INFO

Article history:

Received 20 January 2012

Revised 4 May 2012

Available online 2 July 2012

Keywords:

Millimeter wave (MMW)

Wireless personal area network (WPAN)

Multimode fiber (MMF)

Optical fiber communication

Radio over fiber (RoF)

ABSTRACT

In this paper, we propose and experimentally demonstrate a simple, cost-effective hybrid gigabit fiber-wireless system for in-building wireless access. Simplicity and cost-effectiveness are achieved in all parts of the system by utilizing direct laser modulation, optical frequency up-conversion, combined single mode/multimode fiber transmission and envelope detection. Error-free transmission of 2-Gbps data in 60-GHz band over a composite channel including 10-km standard single-mode fiber (SSMF)/1-km multimode fiber (MMF) and 6.5-m air transmission was successfully achieved.

© 2012 Elsevier Inc. All rights reserved.

1. Introduction

Millimeter wave (MMW) wireless communication is receiving increased research interests. It is aimed at exploring its potential of broadband wireless data transmission in future wireless personal area networks (WPANs), to support bandwidth-hungry services such as high-definition television (HDTV), 3D gaming and high-speed data access. Additionally, the 60-GHz band has been standardized for future WPAN networks by several working groups such as Ecma International - an European association for standardizing information and communication systems, WirelessHD and IEEE 802.15.3c [1–3]. In order to commercialize 60-GHz systems for next-generation high-speed wireless networks, it is highly desirable to develop a system with less complexity and low power consumption transceivers as a large number of remote antenna units (RAUs) and user terminals are to be deployed in such networks. Due to the high atmospheric loss of MMW signals, radio-over-fiber (RoF) technique is generally considered as an attractive solution to extend the reach of MMW wireless networks. In this context, supported by low loss and wide bandwidth transmission of optical fibers, several BSs is connected to one central office (CO) which has centralized functions such as MMW subcarrier generation, data up-conversion, amplification. Several MMW RoF systems have been proposed and demonstrated recently in the literature [4–10].

Regarding the optical fiber plant, standard single-mode fibers (SSMFs) have been widely deployed in optical core/metro/access networks, and well studied in proposed MMW RoF systems [4–10]. On the other hand, multi-mode fibers (MMFs) are predominantly deployed in in-building networks as a backbone for local area networks (LANs) (approximately from 85% to 90%) due to various advantages such as low cost, easy installation and maintenance [11]. Gigabit baseband links over hundred meters of MMF have been deployed [12]. When developing a system to meet the increasing demand for high-bandwidth wireless services, it is greatly encouraged to efficiently utilize this existing infrastructure. Together with SMFs in access networks, the reuse of MMF for distribution of MMW signals through in-building optical networks to WPAN networks will save fiber reinstallation cost. The schematic of such a system is presented in Fig. 1. MMW signal is optically generated at the CO and then distributed to user terminals through a composite channel including SMF, MMF and wireless links. Several experiments on MMF based RoF systems have been reported ([13–15, and references therein]). However, to the best of our knowledge, 60-GHz over MMF system has not been demonstrated yet. The reported highest frequency and data rate so far are 38.8 GHz and 900 Mbps over 100-m MMF [14]. Data transmission over a composite channel has been demonstrated at low bitrate and low RF frequency: 120-Mbps data at 31.14 GHz over 20-km SMF plus 300-m MMF and 3-m wireless link [15]. For future deployment of 60-GHz systems, it is important to evaluate the performance of 60-GHz signal over such composite channel.

* Corresponding author.

E-mail address: ptit@fotonik.dtu.dk (T.-T. Pham).

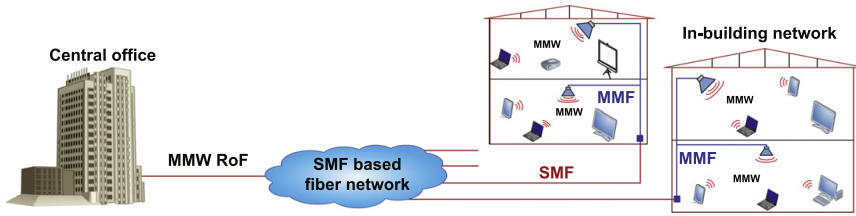


Fig. 1. Distribution of MMW RoF signals over combined SMF and MMF link for in-building broadband wireless access.

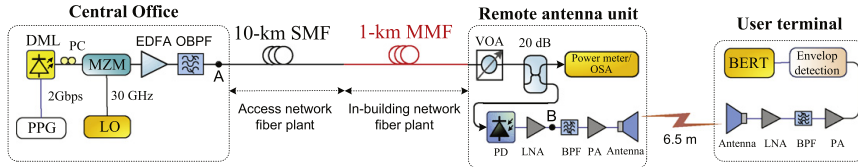


Fig. 2. Experimental setup: PPG: pulse pattern generator, DML: directly-modulated laser, PC: polarization controller, MZM: Mach-Zehnder modulator, EDFA: Erbium doped fiber amplifier, OBPF: optical band-pass filter, VOA: variable optical attenuator, OSA: optical spectrum analyzer, PD: photo-detector, LNA: low-noise amplifier, PA: power amplifier, BPF: band-pass filter, BERT: bit-error-rate tester.

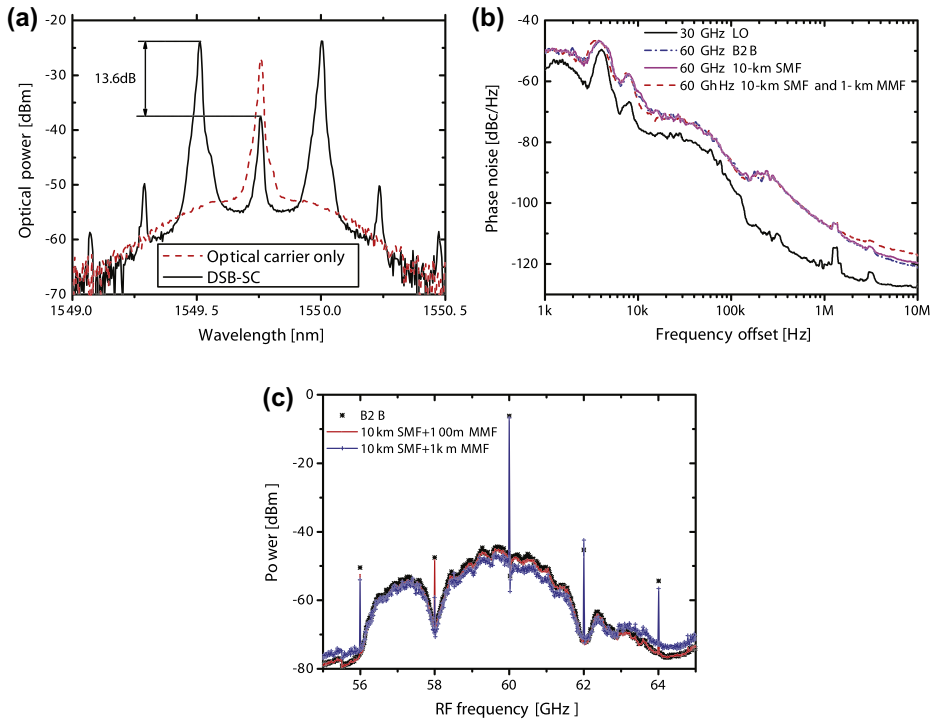


Fig. 3. (a) Optical spectra at point A in Fig. 2, (b) phase noise of RF subcarriers and (c) RF spectra of detected 60-GHz signals with 2-Gbps data at point B in Fig. 2 and -3.0 -dBm received optical power.

In this paper, we report transmission of gigabit data at 60-GHz band with simplified transceivers in end-to-end composite RoF network scenario: access and in-building networks using different types of optical fibers. The link consists of 10-km SMF, 1-km MMF

and 6.5-m wireless. Direct modulation and double-sideband suppressed carrier (DSB-SC) scheme are adopted in the CO to generate 60-GHz subcarrier while simple envelope detection is employed at user terminals. We show that error-free transmission of 2-Gbps

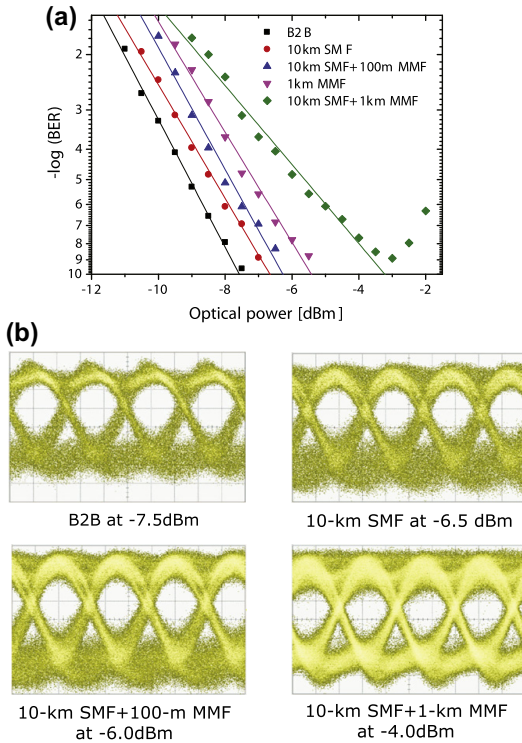


Fig. 4. Measured performance of the system: (a) BER and (b) eye-diagrams (amplitude: 83.5 mV/div and time: 200 ps/div).

data was successfully achieved over the link with less than 4-dB power penalty due to accumulated fiber dispersion.

2. Experimental setup

Fig. 2 illustrates the experimental setup of the in-building wireless access utilizing combined SMF/MMF and simplified wireless transceivers. At the CO, 2-Gbps Pseudo Random Binary Sequence (PRBS) baseband data from a pulse pattern generator (PPG) with a word length of $2^{31}-1$ directly modulated a 1.55- μm laser. To generate a 60-GHz subcarrier, the well-known DSB-SC scheme was utilized. The output from the laser was launched into a Mach-Zehnder modulator (MZM) which was biased at the minimum transmission point and driven by a 30-GHz sinusoid signal from a local oscillator (LO). The output of the MZM was amplified and filtered out amplified spontaneous emission (ASE) noise by an optical band-pass filter (OBPF) with 0.8-nm 3-dB bandwidth. The optical signal was then distributed to a RAU over an optical fiber link composed of 10-km standard SMF and additional 100-m or 1-km MMF. The diameters of core and cladding of the MMF are 50 and 125 μm , respectively. The simple, conventional center-launching technique was used to couple the light from the SMF to the MMF [16]. At the RAU, the optical signal was detected by a broadband 75-GHz photo-detector (PD). The detected 60-GHz signal was amplified and radiated to the air by a horn antenna and received by another one. The wireless link was 6.5 m, which was limited by the available lab space. The received wireless signal was then again amplified and filtered. To simplify the end-user wireless ter-

restrial, electrical envelope detection was employed to down-convert 60-GHz band signal to the baseband. The output signal of the envelope detector was fed to a bit-error-rate tester (BERT) to evaluate the system performance. Both the antennas have 20-dBi gains in 50–75 GHz frequency range and 12 °C beam width. All the amplifiers have 10 GHz bandwidth (55–65 GHz). The power amplifiers (PA) have 28.7-dB gain and 14-dBm P1dB and the low noise amplifiers (LNA) have 16-dB gain. Bandwidth of the BPFs is 5.7 GHz (56.3–62 GHz).

Apart from the utilization of both SMF and MMF plants, this system architecture has some additional important features. Firstly, the use of direct modulation for data and optical frequency up-conversion to MMW band does not require high speed laser. Secondly, the DSB-SC scheme enables the use of low RF frequency LO and avoiding chromatic dispersion induced RF power fading [4–8]. In a wavelength-division multiplexing (WDM) system scenario to support multiple end-users, the MZM can be shared by many WDM channels. Thirdly, envelope detection is a simple demodulation method, which is transparent to RF frequency and does not require any phase-locked LO and mixer for down-conversion. Therefore, in connection with high transmission performance, this scheme is expected to be a very cost-effective solution for broadband 60-GHz in-building wireless networks with the use of simple transceiver, as well as long access reach. Finally, the same RF configuration can be used for uplink to realize a fully cost-effective bidirectional system. The 60-GHz wireless signal from an end-user terminal received by the antenna at the RAU can be down-converted to the baseband using the same envelope detection technique. Then the baseband signal can be transmitted to the BS through the combined MMF/SMF by directly modulating a light source such as a DFB laser or VCSEL.

3. Experimental results and discussion

Fig. 3a shows the optical spectra at the output of the MZM with and without the 30-GHz LO signal. When the LO signal was applied, two first-order sidebands were dominant and the original optical carrier at 1549.75 nm was suppressed approximately 13.6 dB. The influence of optical carrier suppression ratio on the power of the RF signal has been analyzed in [7].

In general, it is important to generate a high quality RF subcarrier to achieve high performance data transmission. The phase noise from the LO does not change the amplitude of a RF signal. However, fiber dispersion such as chromatic dispersion of the SMF, modal dispersion of the MMF causes the phase-to-intensity conversion that, in turn, makes the amplitude of the RF signal vary after fiber transmission. Fig. 3b shows the measured phase noise of the 30-GHz subcarrier from the LO as well as the generated 60-GHz subcarriers at back-to-back (B2B) and after fiber transmission. We can see that the quality of the 60-GHz subcarrier was maintained after fiber transmission due to the correlation of two sidebands [17]. For example, at 100-kHz offset, the phase noise of the 60-GHz subcarrier was only about 5 dB higher than that of the 30-GHz LO. Therefore, we can use a 30-GHz subcarrier from a LO which has similar phase-noise characteristic as the requirement for the 60-GHz subcarrier.

The electrical spectra of the signals at point B in Fig. 2 in cases of B2B and fiber transmission at -3 -dBm optical power are shown in Fig. 3c. The RF spectrum was maintained after 10-km SMF and 100-m MMF. However, there was a slight distortion in the case of 10-km SMF and 1-km MMF due to large modal dispersion of the MMF.

Fig. 4 shows the measured BER curves and eye-diagrams of 2-Gbps data in different transmission cases: B2B, SMF only, MMF only and combined SMF/MMF. The optical power to the PD was controlled by a variable optical attenuator (VOA). We can observe

that chromatic dispersion of 10-km SMF introduced less than 1-dB power penalty. Additional 100-m MMF caused about 0.5-dB power penalty. Suffered from large modal dispersion, the BER performance after 1-km MMF transmission had about 2-dB power penalty. In the case of combined 10-km SMF and 1-km MMF transmission which has both large chromatic dispersion and modal dispersion, the BER curve shows a slightly different slope and the power penalty at a BER of 10^{-9} were approximately 4.3 dB. Additionally, we observed in the experiment that the BER performance rapidly became worse when the received optical power was higher than about -3.0 dBm. That is because the power of the 60-GHz signal was saturated with the RF configuration when high optical power was launched into the PD.

4. Conclusions

We have experimentally demonstrated a gigabit MMW system over a combined-SMF/MMF optical link with simple 60-GHz transceiver based on direct modulation and envelope detection. Error-free transmission was achieved for 2-Gbps data at 60-GHz after 10-km SMF, 1-km MMF and 6.5-m wireless. The experiment proves the feasibility of using SMF in optical access networks in combination with the existing MMF in buildings for distribution of 60-GHz signal direct from a CO to remote in-building antennas enabling a cost-effective solution for next generation gigabit in-building wireless access networks.

Acknowledgments

We would like to thank Thomas Jul from Rohde & Schwarz Denmark A/S for allowing us to use the FSU 67-GHz spectrum analyzer for the experiment.

References

- [1] TC48 – High Rate Wireless Communications, Ecma International. <<http://www.ecma-international.org/memento/TC32-TG20-M.htm>>.
- [2] WirelessHD Consortium. <<http://www.wirelesshd.org>>.
- [3] IEEE 802.15 Working Group for WPAN. <<http://www.ieee802.org/15/>>.
- [4] J. Yu et al., Optical millimeter-wave generation or up-conversion using external modulators, *IEEE Photon. Technol. Lett.* 18 (2006) 265–267.
- [5] Z. Jia et al., Key enabling technologies for optical/wireless networks: optical millimeter-wave generation, wavelength reuse, and architecture, *IEEE/OSA J. Lightw. Technol.* 24 (2006) 1277–1282.
- [6] M.K. Hong et al., Gigabit radio-over-fiber link for converged baseband and millimeter-wave band signal transmission using cascaded injection-locked Fabry–Prot laser diodes, *Opt. Exp.* 17 (2009) 7844–7852.
- [7] M.-K. Hong et al., Gigabit optical access link for simultaneous wired and wireless signal transmission based on dual parallel injection-locked Fabry–Prot laser diodes, *J. Lightw. Technol.* 26 (15) (2008) 2725–2731.
- [8] C. Lim et al., Fiber-wireless networks and subsystem technologies, *IEEE/OSA J. Lightw. Technol.* 28 (2010) 390–405.
- [9] X. Yu et al., Bidirectional radio-over-fiber system with phase-modulation downlink and RF oscillator-free uplink using a reflective SOA, *IEEE Photon. Technol. Lett.* 20 (2008) 2180–2182.
- [10] D. Zibar et al., 16 Gb/s QPSK wireless-over-fibre link in 75–110 GHz band with photonic generation and coherent detection, in: *ECOC2010, Th.9.B.6*, 2010.
- [11] A. Flatman, In-premises optical fiber installed base analysis to 2007, in: *IEEE 802.3 10 GBE over FDDI Grade Fiber Study*, 2004.
- [12] AIEEE 802.15 Working Group for Ethernet. <<http://www.ieee802.org/3/>>.
- [13] A.M.J. Koonen, L.M. Garcia, Radio-over-MMF techniques. Part II: Microwave to millimeter-wave systems, *IEEE/OSA J. Lightw. Technol.* 26 (2008) 2396–2408.
- [14] B.A. Khawaja, M.J. Cryan, Millimetre-wave radio-over-fibre data transmission over multimode fibre, *Microw. Opt. Technol. Lett.* 53 (2011) 254–256.
- [15] A. Nkansah et al., Multilevel modulated signal transmission over serial single-mode and multimode fiber links using vertical-cavity surface-emitting lasers for millimeter-wave wireless communications, *IEEE Trans. Microw. Theory* 55 (2007) 1219–1228.
- [16] D.H. Sim et al., High-speed multimode fiber transmission by using mode-field matched center-launching technique, *IEEE/OSA J. Lightw. Technol.* 27 (2009) 1018–1026.
- [17] X. Yu et al., High carrier suppression double sideband modulation using polarization state rotation filter and optical external modulator, *Opt. Commun.* 267 (2006) 83–87.

[Paper 3]

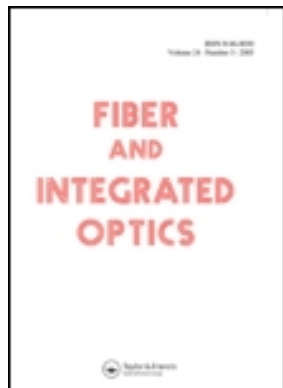
Alexander Lebedev, J. J. Vegas Olmos, Xiaodan Pang, Søren Forchhammer, Idelfonso Tafur Monroy, "Demonstration and Comparison Study for V- and W-band Real-Time HD Video Delivery in Diverse Fiber-Wireless Infrastructure," *Fiber Integr. Opt.*, vol. 32, no. 2, pp. 93-104, 2013.

This article was downloaded by: [DTU Library]

On: 02 September 2013, At: 04:03

Publisher: Taylor & Francis

Informa Ltd Registered in England and Wales Registered Number: 1072954 Registered office: Mortimer House, 37-41 Mortimer Street, London W1T 3JH, UK



Fiber and Integrated Optics

Publication details, including instructions for authors and subscription information:

<http://www.tandfonline.com/loi/ufio20>

Demonstration and Comparison Study for V- and W-Band Real-Time High-Definition Video Delivery in Diverse Fiber-Wireless Infrastructure

Alexander Lebedev^a, J. J. Vegas Olmos^a, Xiaodan Pang^a, Søren Forchhammer^a & Idelfonso Tafur Monroy^a

^a DTU Fotonik, Department of Photonics Engineering, Technical University of Denmark, Kongens Lyngby, Denmark

Published online: 29 Mar 2013.

To cite this article: Alexander Lebedev, J. J. Vegas Olmos, Xiaodan Pang, Søren Forchhammer & Idelfonso Tafur Monroy (2013) Demonstration and Comparison Study for V- and W-Band Real-Time High-Definition Video Delivery in Diverse Fiber-Wireless Infrastructure, *Fiber and Integrated Optics*, 32:2, 93-104, DOI: [10.1080/01468030.2012.760689](https://doi.org/10.1080/01468030.2012.760689)

To link to this article: <http://dx.doi.org/10.1080/01468030.2012.760689>

PLEASE SCROLL DOWN FOR ARTICLE

Taylor & Francis makes every effort to ensure the accuracy of all the information (the "Content") contained in the publications on our platform. However, Taylor & Francis, our agents, and our licensors make no representations or warranties whatsoever as to the accuracy, completeness, or suitability for any purpose of the Content. Any opinions and views expressed in this publication are the opinions and views of the authors, and are not the views of or endorsed by Taylor & Francis. The accuracy of the Content should not be relied upon and should be independently verified with primary sources of information. Taylor and Francis shall not be liable for any losses, actions, claims, proceedings, demands, costs, expenses, damages, and other liabilities whatsoever or howsoever caused arising directly or indirectly in connection with, in relation to or arising out of the use of the Content.

This article may be used for research, teaching, and private study purposes. Any substantial or systematic reproduction, redistribution, reselling, loan, sub-licensing, systematic supply, or distribution in any form to anyone is expressly forbidden. Terms & Conditions of access and use can be found at <http://www.tandfonline.com/page/terms-and-conditions>

Demonstration and Comparison Study for V- and W-Band Real-Time High-Definition Video Delivery in Diverse Fiber-Wireless Infrastructure

ALEXANDER LEBEDEV,¹ J. J. VEGAS OLMOS,¹
XIAODAN PANG,¹ SØREN FORCHHAMMER,¹ and
IDELFONSO TAFUR MONROY¹

¹DTU Fotonik, Department of Photonics Engineering, Technical University of Denmark, Kongens Lyngby, Denmark

Abstract *This article experimentally demonstrates uncompressed high-definition video distribution in V-band (50–75 GHz) and W-band (75–110 GHz) fiber-wireless links achieving 3 m of wireless transmission in both cases. Access architecture is experimentally emulated by deploying single/multi-mode fibers. For the W-band, experimental assessment of passive and active approaches for implementation of remote antenna units is reported. The bit error rate performance of the optical and wireless channels is reported. A successful transmission of real-time uncompressed high-definition video in the V- and W-band fiber-wireless systems is demonstrated with prospects to pave the way for application-focused fiber-wireless connectivity.*

Keywords hybrid optical-wireless architecture, radio-over-fiber, uncompressed high-definition video transmission, W-band wireless

Introduction

The growing usage of wireless technology in consumer devices causes interference and congestion in densely populated wireless hotspots employing unlicensed wireless frequency bands currently adopted by industry, such as Wi-Fi. Recent standardization efforts have led to allocation of unprecedented amounts of unlicensed bandwidth around 60 GHz in V-band (50–75 GHz) [1, 2]. The need to accommodate ever-growing bandwidth requirements leads to an interest in other unlicensed millimeter-wave frequency bands, in particular, those located in E- (60–90 GHz) and W-bands (75–110 GHz). Although the W-band is still in its infancy in terms of radio frequency (RF) component miniaturization, research in integration of W-band wireless systems into fiber architecture is essential to ensure the swift transition of optical networks toward efficient delivery of higher carrier RF signals.

Distributed antenna system (DAS) architectures for remote antenna unit (RAU) locations are considered necessary for efficient fiber support of wireless distribution due to decreased wireless coverage in case of millimeter-wave links (including W-band) [3].

Received 14 December 2012; accepted 17 December 2012.

Address correspondence to Mr. Alexander Lebedev, DTU Fotonik, Department of Photonics Engineering, Technical University of Denmark, Kongens Lyngby, 2800, Denmark. E-mail: alele@fotonik.dtu.dk

Radio-over-fiber (RoF) is widely considered to be a suitable concept for fiber-wireless integration in case of millimeter-wave wireless personal area networks (WPANs) assisted with DAS architecture [4–6]. The RoF approach leads to simplified RAUs, where costly high-frequency RF components are avoided at the RAU, thus leading to simpler and potentially lower cost RAU. Another important advantage of RoF systems is that they may be built transparent to data protocols and modulation formats [7].

Among the potential application scenarios for V- and W-band RoF networks is the delivery of real-time high-definition (HD) video for services such as gaming, e-health monitoring, video conferencing, and surveillance. Several designs for V-band fiber-wireless networks tailored for HD video delivery have been proposed [8, 9]. This study proposes the use of RoF architecture for real-time transfer of uncompressed HD video. Solutions proposed in this article may serve to support the ongoing industrial development to adopt millimeter wave for wireless HD multimedia interface (HDMI) video transmission [2]. The schematics are presented for a fiber-wireless HDMI video transmission system; and its equivalent physical layer performance is then analyzed under the constraints of wireless distance and optical power.

There are ongoing efforts to improve feasibility and efficiency of RoF systems. A major goal is to enable the wireless service to multiple RAUs produced by a single component at the central office (CO). Simultaneous up-conversion of several optical wavelengths has been reported [10]. A different approach to solve up-conversion consists of the up-conversion of several RF carriers onto a single lightwave carrier [11]. The research presented in this article reports on the up-conversion of a single channel; however, if video broadcasting is considered, the present work may fit in the following scenario (see Figure 1).

The latest work on passive remote wireless node architecture for the W-band has been presented for RoF systems tailored for Ethernet services [12]; however, uncompressed video services were not considered and fiber transmission was omitted.

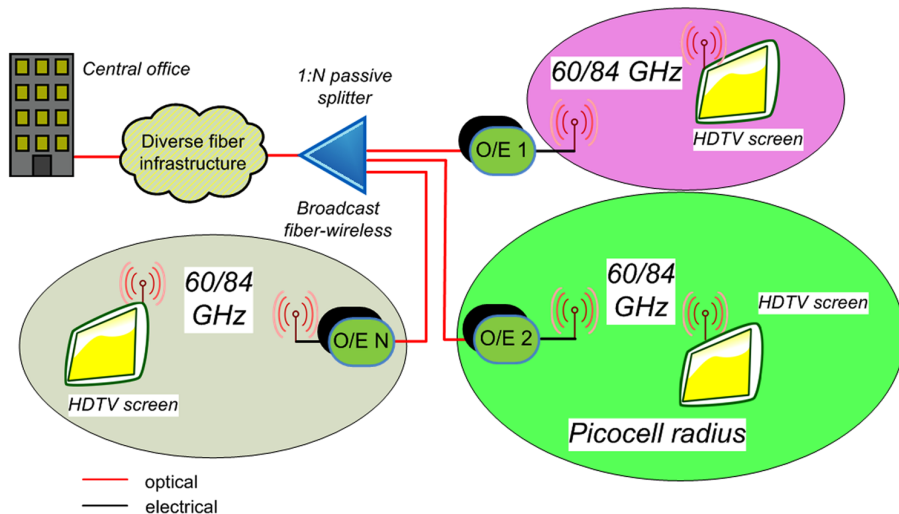


Figure 1. Network scenario for millimeter-wave wireless uncompressed HD video distribution over fiber-wireless networks (O/E: optical-to-electrical conversion; color figure available online).

This study considers both single-mode fiber (SMF) and multi-mode fiber (MMF) access scenarios. There are several potential applications for combined SMF and MMF fiber-wireless access links, among them, in-campus or in-company distribution employing MMFs in the local area network (LAN) interfaced with SMF media coming from the metro/access part of the network. Assessment of the performance when employing MMFs is utterly important to ensure that the diverse pre-existing infrastructure is optimally utilized.

The major novelty of the article is a direct comparison of V- and W-band fiber-wireless systems in terms of bit error rate (BER) performance for the bit-rate enabling real-time uncompressed HD video delivery. V- and W-band access fiber-wireless systems are studied with the analogous power budget in the presence of limitations on reach, dispersion, and non-linearities for fiber access network scenarios.

This article is organized as follows. Section 2 presents the V- and W-band laboratory setups and outlines the order of measurements. Section 3 presents the collected experimental data and discusses achieved experimental results. Finally, a summary and conclusions are provided in Section 4.

Experimental Setup Description

The W-band setup is first given in detail, and an analogous V-band setup is then presented. The overall goal was to replicate W-band measurements with V-band measurements for comparison of the two systems. The experimental setup of the W-band RoF video transmission system is presented in Figure 2, where the main building blocks are a dual-laser RoF transmitter block located at the CO, SMF/MMF distribution, RAU, and the end-user terminal. Two identical external cavity lasers (ECLs) were used for generating lightwave carriers offset by 84 GHz with optical power equal to +15 dBm. High optical power of the optical signals is important to increase the available power budget, which, in the broadcast scenario, increases the possible splitting ratio to enable the maximum number of wireless broadcast units. Baseband data were imposed onto one of the optical carriers by using an optical Mach-Zehnder modulator (MZM) driven by either a pulse pattern generator (PPG) producing a pseudorandom binary sequence (PRBS) with a word length of $2^{11} - 1$ or by an HDMI-to-coax converter. External modulation has been chosen over direct modulation in order to avoid possible frequency chirp.

Subsequently, an erbium-doped fiber amplifier (EDFA) was employed to increase the power budget followed by an optical bandpass filter (OBPF) to reduce out-of-band amplified spontaneous emission (ASE) noise from the EDFA. The EDFA was employed to study the link performance under the constraint of added ASE noise and also to increase the available power budget required to overcome the loss on the coupler, connectors, and fiber and still provide large dynamic range of the optical power values before optical-to-electrical conversion. A 3-dB coupler was used to combine two lightwave carriers before single fiber transmission. The fiber link was composed of 22.8 km of SMF and (or) a 100-m span of MMF. A variable optical attenuator (VOA) was employed to control the optical power impinging the photodiode (PD) in order to estimate the BER performance of the system. Figure 3 depicts the optical spectra after the 3-dB coupler. In the RAU, up-conversion to 84 GHz took place by photo-mixing the two optical carriers at the PD.

This study does not modulate the lightwave with RF directly; however, the RoF transmitter is implemented through coupling of lightwaves produced by two free running lasers. The method employed has been proven to be robust against dispersion-induced RF power fading [13]. Moreover, efficient fiber-wireless transmission on an

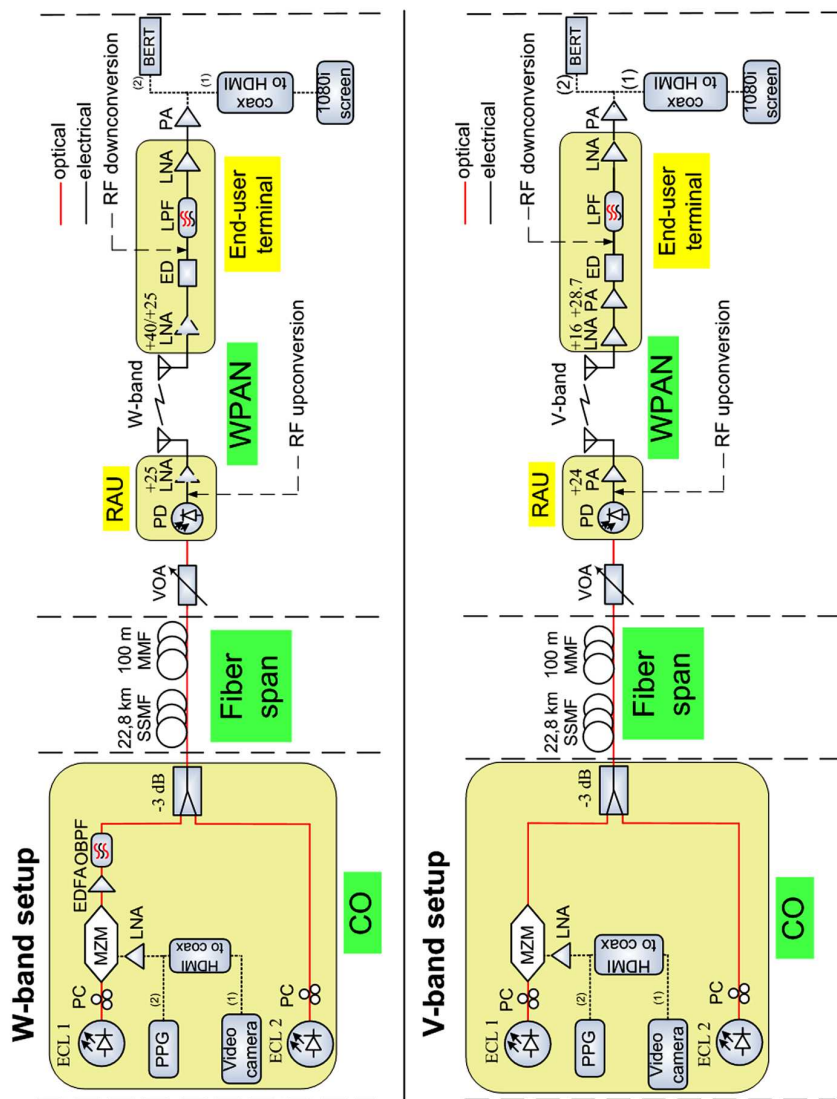


Figure 2. Experimental RoF system with envelope detection for (top) W-band transmission and (bottom) V-band transmission (ECL: external cavity laser, PPG: pulse pattern generator, PC: polarization controller, MZM: Mach-Zehnder modulator, LNA: low-noise amplifier, EDFA: erbium-doped fiber amplifier, OBPF: optical band-pass filter, VOA: variable optical attenuator, PA: power amplifier, BPF: band-pass filter, ED: envelope detector, LPF: low-pass filter, BERT: bit error rate tester; color figure available online).

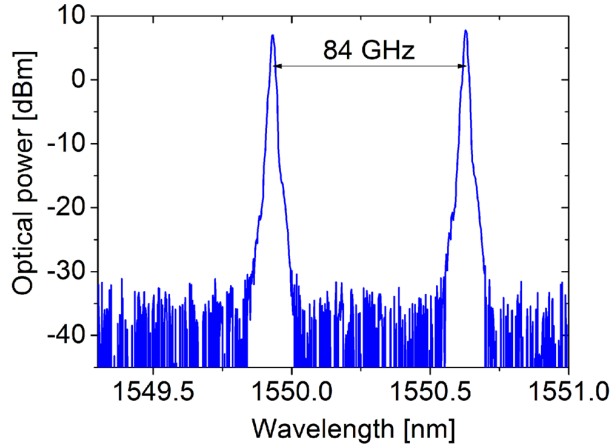


Figure 3. Optical spectra of W-band dual-laser RoF signal incident to the PD (color figure available online).

84-GHz RF carrier is currently most feasible with a dual-laser scheme, since methods that involve modulation of a lightwave with an RF signal, such as double sideband (DSB) or double sideband with suppressed carrier (DSB-SC), would require very high-frequency modulators with bandwidth exceeding 42 GHz and 84 GHz for DSB-SC and DSB schemes, respectively.

Both passive and active RAU approaches were studied experimentally. For the case of an active RAU, a 25-dB gain W-band amplifier was used before feeding the 84-GHz RF signal to an antenna for up to 3 m of wireless transmission. For the case of a passive RAU, the signal was radiated directly from the output of the PD. The transmitting and receiving antennas used in the experiment are commercially available horn antennas with 25-dBi gain. After receiving the signal with an antenna and W-band double-stage amplification (40-dB gain), envelope detection (ED) was employed for down-conversion. ED for RoF setups can be used efficiently for detection of on-off keying (OOK) signals [12, 14]. ED is particularly suitable in case of end-to-end video data communication when ultra-high speed data rates (in excess of several gigabits) are not required. Afterward, a baseband 20-dB-gain low noise amplifier (LNA) and a power amplifier (PA) 18-dB-gain PA were used to increase the peak-to-peak voltage level, as required for BER tester (BERT) operation (more than 250 mV).

The experimental measurements were divided into three phases. In Figure 2, changing parts of the setup are indicated with a dashed line. First, the MMF and SMF fiber architectures were characterized for an active RAU case (with the 25-dB-gain LNA at the RAU) employing a PPG configured to produce pulses of the same bit-rate and peak-to-peak voltage levels as those from the HDMI-to-coax video converter. Thereafter, PRBS transmission was performed using the MMF or SMF fiber link for a passive RAU case (without the +25/+40 LNA at the RAU). Finally, the transmission of an uncompressed 1080i video (bit-rate of 1.5 Gbps) was performed.

The video transmitter is designated as “(1)” in Figure 2. A commercially available video camera was used to produce a 1080i uncompressed video signal at its output. The characteristics of the video signal are as follows: framerate of 60 fields per second

(interlaced), 1,920 × 1,080 resolution, 4:4:4 color format, bit depth of 8 bits per color. The camera was connected directly to the commercially available HDMI-to-coax converter that produces non-return-to-zero (NRZ) electrical pulses on its output when given an HDMI video signal on its input. At the receiving end of the system, a coax-to-HDMI converter was placed, then a 1080i capable screen.

The V-band laboratory setup was assembled in order to replicate the W-band setup and perform the comparison study. The difference is that the EDFA was not added before the transmission through the fiber. An EDFA was added in the case of the W-band setup to achieve higher levels of optical power incident to the PD to increase the RF power level of generated 84-GHz carrier for the passive transmitter schematics.

Due to limitations in the equipment, slightly different high-frequency amplification components were used in the case of V-band measurements. A 24-dB-gain PA was used at the transmitter side, and a cascade of a 16-dB-gain LNA with a 28.7-dB-gain PA was used at the receiver side. For the V-band setup, the measurements for an active transmitter were performed only in order to benchmark V-band and W-band system performances.

Results and Discussion

W-Band Passive and Active RAUs Investigation

This section presents the measurement results for BER values, optical power levels, and wireless distances for the bit-rate of video (1.5 Gbps). Figure 4 presents two sets of results that characterize the performance of the optical channel and the wireless channel in case of active wireless transmitter. The behavior of the optical channel is shown with two series of data points at 2 and 3 m of wireless transmission for the optical back-to-back (B2B), 22.8-km SMF only and for the 22.8-km SMF combined with 100 m of MMF. The curves show the expected behavior at a distance of 2 m; the optical B2B shows the best performance, and the SMF transmission only and combined SMF-MMF transmission show at most 1 dB of penalty compared to the B2B case. This reflects the fact that short spans of MMF have high length-bandwidth product and do not deteriorate the performance of the system operating at the same optical power level at the PD. Nevertheless, the use of MMF introduces coupling losses on SMF-MMF and MMF-SMF connections and therefore contributes to deterioration of the power budget.

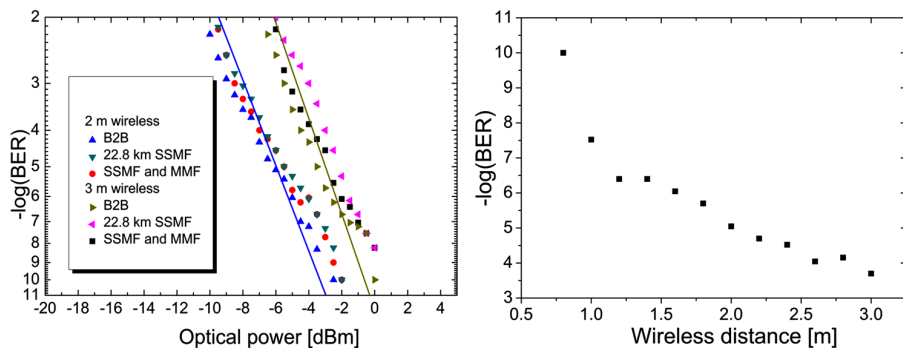


Figure 4. BER as a function of (left) optical power and (right) wireless distance for an active transmitter for optical B2B transmission (color figure available online).

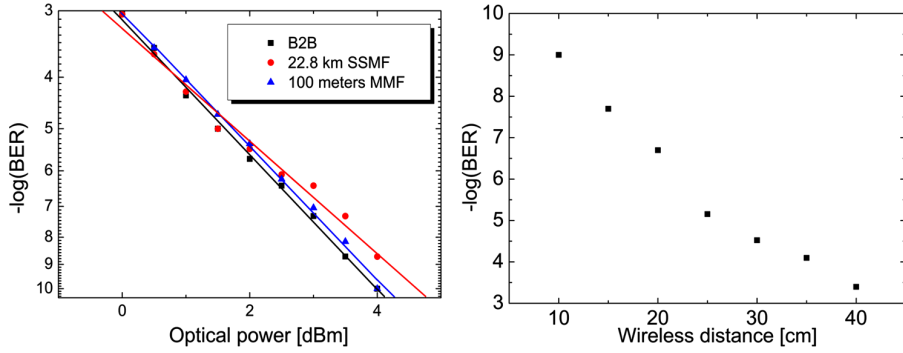


Figure 5. BER as a function of (left) optical power and (right) wireless distance for a passive transmitter with a 20-dB-gain amplifier at the receiver (color figure available online).

The results for 3 m of air transmission represent different behavior because of the higher power before the radiation for 3 m of distance. Figure 4 also shows the distance-dependent behavior of the wireless channel for the active wireless transmitter at the optical power level of -5 dBm.

To study the passive RAU behavior, the LNA was removed at the RAU, and the optical power at the input of the PD was increased to achieve lower BER values. Two cases are explored: (1) setting the amplification value at the receiver to $+25$ dBm and (2) setting the amplification value at the receiver to $+40$ dBm.

Applying 25-dB-gain amplification proves to be insufficient to communicate the data for long wireless distance, as depicted in Figure 5. At the same time, it is shown that the results for different fibers indicate no penalty associated with fiber transmission. It is important to note that the noise figure of the 25-dB-gain amplifier is less. This can be used as an advantage for very short wireless data links communication, similar to [15].

Passive RAU wireless transmission assisted with a $+40$ -dB-gain amplifier at the receiving end of the system exhibits the performance as depicted in Figure 6. Note that error-free performance was not achieved at the distance of 1 m, which is limited by

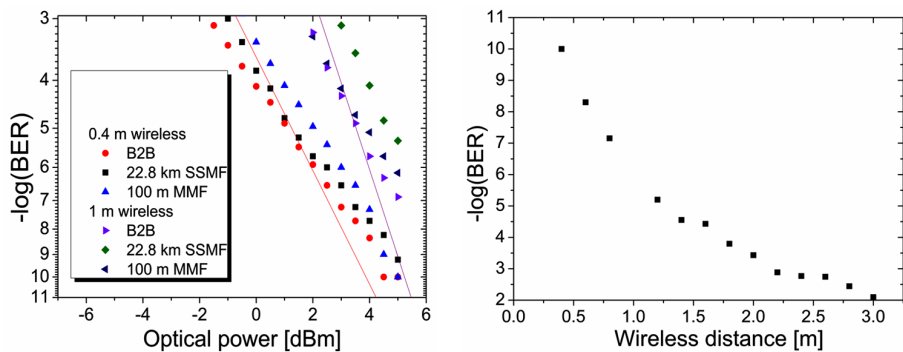


Figure 6. BER as a function of (left) optical power and (right) wireless distance for a passive transmitter (color figure available online).

the specified maximum optical power into the PD. The results show the expected linear performance at the wireless distance of 0.4 m and 1 m. It is important to note that at higher optical power levels, MMF and SMF transmissions show similar results. This means an absence of non-linearities impacting the BER, because otherwise, in the case of MMF, the larger core size would result in a higher threshold for non-linearities and thus better performance. At the same time, wireless distances in case of the passive RAU are significantly shorter.

Despite inferior performance in the case of a passive RAU, close proximity WPAN applications are feasible, giving the advantage of a simplified, energy-efficient remote wireless terminal. Figure 6 also shows the wireless channel behavior for the passive transmitter at the optical power level of -5 dBm.

The use of ED allows great simplification of the detection and the performance of electrical down-conversion from RF to baseband using only passive equipment. Similar work has already been done in V- and W-bands [12, 14]. The main limitation is the limitation on bandwidth. The fact that error-free BER can be achieved at 1.5 Gbps benchmarks the performance of the W-band envelope detectors for 1080i uncompressed HD video transmission.

V-Band Setup Performance: Comparison of V- and W-Band Dual-Laser RF Generation Schemes for Real-Time Uncompressed 1080i Video Delivery

This section compares the performance of W-band and V-band links in terms of BER performance as a function of decreasing optical power.

Figure 7 depicts BER performance of the V-band setup. W-band and V-band fiber-wireless transmission systems based on a dual-laser RF generation scheme show similar performance with penalty in case of the W-band wireless transmission (see Figure 6); however, the slope of BER curves is steeper in case of the V-band. These differences

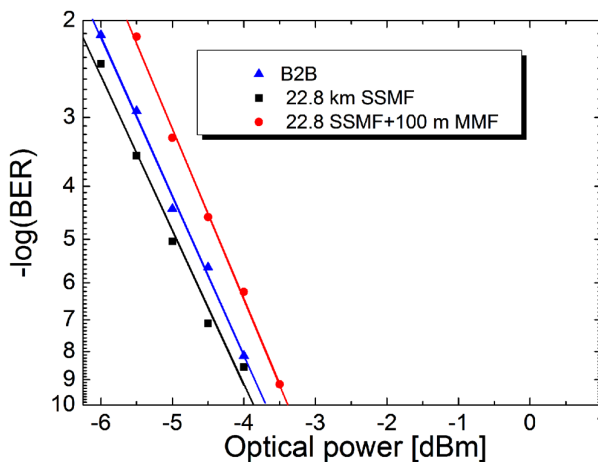


Figure 7. BER as a function of optical power for 3 m of wireless transmission (color figure available online).

are explained by a higher free space path loss that is expected for W-band links, slight differences in the power budget, and components performance, and it is consistent with previous reports in the area. These experimental results open the prospects to enable multi-band millimeter-wave wireless connectivity supported with a fiber infrastructure.

This work has used V- and W-band waveguide experimental equipment. The frequency range of the W-band and E-band waveguide equipment overlaps in the range of 75–90 GHz. Thus, the 84-GHz frequency used for W-band transmission is compatible with E-band wireless systems that are currently being introduced in the industry.

Demonstration of Real-Time 1080i Uncompressed Video Transmission and Video Performance Analysis

Commercially available HDMI-to-coax/coax-to-HDMI converters were used for video transmission. The situations of low percentage of packet loss, when video error-concealment tools can be employed to conceal the packet loss artifacts efficiently, were not encountered. Instead, either perfect performance was observed or the video transmission was stopped. Therefore, evaluation of the video transmission performance with the commonly used peak signal-to-noise ratio (PSNR) metric is not presented.

BER level is a crucial characteristic defining the quality of transmitted video. The video signal exhibited high sensitivity to bit errors, and it is therefore of utmost importance to keep the signal-to-noise ratio (SNR) as high as possible. Given the channel behavior in Figures 4–7, the use of channel coding is suggested as applied for the 60-GHz frequency in [2]. Employing channel coding, error-free rates for more than 2 m in both passive and active transmitter cases can be achieved with a reasonable number of overhead bits (pre-coded BERs of 10^{-5} and 10^{-3} for active and passive cases, respectively). The maximum distance of 3 m for a passive transmitter case will result in an excessive number of overhead bits. For a passive and an active case, video exhibited higher performance in the case of a passive RAU for the equivalent distances since an amplifier that introduces a noise figure of 4.5 dB was not employed.

Figure 8 depicts the laboratory setup where the video camera generating the video signal is pointed to the transmitting side of the system. After the signal has been transmitted and received successfully, it is displayed on a 1080i screen. The receiving end of the system is depicted behind the screen on the photograph.

Conclusions

The performance analysis is presented for transmission of real-time uncompressed 1080i HD video in the V- and W-band hybrid fiber-wireless architectures employing simplified receiver for down-conversion of the RF signal. Furthermore, the channel for the equivalent video bit-rate of 1.5 Gbps is characterized. Based on the experimental results, it can be concluded that V- and W-band dual-laser RF generation fiber-wireless systems can be regarded as viable candidates to provide fiber support in a high-frequency WPAN, e.g., for uncompressed real-time HD video delivery. Diverse fiber infrastructure is considered, and it is concluded that MMFs and SMFs can serve as a suitable media to connect the CO and the RAU in V- and W-band RoF transmission systems satisfying the requirements for reach, dispersion, and non-linearities in access fiber-wireless systems. Future work includes estimation and comparison of wireless channel loss for V- and W-band systems and quantification of the optical signal-to-noise ratio (OSNR) degradation effect of an EDFA on the link.

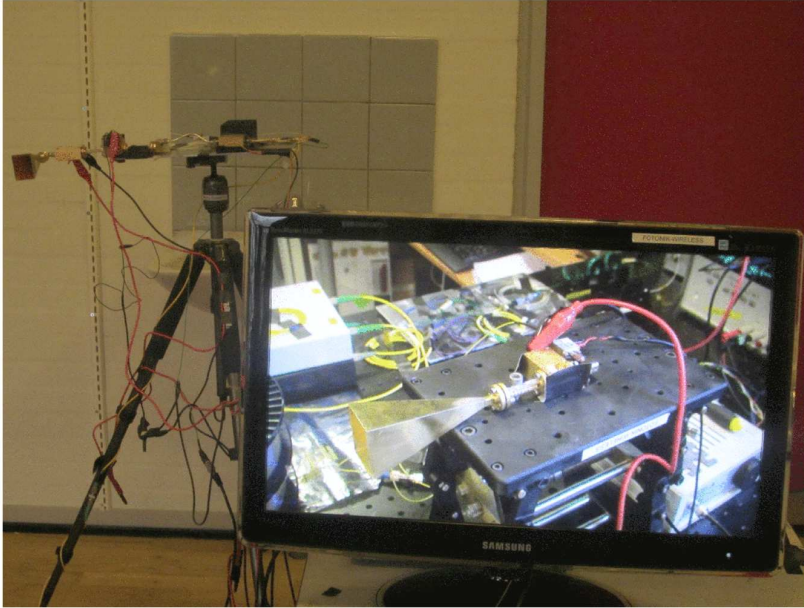


Figure 8. Photograph of the setup depicting wireless transmitter and wireless receiver (color figure available online).

References

1. Yong, S.-K. 2011. *60 GHz Technology for Gbps WLAN and WPAN: From Theory to Practice*, chapter 1. Wiley.
2. <http://www.wirelesshd.org/about/specification-summary/>.
3. Parker, M. C., Walker, S. D., Llorente, R., Morant, M., Beltrán, M., Möllers, I., Jäger, D., Vázquez, C., Montero, D., Librán, I., Mikroulis, S., Karabetsos, S., and Bogris, A. 2010. Radio-over-fibre technologies arising from the building the future optical network in Europe (BONE) project. *IET Optoelectronics* 4(6):247–259.
4. Lim, C., Nirmalathas, A., Bakaul, M., Gamage, P., Lee, K.-L., Yang, Y., Novak, D., and Waterhouse, R. 2010. Fiber-wireless networks and subsystem technologies. *IEEE Journal of Lightwave Technology* 28(4):390–405.
5. Zin, A. M., Bongsu, M. S., Idrus, S. M., and Zulkifli, N. 2010. An overview of radio-over-fiber network technology. Paper ICP2010-85. *International Conference on Photonics (ICP)*, Langkawi, Malaysia, July 5–7.
6. Iezekiel, S. 2009. *Microwave Photonics: Devices and Applications*, chapter 1. Wiley.
7. Xiao, S.-Q., Zhou M.-T., and Zhang, Y. 2007. *Millimeter Wave Technology in Wireless Pan, Lan, and Man*, chapter 11. CRC Press.
8. Guillory, J., Tanguy, E., Pizzinat, A., Charbonnier, B., Meyer, S., Li, H. W., and Algani, C. 2011. Radio over fiber tunnel for 60 GHz wireless home network. Paper OWT6. *Conference on Optical Fiber Communication (OFC), Collocated National Fiber Optic Engineers Conference (OFC/NFOEC)*, Los Angeles, CA, March 6–11.
9. Guillory, J., Tanguy, E., Pizzinat, A., Charbonnier, B., Meyer, S., Algani, C., and Li, H. 2011. A 60 GHz wireless home area network with radio over fiber repeaters. *IEEE Journal of Lightwave Technology* 29(16):2482–2488.
10. Griffin, R. A. 2000. DWDM aspects of radio-over-fiber. Paper MH3. *Lasers and Electro-Optics Society 2000 Annual Meeting (LEOS 2000)*, Rio Grande, Puerto Rico, November 13–16.

11. Chowdhury, A., Chien, H.-C., and Chang G.-K. 2010. Demonstration of simultaneous all-optical up-conversion of Gigabit wireless services at 60-GHz and 64-GHz in converged optical wireless system carried by single wavelength lightwave. Paper OWQ5. *Conference on Optical Fiber Communication (OFC), Collocated National Fiber Optic Engineers Conference, (OFC/NFOEC)*, San Diego, CA, March 21–25.
12. Babel, S., Perentos, A., Fedderwitz, S., Kunz, B., Iezekiel, S., and Stöhr, A. 2011. 100 GHz band photonic wireless system employing passive RoF transmitters. Paper C12. *International Symposium on Green Radio over Fibre & All Optical technologies for Wireless Access Networks (GROWAN)*, Brest, France, June 15–17.
13. Gliese, U., Nørskov, S., and Nielsen, T. N. 1996. Chromatic dispersion in fiber-optic microwave and millimeter-wave links. *IEEE Transactions on Microwave Theory and Techniques* 44(10):1716–1724.
14. Pham, T. T., Lebedev, A., Beltrán, M., Yu, X., Llorente, R., and Tafur Monroy, I. 2012. Combined single-mode/multimode fiber link supporting simplified in-building 60-GHz gigabit wireless access. *Optical Fiber Technology* 18(4):226–229.
15. www.transferjet.org/tj/transferjet_overview.pdf.

Biographies

Alexander Lebedev received his Dipl.-Ing. in physics and technique of optical communication from the Bonch-Bruevich Saint-Petersburg State University of Telecommunications, Russia, in 2010. He is currently pursuing his Ph.D. at DTU Fotonik, Technical University of Denmark. His research interests are in the area of high-definition video transmission in fiber-wireless communication systems.

J. J. Vegas Olmos has been an assistant professor at the Metro-Access and Short Range Systems group of the Technical University of Denmark, DTU Fotonik, since 2011. He received his Ph.D. in 2006 from TU Eindhoven, The Netherlands. He was further trained at Osaka University as a JSPS Fellow and subsequently worked as senior researcher at Hitachi Central Research Laboratory, Tokyo, Japan.

Xiaodan Pang received his B.Sc. in optical information science and technology from Shandong University, Jinan, China, in 2008, and his M.Sc. in photonics from the Royal Institute of Technology, Stockholm, Sweden, in 2010. He is currently pursuing his Ph.D. in optical communications engineering at DTU Fotonik, Technical University of Denmark. His research interests are in the area of hybrid optical fiber-wireless communication systems.

Søren Forchhammer received his M.S. in engineering and Ph.D. from the Technical University of Denmark, Lyngby, in 1984 and 1988, respectively. Currently, he is a professor with DTU Fotonik, Technical University of Denmark, where he has been since 1988. He is head of the Coding and Visual Communication Group at DTU Fotonik. His main interests include source coding, image and video coding, distributed video coding, processing for image displays, two-dimensional information theory, and visual communications.

Idelfonso Tafur Monroy is currently professor and head of the Metro-Access and Short Range Communications Group of the Department of Photonics Engineering at the Technical University of Denmark. He graduated from the Bonch-Bruevich Institute of Communications, St. Petersburg, Russia, in 1992, where he received his M.Sc. in multichannel telecommunications. In 1996, he received a Technology Licentiate in telecommunications theory from the Royal Institute of Technology, Stockholm, Sweden. The same year, he joined the Electrical Engineering Department of Eindhoven University of Technology, The Netherlands, where he earned his Ph.D. in 1999 and worked as

an assistant professor until 2006. He has participated in several European research framework projects in photonic technologies and their applications to communication systems and networks. He is currently involved in the ICT European projects GiGaWaM and EURO-FOS and is the technical coordinator of the ICT-CHRON project. His research interests are in hybrid optical-wireless communication systems, high-capacity optical fiber communications, digital signal processing for optical transceivers for baseband and radio-over-fiber links, and the application of nanophotonic technologies in the metropolitan and access segments of optical networks, as well as in short range optical-wireless communication links.

[Paper 4]

Alexander Lebedev, Juan Jose Vegas Olmos, Miguel Iglesias, Søren Forchhammer, Idelfonso Tafur Monroy, "A novel method for combating dispersion induced power fading in dispersion compensating fiber," *Opt. Express*, vol. 21, no. 11, pp. 13617-13625, 2013.

A novel method for combating dispersion induced power fading in dispersion compensating fiber

Alexander Lebedev,* J. J. Vegas Olmos, Miguel Iglesias, Søren Forchhammer, and Idelfonso Tafur Monroy

DTU Fotonik, Dept. of Photonics Engineering, DTU, Technical University of Denmark, Kgs. Lyngby, Denmark
*alele@fotonik.dtu.dk

Abstract: We experimentally investigate the performance of 60 GHz double sideband (DSB) radio over fiber (RoF) links that employ dispersion compensating fiber (DCF). Error free transmission of 3 Gbps signals over 1 m of wireless distance is reported. In order to overcome experimentally observed chromatic dispersion (CD) induced power fading of radio frequency (RF) signal, we propose a method for improvement of RF carrier-to-noise (C/N) ratio through introduction of a degree of RF frequency tunability. Overall results improve important aspects of directly modulated RoF systems and demonstrate the feasibility of high carrier frequency and wide bandwidth RF signals delivery in RoF links including DCF fiber. Error free performance that we obtain for 3 Gbps amplitude shift-keying (ASK) signals enables uncompressed high-definition 1080p video delivery.

©2013 Optical Society of America

OCIS codes: (060.2330) Fiber optics communications; (060.5625) Radio frequency photonics.

References and links

1. Cisco white paper, "Cisco visual networking index: global mobile data traffic forecast update, 2012-2017," (Cisco, 2012).
http://www.cisco.com/en/US/solutions/collateral/ns341/ns525/ns537/ns705/ns827/white_paper_c11-520862.pdf.
2. Ericsson white paper, "Traffic and market data report," (Ericsson, 2011).
<http://hugin.info/1061/R/1561267/483187.pdf>.
3. Ericsson white paper, "Heterogeneous networks," (Ericsson, 2012).
<http://www.ericsson.com/res/docs/whitepapers/WP-Heterogeneous-Networks.pdf>.
4. M. C. Parker, S. D. Walker, R. Llorente, M. Morant, M. Beltrán, I. Möllers, D. Jäger, C. Vázquez, D. Montero, I. Librán, S. Mikroulis, S. Karabetsos, and A. Bogris, "Radio-over-fibre technologies arising from the building the future optical network in Europe (BONE) project," *IET Optoelectron.* **4**(6), 247–259 (2010).
5. C. Lim, A. Nirmalathas, M. Bakaul, P. Gamage, L. Ka-Lun, Y. Yizhu, D. Novak, and R. Waterhouse, "Fiber-Wireless Networks and Subsystem Technologies," *J. Lightwave Technol.* **28**(4), 390–405 (2010).
6. A. M. Zin, M. S. Bongsu, S. M. Idrus, and N. Zulkifli, "An overview of radio-over-fiber network technology," in *Proceedings of IEEE International Conference on Photonics*, (Institute of Electrical and Electronics Engineers, San Francisco, 2010), paper ICP2010–85.
7. R. Herschel and C. G. Schaeffer, "Architectures for multiband multi gbps radio-over-fiber systems," in *Proceedings of 12th ITG Conference on Photonic Networks* (Institute of Electrical and Electronics Engineers, Leipzig, Germany, 2011), paper 24.
8. Vubiq specification datasheet, "60 GHz receiver waveguide module," (Vubiq, 2013).
<http://www.vubiq.com/pdf/Data%20Sheet%20V60RXWG2%20rev1.3.pdf>.
9. WirelessHD white paper, "WirelessHD Specification Version 1.1 Overview," (WirelessHD, 2010).
<http://www.wirelesshd.org/pdfs/WirelessHD-Specification-Overview-v1.1May2010.pdf>.
10. Siversima white paper, "MM-wave converter series for high capacity wireless transfer," (Siversima, 2010).
http://www.siversima.com/wp-content/uploads/2011/10/high-capacity-wireless-transfer_111010.pdf.
11. R. Hofstetter, H. Schmuck, and R. Heidemann, "Dispersion effects in optical millimeter-wave systems using self-heterodyne method for transport and generation," *IEEE Trans. Microw. Theory* **43**(9), 2263–2269 (1995).
12. K. Kitayama, "Ultimate performance of optical DSB signal-based millimeter-wave fiber-radio system: effect of laser phase noise," *J. Lightwave Technol.* **17**(10), 1774–1781 (1999).
13. A. Stohr, K. Kitayama, and T. Kuri, "Fiber-length extension in an optical 60-GHz transmission system using an EA-modulator with negative chirp," *IEEE Photon. Technol. Lett.* **11**(6), 739–741 (1999).

14. A. Ng'oma, Sh. Po-Tsung, J. George, F. Annunziata, M. Sauer, L. Chun-Ting, J. Wen Jr., Jyehong, and S. Chi, "21 Gbps OFDM wireless signal transmission at 60 GHz using a simple IMDD radio-over-fiber system," Conference on Optical Fiber Communication, collocated National Fiber Optic Engineers Conference (Optical Society of America, 2010), paper OTuF4.
15. M. Weiß, "60 GHz photonic millimeter-wave communication systems," PhD dissertation, University of Duisburg-Essen, 2010.
16. H. Sun, M. C. Cardakli, K.-M. Feng, J.-X. Cai, H. Long, M. I. Hayee, and A. E. Willner, "Tunable RF-powerfading compensation of multiple-channel double-sideband SCM transmission using a nonlinearly chirped FBG," *IEEE Photon. Technol. Lett.* **12**(5), 546–548 (2000).
17. B. Hraimel, Zh. Xiupu, M. Mohamed, and W. Ke, "Precompensated optical double-sideband subcarrier modulation immune to fiber chromatic-dispersion-induced radio frequency power fading," *J. Opt. Commun. Netw.* **1**(4), 331–342 (2009).
18. H. Sotobayashi and K. Kitayama, "Cancellation of the signal fading for 60 GHz subcarrier multiplexed optical DSB signal transmission in nondispersion shifted fiber using midway optical phase conjugation," *J. Lightwave Technol.* **17**(12), 2488–2497 (1999).
19. A. Lebedev, J. J. Vegas Olmos, X. Pang, S. Forchhammer, and I. Tafur Monroy, "Demonstration and comparison study for V- and W-band real-time high-definition video delivery in diverse fiber-wireless infrastructure," *Fiber Integrated Opt.* **32**(2), 93–104 (2013).
20. T. T. Pham, A. Lebedev, M. Beltrán, X. Yu, R. Llorente, and I. Tafur Monroy, "Combined singlemode/multimode fiber link supporting simplified in-building 60-GHz gigabit wireless access," *Opt. Fiber Technol.* **18**(4), 226–229 (2012).
21. J. Ma, J. Yu, C. Yu, X. Xin, J. Zeng, and L. Chen, "Fiber dispersion influence on transmission of the optical millimeter-waves generated using LN-MZM intensity modulation," *J. Lightwave Technol.* **25**(11), 3244–3256 (2007).
22. G. Hilt, "Optical transmission and upconversion of microwave signals in radio-over-fiber telecommunication Systems," PhD dissertation, L'institut National Polytechnique De Grenoble, (1999).
23. H. Schmuck, "Comparison of optical millimetre-wave system concepts with regard to chromatic Dispersion," *Electron. Lett.* **31**(21), 1848–1849 (1995).
24. U. Gliese, S. Norskov, and T. N. Nielsen, "Chromatic dispersion in fiber-optic microwave and millimeter wave links," *IEEE Trans. Microw. Theory* **44**(10), 1716–1724 (1996).

1. Introduction

The introduction of diverse bandwidth-demanding services requires an upgrade of current networks in order to provide higher bitrates for the end-user. Traffic generated by wireless/mobile services is predicted to grow at a fast pace with dominant applications such as data, file sharing, video, voice over internet protocol (VOIP) and gaming [1, 2]. Video traffic is predicted to increase at a highest annual growth rate compared to other services (taking up more than 70 percent of the overall traffic) [1].

In this work, we study the performance of heterogeneous links, which include fiber and wireless spans. In a recent report on heterogeneous networks [3], the use of distributed antenna systems (DAS) architecture is suggested in order to provide wired infrastructure for wireless traffic generated by the end-user, where antennas are located very densely with one antenna covering several rooms or even a single room. Among the physical layer fiber optic wired-wireless communication solutions for DAS network architecture, radio over fiber (RoF) stands out by addressing two important requirements: the need to simplify a remote antenna unit (RAU), potentially providing a solution only with passive components, and the need to centralize the signal processing at the common point for the optical and the electrical signal. An overview of RoF technology principles, advantages and recent advances can be found in [4–7].

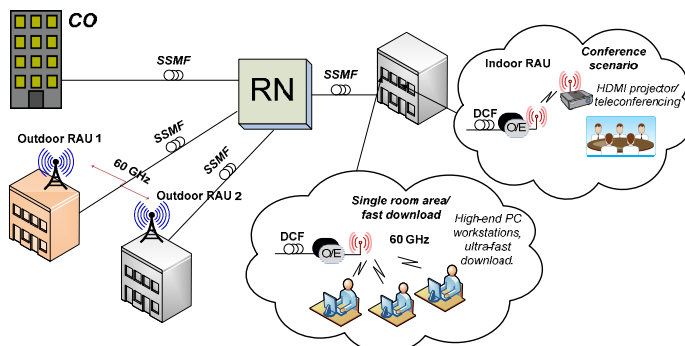


Fig. 1. Network scenario for 60 GHz RoF system. RAU: remote antenna unit, CO: central office, O/E: optical to electrical conversion, RN: remote node, DCF: dispersion compensating fiber, SSMF: standard single mode fiber.

Recent developments in component miniaturization have led to the appearance of commercially available solutions of 60 GHz up- and down-conversion integrated modules [8–10]. In order to provide seamless infrastructure for the electrical RF signal transfer between the central office (CO) and the RAU, we suggest that future fiber networks will need to transport the 60 GHz signals through the fiber span by means of direct intensity modulation of the lightwave that imposes double sideband (DSB) modulation on the carrier. Work on RoF DSB transmission has been widely reported, including methods to overcome the drawbacks of DSB modulation [11–13] and more recently reporting on ultra high bitrate wireless transmission (21 Gbps) through 500 meters of fiber [14]. Alternatives for DSB modulation, namely optical single sideband (OSSB) modulation and double sideband modulation with suppressed carrier (DSB-SC), have been studied and used extensively for RoF setups due to their increased tolerance against impairments. However, there are drawbacks for these approaches, such as a high optical power loss when we bias at the minimum point on a transfer characteristic of the Mach-Zehnder modulators (MZM), as in case of DSB-SC modulation, or high degree of complexity and accuracy in the optical filtering as in case of OSSB modulation. A thorough overview of photonic RF signal generation techniques can be found in [15].

In Fig. 1, we consider a network scenario for the 60 GHz fiber-wireless link that is capable of serving diverse applications. Our target application is real-time high definition (HD) uncompressed video transmission for business teleconferencing. Motivations for uncompressed video transmission include reduced latency and energy consumption. In this paper, we characterize the fiber-wireless system for a bitrate of 3 Gbps. The 3 Gbps bitrate would be sufficient to deliver 1080p uncompressed HD video. Systems of this bitrate that may also be alternatively used for ultra fast data download as indicated in the Fig. 1. Both of these applications may not be served by coaxial links combined with Wi-Fi if we consider the 3Gbps bitrate.

In the fiber architecture considered in this paper, photonic 60 GHz upconversion takes place at the remote node (RN). The metropolitan optical infrastructure is used to deliver the baseband signal from the CO to the RN. We consider that upconversion is made at the RN serving as an interface between metro and access parts of the network. In this scenario, a coil of dispersion compensating fiber (DCF) could be installed at the end-user site to compensate the effects of chromatic dispersion on a digitally modulated lightwave. The fiber-distributed 60 GHz wireless signals could subsequently serve in both indoor and outdoor wireless scenarios.

DCF is typically used for dispersion management in long reach optical fiber links. In this paper, we investigate the transmission of DSB modulated lightwave through DCF. Transmission of DSB signals in dispersive fiber media leads to appearance of phase change between the carrier and the sidebands that, after photomixing, results in RF carrier-to-noise (C/N) ratio degradation as a function of fiber distance and electrical oscillator frequency. A number of methods have been proposed for compensating RF C/N degradation that employ diverse fiber optics tools and electrical precompensation [13, 16–18]. In this paper, we show through experiment and simulation that the use of DCF for a lightwave modulated by an RF signal will be severely constrained by chromatic dispersion (CD) induced RF power fading. We then propose the algorithm to combat the RF power fading.

The novel contribution of this paper is twofold. First, this paper presents a 3 Gbps synchronous detection 60 GHz DSB RoF link operating below 10^{-9} BER level. The link's bitrate enables transmission of 1080p HD uncompressed video with an “off-the-shelf” hardware. Second, we study the transmission of DSB signals in DCF. Based on experimental results and modeling, we propose a method for improvement of the RF C/N ratio after the photomixing. Our proposed solution produces the reduction in CD induced degradation of RF C/N ratio and at the same time does not require a change in fiber infrastructure.

This paper is organized as follows: in Section 2 we present the laboratory setup and experimental performance assessment of the DSB 60 GHz DCF RoF link. In Section 3, we first present an analytical description for CD induced RF power fading in case of SMF and DCF based 60 GHz RoF links. Based on the observation of frequency-dependent behavior of CD induced RF C/N penalty for the DCF and SMF links, we propose a new algorithm for compensation of RF power fading. Finally, we provide a summary and conclusions in Section

2. Experimental setup for 60 GHz RoF employing DCF Fibers

The experimental setup of the 60 GHz DSB RoF system is presented in Fig. 2. A baseband data signal generated by a pulse pattern generator (PPG) producing a pseudorandom binary sequence (PRBS) with a word length of $2^{15}-1$ was mixed with a 58.24 GHz electrical signal from a factor-4 multiplied 14.56 GHz sinusoidal electrical signal. A lightwave carrier with a power of 6 dBm was generated by a laser diode (LD) of 1550 nm wavelength with less than 100 kHz line width. It was then modulated with the RF-upconverted signal through driving a Mach-Zehnder modulator (MZM) (35 GHz of –3dB electrical bandwidth) biased at its quadrature point. An Erbium doped fiber amplifier (EDFA) was employed, followed by a 2 nm bandwidth optical bandpass filter (OBPF) to reject out-of-band amplified spontaneous emission (ASE) noise introduced by the EDFA. The fiber link was composed of either 50 or 100 meters of DCF. The dispersion parameter of the DCF fiber employed is -108 ps/(nm*km). After photodetection, we used a 16 dB gain 55-65 GHz bandwidth low noise amplifier (LNA) and a 28.7 dB gain 55-65 GHz bandwidth power amplifier (PA) to increase the signal power before radiation.

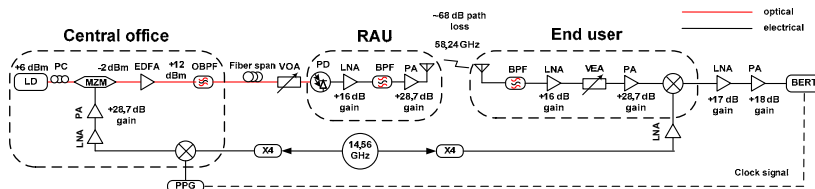


Fig. 2. Experimental setup of the 60 GHz DSB RoF system. LD: laser diode, PC: polarization controller, MZM: Mach-Zehnder modulator, EDFA: Erbium doped fiber amplifier, OBPF: optical bandpass filter, DCF: dispersion compensating fiber, VOA: variable optical attenuator, PD: photodiode, LNA: low noise amplifier, PA: power amplifier, BPF: bandpass filter, VEA: variable electrical attenuator, PPG: pulse pattern generator, BERT: bit error rate tester.

We employed commercially available high-directivity (25 dBi gain) horn antennas in order to improve the wireless link budget. 55–65 GHz bandpass filters (BPF) on the receiving and the transmitting side were used in order to reject out-of-band noise added by the photodiode (PD) and amplifiers. On the receiving side, we employed a variable electrical attenuator (VEA) to avoid the saturation of the amplifier. After reception of the signal, filtering and amplification, we downconverted the signal by means of mixing with the electrical oscillator synchronized in phase and frequency with the RF component of the detected signal. We employed a single electrical oscillator for the up- and down-conversion, however for a real-life implementation, when separate oscillators are implemented, phase locked loop (PLL) is required to be installed.

We employed a mixing technique to downconvert the data signal with the help of electrical oscillator in order to achieve 3 Gbps of bitrate for a wireless distance of 1 m. Alternative envelope detection techniques suffer from limitations on the bandwidth [19, 20]. We then used a baseband LNA (17 dB gain) and a PA (18 dB gain) to increase the peak-to-peak voltage level for the bit error rate tester (BERT) operation.

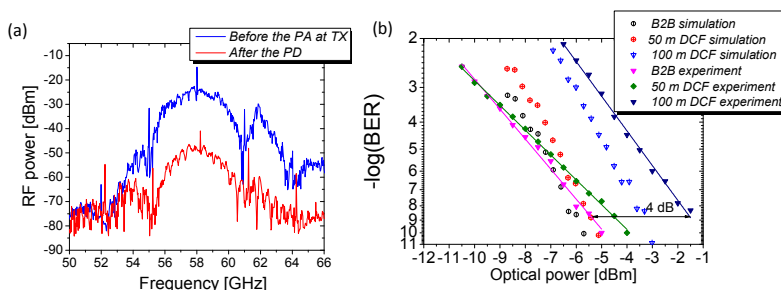


Fig. 3. (a) Experimentally measured electrical spectra of the signal before E/O and after O/E conversion, (b) BER curves as a function of the optical power.

Figure 3(a) shows the experimentally measured electrical spectrum of the signal before the PA at the CO side and after the PD at the optical receiver side. We observe a 30 dB reduction of the signal power after transmission through the analog optical link; this reduction is overcome by using a cascade of the LNA and the PA before radiation.

The performance of the system in terms of BER is depicted in Fig. 3(b). We observe that the system performance is degraded significantly depending on the length of the fiber span; there is a 4 dB penalty between 50 m and 100 m spans. We attribute this effect to the distance-dependent CD induced RF C/N penalty. This severe penalty is caused due to the fact that we transmit through the fiber with high absolute value of the dispersion parameter. In Fig. 3(b), we present the results of both simulation and experiment of 60 GHz fiber-wireless system performance under a constraint of dispersion. Simulation was performed using the VPI software. The difference in the slope between the simulation and the experimental performance is attributed to the ambiguity in noise levels between the simulation and the laboratory setup. Simulation that we performed was focused on the estimate of CD induced RF C/N ratio degradation and certain aspects of the system performance have been simplified. The overall system noise sources include high frequency electrical amplifiers noise, shot noise of the PD, thermal noise, and ASE noise. Dispersion also contributes synchronization loss between sidebands and imposes deterioration on an eye-diagram as a function of fiber distance [21].

Analytical description of the CD induced RF C/N penalty and a novel algorithm to combat it are presented in the next section.

3. Method of improvement of RF C/N ratio through frequency tuning of the RF carrier

In this section, we propose an algorithm for compensation of RF power fading in DSB link based on observation of the increasing frequency periodicity of the RF carrier fading for increasing fiber link length. We present the improvement in C/N performance achievable with the software implementation of the frequency tuning algorithm.

Number of sophisticated solutions to combat the CD induced RF power fading have already been proposed and implemented in the field - such as employing transmitters with negative chirp [13], tunable compensation with Fiber Bragg Gratings (FBG) [16], through applying optimum electrical phase shift [17] and midway optical phase conjugation [18]. The novelty of our approach consists in the fact that we do not consider generation of a certain frequency, but we consider a transmission within a certain band for a given frequency shift of the local oscillator that is allowable, then we define the optimum frequency for transmission for a given fiber length and what effect it brings for the improvement of the impaired C/N ratio.

CD induced power fading effect is described analytically in references [22–24]; we only present the final formula as in [23]. Equation (1) reflects that C/N ratio of the RF signal recovered after the RoF link depends on dispersion parameter, fiber link length and frequency of the electrical oscillator.

$$P_{el}(t) \approx I_{PD}^2(t) \approx \cos^2[\varphi_d(\omega_m)] \approx \cos^2\left[\pi cDL(f_{RF}/f_c)^2\right] \quad (1)$$

where c is a light velocity, D is a dispersion parameter, in our calculations, we set it to 18 ps/(nm*km) for SSMF and -108 ps/(nm*km) for DCF, L is a fiber length, f_{RF} is a cyclic frequency of an electrical oscillator, which in our case is equal to 58.24 GHz, f_c is a frequency of a lightwave, we set it to 193.1 THz.

Equation (2) represents the value of RF C/N penalty in a logarithmic scale:

$$Penalty_{C/N} = 10 \log \left| \frac{X_{OUT}(f_c)_{fiber}}{X_{OUT}(f_c)_{nofiber}} \right| \quad (2)$$

$X_{OUT fiber}$ and $X_{OUT nofiber}$ is the signal power with and without fiber transmission.

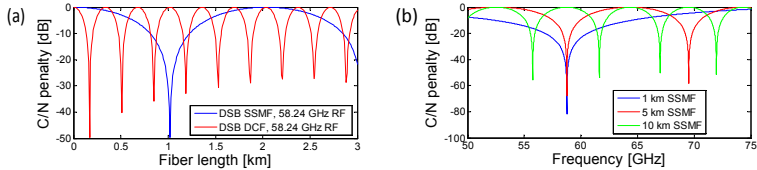


Fig. 4. Dispersion-induced power fading as a function of (a) fiber length for SSMF and DCF, (b) RF carrier frequency for SSMF.

In Fig. 4(a) we present the results of numerical calculation of CD induced RF power fading based on Eq. (1) and Eq. (2) for DCF and SSMF for a fixed frequency of the local oscillator. We see from Fig. 4(a) that the CD induced fading in case of DCF has higher periodicity along the fiber length. We chose the same RF carrier (58.24 GHz) for analytical estimation as was used throughout the experimental part of the work; it shows coherence with the experimental data where more severe constant power fading was observed in case of DCF. The first dip in C/N ratio for DCF occurs at 170 m length compared to 1020 meters for the first dip length for SSMF. The first -3 dB penalty occurs at 510 m and 85 m for SSMF and DCF respectively.

The Fig. 4(b) reflects the fact that there is a set of frequencies for a given fiber length that produces minimum CD induced RF C/N degradation. For example, as depicted in Fig. 4(b) 10 km SSMF span has 5 optimal frequencies in V-band range.

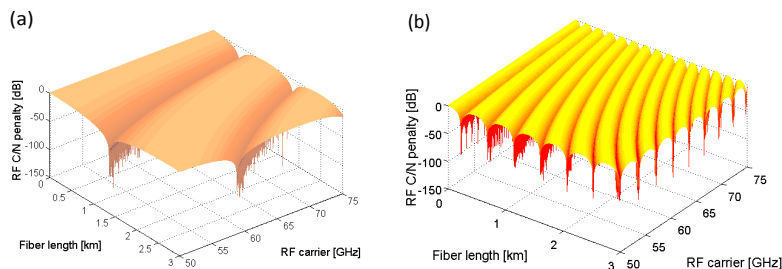


Fig. 5. Dispersion induced power fading as a function of frequency and fiber length for SSF (a) and DCF (b).

In Fig. 5, we depict the surface plots for the combined effects of distance-dependent and frequency-dependent RF power fading in case of SSF and DCF. It is visible that periodicity of fading for DCF is higher in both frequency domain and along the fiber length. We then present the algorithm to overcome CD induced RF power fading for a given bandwidth of local oscillator tuning.

Tunability in frequency domain is important notion to consider given that RF oscillators that are produced currently by the industry are frequency tunable, and thus the frequency of an oscillator can be adjusted in order to improve RF C/N ratio for a given length of deployed fiber. It is also important to note that the periodicity of the fading is increasing with the increase in fiber length, thus, for longer distances of fiber, we need less tuning bandwidth to obtain the same improvement in C/N ratio. At the same time, we also need to note from Fig. 4 and Fig. 5 that, with increase in the fiber length, the -3 dB bandwidth of minimum fading values for the signal decreases. Our numerical simulations indicate that a -3 dB bandwidth of 6 GHz occurs for V-band signals with this type of DCF in distances above 800 m.

We make the following assumptions for the model: we do not have the prior knowledge of the fiber distance for the deployed link, and we have a low data rate link to transmit the control signals from the optical receiver to the optical transmitter. Low data rate link may be a part of a larger packet-based network, where the 60 GHz fiber-wireless connection serves as a backbone.

It is important that we have sufficient amount of bandwidth in the wireless part of the link to allow the frequency tunability without breaking the unlicensed frequency allocation borders. The range of frequencies allocated for unlicensed use around 60 GHz varies from country to country, for instance, in Europe the frequency is allocated within 57-66 GHz bandwidth [9]. According to [9], a channel bandwidth can occupy up to 2160 MHz. The bandwidth of a main lobe of our signal is approximately 6 GHz. However, the proposed algorithm will work also with lower bandwidth signals. In order to enable 3 Gbps error free transmission in 2160 MHz band defined by [9], QAM-16 modulation is necessary for a single carrier transmission.

The concept of the algorithm is as follows:

- 1) At the CO (or the RN depending on the scenario,) electrical oscillator frequency is set in a 60 GHz unlicensed band (our choice-58.24 GHz).

- 2) The RF is swept with an arbitrary step (we chose 0.01 GHz) at the transmitter and values of RF power after the photodiode are stored.
- 3) RF power values are sent to the transmitter through the low datarate channel, where the frequency that resulted in maximum RF power at the output of the photodiode is selected.

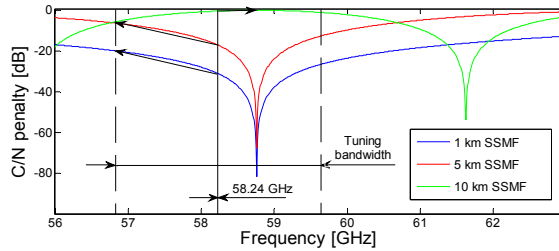


Fig. 6. An example of the algorithm performance for 1, 5 and 10 km of SSMF transmission.

Figure 6 is a close-up of a Fig. 4(b) where tuning is depicted for SSMF. Originally, frequency is set to 58.24 GHz. For 1 km and 5 km of fiber distance, the necessary frequency shift to improve the C/N ratio is the largest possible tuning shift (-1.4 GHz), however, for 10 km distance, the necessary shift is 0.52 GHz. The algorithm for DCF has the same principle of operation as depicted in Fig. 6.

Figure 7 and Fig. 8 depict the results of frequency-tuning based optimization under the constraints of tuning bandwidth (2.8 GHz as in commercially available module that was used for the experiment) and RF-spectrum allocation.

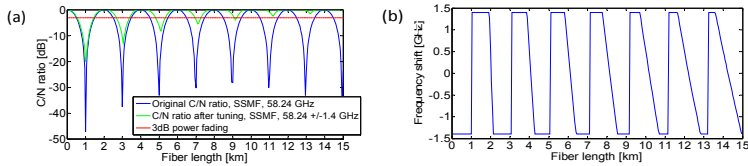


Fig. 7. (a) Improvement of C/N ratio with a frequency tuning method for SSMF, (b) the required frequency shift to produce the improvement of the C/N ratio for SSMF case.

It's important to note that the frequency tuning algorithm produces superior performance at longer lengths of fiber since as we may see from the Fig. 4(b) the frequency-dependent fading dips occur more often at longer spans of fiber. Our proposed method for CD induced RF power fading compensation brings performance at no more than 3 dB RF power penalty at the distance of around 11 km for SSMF and at the distance of 1.8 km for DCF fiber. We also see that, at lower fiber distances, maximum absolute carrier frequency shift is the preferred choice, but, as the distance increases, the algorithm selects the lower frequency shifts more often. It is due to the fact that the frequency periodicity of fading is increasing with distance that there is a smaller frequency shift required that can lead to a maximum possible improvement of RF C/N ratio inside of the tuning bandwidth.

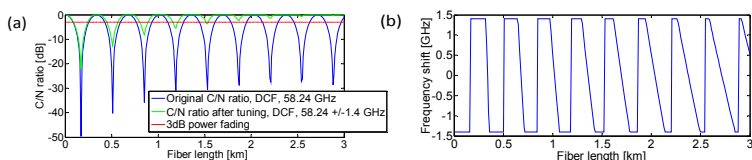


Fig. 8. (a) Improvement of C/N ratio with a frequency tuning method for DCF, (b) the required frequency shift to produce the improvement of the C/N ratio for DCF.

We show that although DCF fiber has more frequent occurrence of CD induced RF power fading, when we employ the algorithm for frequency tuning, we may achieve better performance for DCF fiber compared to the case of SSMF.

Future work includes a laboratory implementation that requires installation of automatically controlled V-band power meter storing the power values. Once the frequency is swept at the transmitter, the RF power values are stored at a power meter on the receiving side, they can then be communicated to the transmitter using an available uplink channel where the decision on appropriate frequency shift is made and a new frequency is set through the automatic control of the RF-generating board.

4. Conclusions

We experimentally demonstrated a 60 GHz DSB RoF synchronous detection link capable of transmitting 1080p uncompressed video. We studied CD induced RF degradation for DCF through experiment, simulation and analytical assessment. The experimental results have indicated severe degradation of RF carrier after photomixing in case of DCF deployment, which agrees well with simulation and analytical solution. Analytical results presented in this paper indicate that increase in absolute value of dispersion parameter, e.g. when we employ DCF, increases the periodicity of CD induced RF degradation. Based on experimental results and modeling, we then proposed an algorithm for frequency tuning of the electrical oscillator that uses an advantage of the wide 60 GHz bandwidth.

Acknowledgment

J. J. Vegas Olmos acknowledges the Marie Curie program for partly funding this research through the WISCON project.

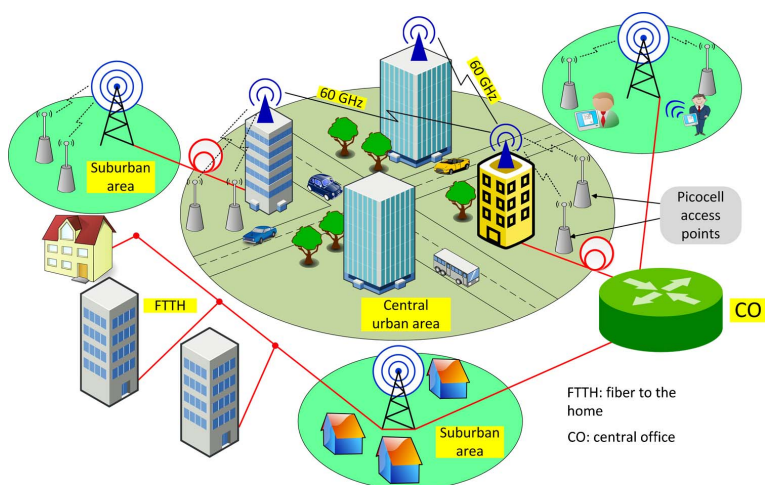
[Paper 5]

Alexander Lebedev, Xiaodan Pang, J. J. Vegas Olmos, Marta Beltran, Roberto Llorente, Søren Forchhammer, Idelfonso Tafur Monroy, "Feasibility study and experimental verification of simplified fiber-supported 60 GHz picocell mobile backhaul links," *IEEE Photon. J.*, vol. 5, no. 4, pp. 7200913, August 2013.

Feasibility Study and Experimental Verification of Simplified Fiber-Supported 60-GHz Picocell Mobile Backhaul Links

Volume 5, Number 4, August 2013

Alexander Lebedev
Xiaodan Pang
J. J. Vegas Olmos
Marta Beltrán
Roberto Llorente
Søren Forchhammer
Idelfonso Tafur Monroy



DOI: 10.1109/JPHOT.2013.2277011
1943-0655 © 2013 IEEE

Feasibility Study and Experimental Verification of Simplified Fiber-Supported 60-GHz Picocell Mobile Backhaul Links

Alexander Lebedev,¹ Xiaodan Pang,¹ J. J. Vegas Olmos,¹ Marta Beltrán,²
Roberto Llorente,² Søren Forchhammer,¹ and Idefonso Tafur Monroy¹

¹DTU Fotonik, Department of Photonics Engineering, Technical University of Denmark,
2800 Kongens Lyngby, Denmark

²Valencia Nanophotonics Technology Center, Universidad Politécnica de Valencia,
46022 Valencia, Spain

DOI: 10.1109/JPHOT.2013.2277011
1943-0655 © 2013 IEEE

Manuscript received July 5, 2013; revised July 29, 2013; accepted July 30, 2013. Date of current version August 20, 2013. The work of J. J. Vegas Olmos was supported in part by the Marie Curie Program through the WISCON project. M. Beltrán and R. Llorente were supported by the Spain National Plan TEC2012-38558-C02-01 MODAL project. Corresponding author: A. Lebedev (e-mail: alele@fotonik.dtu.dk).

Abstract: We propose and experimentally demonstrate a fiber-wireless transmission system for optimized delivery of 60-GHz radio frequency (RF) signals through picocell mobile backhaul connections. We identify advantages of 60-GHz links for utilization in short-range mobile backhaul through feasibility analysis and comparison with an alternative E-band (60–90 GHz) technology. The 60-GHz fiber-wireless-fiber setup is then introduced: two spans of up to 20 km of optical fiber are deployed and bridged by up to 4 m of wireless distance. The 60-GHz radio-over-fiber technology is utilized in the first span of fiber transmission. The system is simplified and tailored for delivery of on-off keying data signals by employing a single module for lightwave generation and modulation combined with a simplified RF downconversion technique by envelope detection. Data signals of 1.25 Gb/s are transmitted, and a bit-error-rate performance below the 7% overhead forward-error-correction limit is achieved for a range of potential fiber deployment scenarios. A spurious free dynamic range of 73 dB-Hz^{2/3} is attained for a frequency-doubling photonic RF upconversion technique. The power budget margin that is required to extend the wireless transmission distance from 4 m to a few hundred meters has been taken into account in the setup design, and the techniques to extend the wireless distance are analyzed.

Index Terms: Microwave photonics, radio over fiber, optical communications.

1. Introduction

Mobile traffic is predicted to grow at a fast pace with video and data communication playing a larger role than voice communication and boosting the capacity requirements [1], [2]. There is a strong demand for larger capacity short range backhaul links supporting picocell connections in dense urban areas [3]. In metropolitan small cell wireless backhaul for picocell wireless networks, the maximum capacity provision is essential, and the cell site spacing is limited to less than 1 km distance [3].

The 60 GHz wireless technology has been already widely adopted by industry for applications such as wireless Gigabit Ethernet bridges reaching distances up to 1 km [4]–[6] and high-definition multimedia interface (HDMI) cable replacement [7]. There is an ongoing research and industrial development in application of the 60 GHz technology for the wireless personal area networking (WPAN) [8], data center interconnects [9]–[11] and mobile backhaul links [12], [13].

Telecommunication services such as broadband compressed and uncompressed high-definition (HD) video transmission in the 60 GHz electrical only [14]–[16] and combined 60 GHz fiber-wireless setups [17]–[22] have been recently reported. Advantages of the 60 GHz links for bandwidth-demanding applications include unlicensed operation in up to 9 GHz of spectrum depending on the national wireless spectrum regulations, availability of narrow-beam compact antennas, and a high level of frequency reuse [23].

Recent industrial reports indicate the rapid progress in the 60 GHz electrical signal generation and component miniaturization [7], [8], [24]. As a result of these developments, there appears also a growing need to transport the RF signals across the optical fiber infrastructure. Photonic RF generation techniques are complementary to electronic techniques and are deployed for low-loss, low electromagnetic interference interconnection of wireless base stations (BS) to the central office (CO) over preexisting fiber infrastructure [25]. The recent development of highly linear high power photoreceivers [26] combining advancements in optoelectronics and mm-wave electronics further strengthens the potential for commercial deployment of 60 GHz fiber-wireless links.

For mm-wave radio transmission, the simplicity and low cost of BS is advantageous as utilization of the mm-wave bands would require a large number of BSs within a small geographical area. In order to simplify the BSs in a network with a fiber connection between the CO and the BS, a radio over fiber (RoF) technology was proposed. In RoF, the BSs are simplified to perform the functions of optical-to-electrical (O/E) conversion, RF amplification and filtering, while expensive mm-wave radio frequency (RF) generation and mixing are avoided at the BSs [27]–[32]. Generation of RoF signals can be performed with diverse optical components [33]–[36] and can be designed transparent to advanced modulation formats [37].

In this paper, we study the application of the 60 GHz wireless technology for providing Gigabit picocell wireless backhaul links fully integrated in a metro/access fiber network. State-of-the-art research on the fiber-wireless mobile backhaul links includes studies on microwave and E-band (60–90 GHz) technologies [38], [39]. In this work, we argue that the deployment of the 60 GHz links for fiber-supported picocell wireless backhaul is beneficial in terms of the link budget, the installation time and the capacity availability for the unlicensed use.

We propose a simplified system in which integrated distributed feedback laser and electro-absorption modulator (DFB-EAM) modules are used for the lightwave generation and data modulation in both RoF and baseband fiber links. It is important to consider the low-cost broad linewidth optical signal generation with a DFB laser in order to tailor the system for simplified on-off keying (OOK) modulation/envelope detection systems suitable for wireless Gigabit backhaul transmission. A broader linewidth of the laser is also reported to increase the threshold for the stimulated Brillouin scattering (SBS) effect [40].

Bit error rate (BER) performance below the 7% overhead forward error correction (FEC) limit for 1.25 Gbps data signal is reported for transmission through a standard single mode fiber (SSMF) link of 20 km, 4 m of wireless distance, and a second span of 20 km SSMF. Given that the wireless distance performance is only tested for up to 4 m because of laboratory space limitations, we propose and analyze methods for further wireless distance extension. In this paper, we significantly extend our work presented in [41] through the report on spurious free dynamic range (SFDR), the feasibility study, updated and extended state-of-the-art in the field and the revised conclusions.

This paper is organized as follows: In Section 2, network architecture of the proposed 60 GHz mobile backhaul system is presented. In Section 3, the feasibility of deployment of 60 GHz links for picocell mobile backhaul connections is analyzed in comparison to the E-band technology. In Section 4, the experimental setup for validation of the proposed architecture is presented. Measurements of the dynamic range of the RoF system in terms of nonlinearities are presented in Section 5. The experimental data are analyzed and the results are discussed in Section 6. Finally, we conclude the paper in Section 7.

2. Network Architecture and Potential Application Scenarios

In densely populated metropolitan areas, deployment of new mobile backhaul connections on a wire becomes prohibitive due to increased installation time and decreased economical feasibility

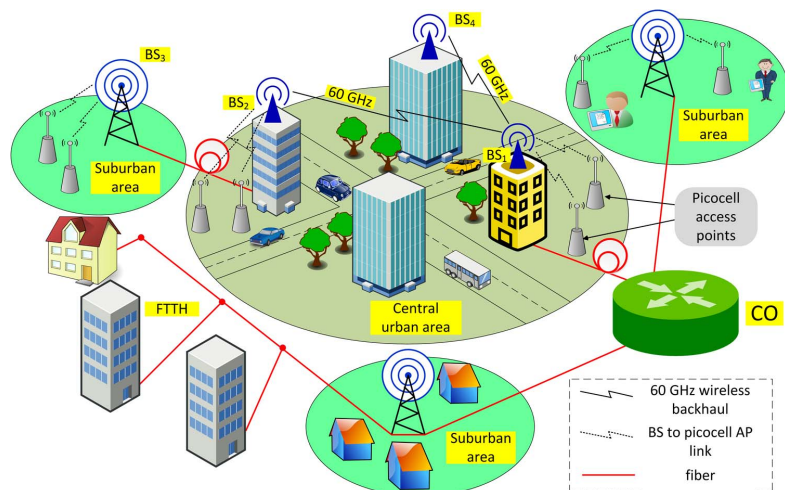


Fig. 1. Network scenario for the 60 GHz urban picocell mobile backhaul link fully supported with a diverse fiber infrastructure. CO: central office, BS: base station, FTTH: fiber to the home. BS₁ and BS₂ operate on the 60 GHz frequency, BS₃ is suggested to operate in the lower frequency licensed bandwidth.

[42]. Contrary to wired solutions, point-to-point mm-wave links can be installed quickly with wireless access points mounted on roofs, walls, or telecommunication poles. As shown in Fig. 1, BS₁–BS₂ link represents the urban mobile backhaul connection. Fiber interface to the BS₁ and the BS₂ provides connection to the CO and the suburban BS₃, respectively. BS₁, BS₂, and BS₄ are supporting multiple urban picocells, and BS₃ is supporting the suburban picocells. By adding a fiber connection from BS₂ to BS₃, a hybrid solution for metropolitan/suburban backhaul of picocell networks is provided.

We employ optical fiber for the RF signal delivery from the CO to the BS₁. The data are then transmitted wirelessly to the BS₂ on the 60 GHz RF carrier. Outside of the central urban area, backhauling is then performed using preexisting optical fiber infrastructure (BS₂–BS₃ connection). The signal arrives to the BS₃ in a baseband format where it can be subsequently upconverted for BS-access point communication.

It is also important to point out that the fiber infrastructure is expected to be shared between baseband digital systems providing broadband fiber-to-the-home (FTTH) services simultaneously with backhaul traffic delivery. This architecture can also be extended to fit the RF generation and delivery in wavelength division multiplexing (WDM) systems [43], [44], enabling simultaneous delivery of the 60 GHz RF carrier in CO–BS₁–BS₂ and CO–BS₁–BS₄ directions.

3. Feasibility Modeling of Wireless Mobile Backhaul Links Transmission in the 60 GHz Band

In this section, we perform a large-scale mm-wave channel modeling in which V (50–75 GHz) and E (60–90 GHz) band line-of-sight (LOS) outdoors RF transmission systems are compared. We argue that the use of the 60 GHz technology is advantageous for the point-to-point picocell mobile backhaul deployment on distances up to a few hundred meters.

Attenuation of the RF signals during air transmission for the LOS outdoors case consists of two major components: the free space path loss and the loss due to atmospheric absorption on molecules of oxygen and water vapor. We place the center frequencies in V- and E-band at the centers of

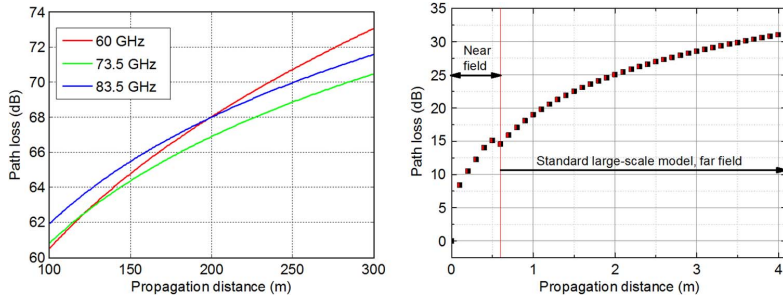


Fig. 2. The combined free space path loss and atmospheric absorption as a function of wireless transmission distance for E- and V-band outdoors links (left) and indoor V-band links (right).

spectrum windows available for unlicensed and ‘light licensing’ deployment (60 GHz, 73.5 GHz, and 83.5 GHz).

The free space path loss is calculated using the Friis transmission equation. By including the attenuation of the signal related to atmospheric absorption, we arrive to the Eq. (1) for calculation of the path loss for air transmission:

$$\alpha = 20 \log_{10} \left(\frac{4\pi R}{\lambda} \right) + L_{gas} - G_{tx} - G_{rx}, \quad (1)$$

where R (m) is a transmission distance, λ (m) is a wavelength of the signal, L_{gas} (dB) is the atmospheric absorption related attenuation, G_{tx} and G_{rx} are gain of transmitting and receiving antennas respectively (we set these to 25 dBi each). Gaseous attenuation including both water vapor and oxygen-related absorption peaks at the 60 GHz frequency reaching the value of approximately 15 dB/km due to the absorption peak on oxygen molecules, however across E-band combined attenuation on molecules of oxygen and water vapor is measured to be about 0.4 dB/km [45]. In order to compare the performance of V- and E-band systems for wireless distances suitable for dense metropolitan backhaul of picocell networks, we plot the results of numerical calculation for the combined signal attenuation in Fig. 2 (left).

From Fig. 2 (left), it can be seen that the 60 GHz transmission link shows a lower path loss in a range of about 200 m compared to the E-band solution centered at 83.5 GHz and at about 130 meters for 73.5 GHz centered E-band link, the attenuation penalty does not exceed 3 dB in the links up to 300 m. Thus, the 60 GHz links can achieve performance superior/close to the E-band links in the range up to a few hundred meters in terms of added contributions from the free space path loss and atmospheric absorption on the molecules of oxygen and water vapor.

In Fig. 2 (right) the 60 GHz path loss for indoor wireless distances is presented. We have first experimentally measured the RF attenuation in a near-field area where the standard Friis transmission equation does not apply. The Fraunhofer distance defining the border between near- and far-field propagation is calculated according to:

$$d_f = \frac{2D^2}{\lambda}, \quad (2)$$

where D is the largest dimension of an antenna, in our case it is equal to 0.039 m, and λ is a wavelength of the radio signal. The results show a close match around the Fraunhofer distance between experimentally measured values of attenuation in the near field and values calculated according to Eq. (1) in the far field.

Using the Eq. (1), we obtain that, in order to extend the wireless distance from 4 m to 300 m, 42 dB improvement in the electrical link budget is required. It is therefore critical that we design the laboratory setup capable to accommodate this requirement.

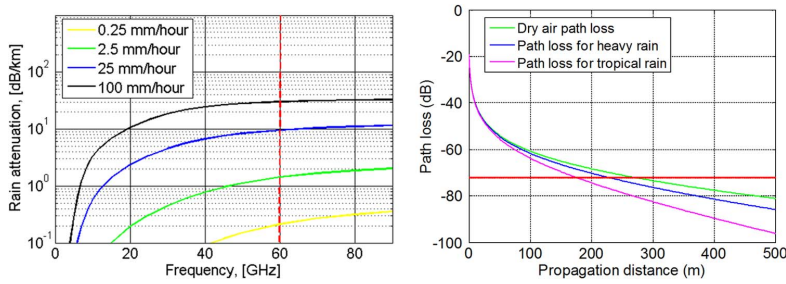


Fig. 3. Rainfall attenuation as a function of frequency (left) and combined path loss and rainfall attenuation for 60 GHz RF propagation versus required SNR level (right) as a function of wireless distance.

Another important performance criterion for wireless communication is stability of the link under the weather influence. In this paper, we analyze the influence of rain on transmission performance. An estimate of the rain attenuation is given by:

$$\gamma_R = kR^\alpha, \quad (3)$$

where γ_R (dB/km) is the specific rain-related attenuation, and R (mm/hour) is the rain rate parameter differentiating the intensity of a rainfall. The coefficients k and α are frequency dependent and may be either determined by curve-fitting equations or through a set of specified values given in Recommendation P.838-2 [46]. Rain types are separated as a ‘drizzle: 0.25 mm/hour’, a ‘light rain: 2.5 mm/hour’, a ‘heavy rain: 25 mm/hour’, and a ‘tropical rain: 100 mm/hour’ [3]. Fig. 3 (left) presents the simulation results based on the recommendation.

60 GHz links have slightly lower rainfall attenuation values compared to E-band links as depicted in Fig. 3 (left). In Fig. 3 (right) we display the effect that the ‘heavy’ and the ‘tropical’ rain will have on the operation of the 60 GHz link in terms of shortening the transmission distance for a given signal-to-noise ratio (SNR) required at the receiver. We define the limit on the path loss by the closeness of the 60 GHz RF signal power to the noise floor defined by the Johnson noise. The path loss margin β available for a given requirement on the SNR (we set SNR of 18 dB which for envelope-detected signals yields BER less than 10^{-12}), given bandwidth of the signal ($B = 2.5$ GHz), given RF power before the antenna ($P_{tx} = 10$ dBm) is then equal to:

$$\beta = P_{tx} - 10\log_{10}(1000 \times kt) - 10\log_{10}(B) - SNR, \quad (4)$$

where k is a Boltzmann’s constant, and t (K) is a room temperature. We have calculated β to be equal to 72 dB for our bitrate. The values of path loss are then calculated as a sum of (1) and (3) for antenna gain of 25 dBi. As we see in Fig. 3 (right), the influence of weather conditions shortens the reliable wireless link length, however, in order to combat this, FEC techniques are typically used [4], [6]. It is also clear from Fig. 3 (right) that the reliable link length can be extended by increasing the power at the transmitter or increasing the antenna gain.

Given the modeling results, it is clear that the 60 GHz links are a good solution for the picocell backhaul transmission systems on a distance up to a few hundred meters in terms of combined effects of the free space path loss, the atmospheric absorption and the possible rain attenuation. There are few additional aspects that have to be considered before making a choice between V- or E-band links for deployment in picocell mobile backhaul. First, V-band links provide unlicensed operation, when E-band transmission requires light licensing which may incur additional delays in the link installation time. Second, the current market costs of the equipment based on the V-band technology are lower than that of the E-band links [4]. Last, with a quick reduction of power level when the signal is following other than the LOS path, superior multipath interference immunity and high frequency reuse are enabled for 60 GHz systems.

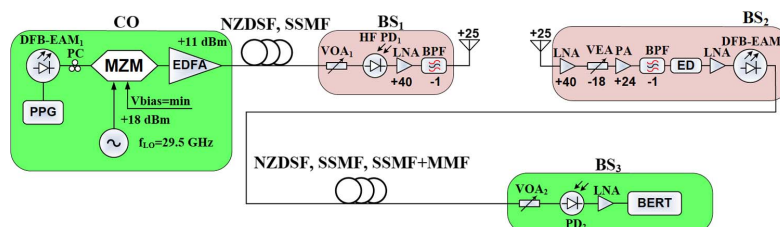


Fig. 4. Laboratory setup for a fiber-wireless-fiber 60 GHz link. DFB-EAM: distributed feedback laser integrated with an electro-absorption modulator, PPG: pulse pattern generator, MZM: Mach-Zehnder modulator, LO: local oscillator, EDFA: Erbium doped fiber amplifier, HF PD: high frequency photodiode, LNA: low noise amplifier, BPF: bandpass filter, VOA: variable optical attenuator, VEA: variable electrical attenuator, PA: power amplifier, ED: envelope detector, BERT: bit error rate tester, CO: central office, BS: base station, SSF: standard single mode fiber, NZDSF: non-zero dispersion shifted fiber, MMF: multimode fiber.

We believe that the feasibility study presented in this section supports the relevance of studying the 60 GHz links for picocell mobile backhaul. In the next sections, a simplified 60 GHz fiber-wireless-fiber setup is built, and its performance is characterized experimentally.

4. Experimental Setup Description

The schematics of the experimental setup of the 60 GHz fiber-wireless picocell mobile backhaul link including two spans of fiber and a single 60 GHz wireless link in between is presented in Fig. 4. Four subsystems are emulated: a CO transmitter and three BSs (BS_1 – BS_3). RoF generation and data modulation are located at the CO; BS_1 performs the O/E conversion and amplifies the 60 GHz RF signal before the radiation, BS_2 performs the RF downconversion and remodulation onto the lightwave. BS_3 recovers the original baseband data by O/E conversion.

A DFB-EAM module was used to produce a lightwave at a wavelength $\lambda = 1550$ nm with 4 dBm of optical power. A 1.25 Gbps nonreturn to zero (NRZ) pseudorandom binary sequence (PRBS) with a word length of $2^{15} - 1$ generated by a pulse pattern generator (PPG) was directly modulated onto the lightwave at the DFB-EAM₁. The use of the DFB-EAM for lightwave generation and data modulation relaxes requirements for a peak-to-peak voltage of the electrical signal driving the modulator and simplifies the overall system installation. Chirp effects common to EAM technology were controlled through application of an optimal voltage.

RF modulation of the lightwave was performed using a single-drive Mach-Zehnder modulator (MZM). A polarization controller (PC) was placed before the MZM in order to minimize the polarization-dependent loss. The MZM was biased at a minimum transmission point and driven by a high-power sinusoidal local oscillator (LO) RF (+18 dBm, $f_{LO} = 29.5$ GHz), resulting in a suppression of the original optical carrier and increase of optical power in upper and lower sidebands separated by twice the original RF frequency $2f_{LO}$. This technique for generation of RoF signals is known as an optical carrier suppression (OCS) technique [47]. By using the OCS method, the requirements for high frequency RF components at the CO are alleviated, and high quality phase noise performance is obtained due to the fact that upper and lower sidebands are produced by the same laser. The optical spectrum of the generated double-sideband with a suppressed carrier (DSB-SC) signal is presented in Fig. 5 (left). A suppression of the optical carrier relative to the RF-produced sidebands of approximately 20 dB was achieved constrained by both the polarization alignment and the extinction ratio of the modulator.

The signal was subsequently coupled into an Erbium doped fiber amplifier (EDFA) in order to improve the power budget before the launch into the fiber. Subsequently, fiber transmission was performed through SSF and non-zero dispersion shifted fiber (NZDSF). We detected the electrical RF signal through photomixing at a 75 GHz bandwidth p-i-n photodiode (PD₁). The variable optical attenuator (VOA₁) was placed before the PD₁ in order to control the power entering the PD₁. After

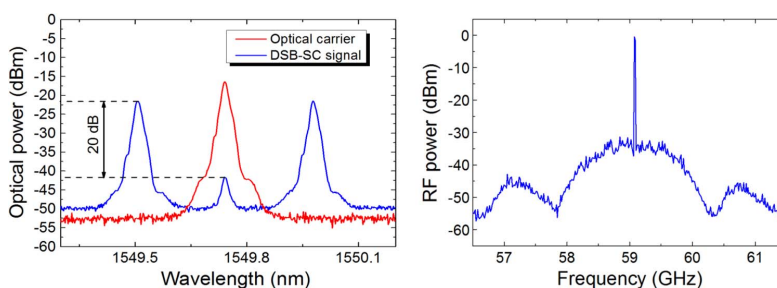


Fig. 5. Optical spectra of the transmitted signal (left) and RF spectrum of the signal before radiation (right).

photomixing, the 60 GHz RF signal was amplified with a 40 dB gain double-stage low noise amplifier (LNA), passed through a bandpass filter and radiated with a horn antenna (+25 dBi gain). The spectrum of the modulated RF signal is depicted in Fig. 5 (right). The path loss for 4 m wireless distance including the combined gain of antennas (50 dBi) is equal to approximately 31 dB which was calculated using the Eq. (1) presented in Section 3. The equivalent omnidirectional path loss (antenna gain is excluded) is equal to 81 dB.

After reception with an equivalent antenna, the signal was amplified with a 40 dB gain LNA. We have then employed a variable electrical attenuator (VEA) and a power amplifier (PA) in order to emulate the effect of the possible wireless distance extension on the system performance. The VEA has been set to attenuate the signal by 18 dB throughout the measurements. The signal was then filtered and the data signal were downconverted from RF into baseband at a zero-biased Schottky diode serving as an envelope detector (ED). We refer the readers to [48] for a thorough study on basic principles of Schottky diodes' operation. Main advantage of the envelope detection technique is that it allows performing the RF signal downconversion without using an RF LO and a phase locked loop circuitry required for the synchronous mixing detection technique. Following the ED, the signal was amplified to bring the peak-to-peak voltage level of the signal to a value required for effective driving of the DFB-EAM₂.

After the subsequent remodulation on the lightwave, the signal was passed through diverse types of optical fiber. We have included multimode fiber (MMF) in a second span of fiber transmission in order to address the fiber distribution in network connections where the metro/access delivery is integrated with MMF-wired local area network (LAN) distribution. The baseband electrical data were finally recovered with a 10 GHz bandwidth p-i-n PD. After amplification, it was fed to a BER tester (BERT) for further signal quality evaluation.

5. Characterization of the SFDR

An SFDR measurement is needed in order to quantify performance of the RoF system in terms of nonlinearities of link components, i.e. appearance of spurious harmonics of the RF signal that are located in the bandwidth of data modulation and contribute to BER deterioration. The SFDR of the system is the range between the smallest signal that can be transmitted and received by the system and the largest signal that can be introduced into the system without creating distortions above the noise floor after detection in the bandwidth of interest [49]. SFDR gives better system performance estimate than maximum achievable SNR which is constrained by noise floor and saturation only. Given that in order to extend the wireless link distance for outdoor scenarios we need to improve the power budget, we have measured the SFDR including EDFA and increased optical power into the PD.

In Fig. 6, we present the setup for measuring the SFDR of the modulation and upconversion block in the system. We built the SFDR setup based on a part of the general setup—a link between the CO and the BS₁. The signal is then analyzed directly on the output of the PD.

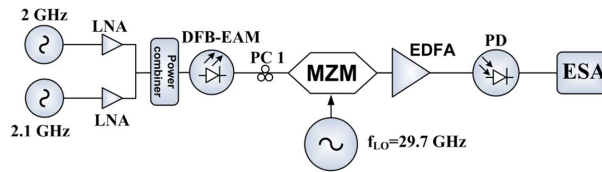


Fig. 6. Laboratory setup for measuring SFDR. LNA: low noise amplifier, DFB-EAM: distributed feedback laser integrated with electro absorption modulator, PC: polarization controller, LO: local oscillator, MZM: Mach-Zehnder modulator, EDFA: Erbium doped fiber amplifier, PD: photodiode, ESA: electrical spectrum analyzer.

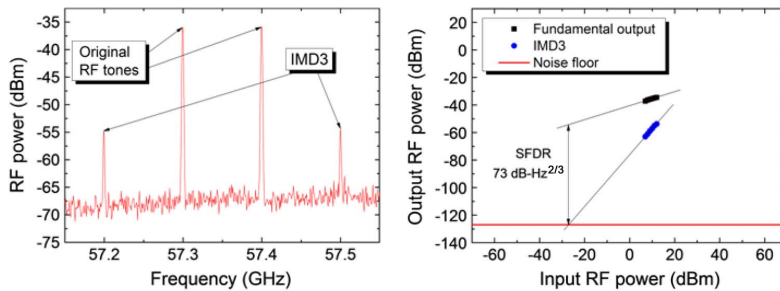


Fig. 7. SFDR measurement for a chosen RF generation technique.

Two RF tones modulating the DFB-EAM were located at 2 GHz (f_1) and 2.1 GHz (f_2) RF frequency; the f_{LO} was set to 29.7 GHz. According to [49], third order intermodulation (IMD3) components are expected to be located at $59.4 \text{ GHz} + 2 \times f_1 - f_2 = 57.5 \text{ GHz}$ and $59.4 \text{ GHz} + 2 \times f_2 - f_1 = 57.2 \text{ GHz}$. Fig. 7 (left) shows the RF spectra including the original RF tones and IMD3 tones. The optical power at the PD was set to 5 dBm throughout the SFDR measurement. It should be noted that the SFDR was measured for a transmitter including EDFA, which increases the noise level at the PD, but gives characterization of the system suitable for extended optical and wireless transmission.

Increasing RF power modulating the lightwave improves the SNR, however, the IMD3 distortion is increasing at a faster rate than the signal. As seen in Fig. 7 (right), we achieved the SFDR value of $73 \text{ dB-Hz}^{2/3}$ that is comparable to results obtained by other authors who use similar frequencies of two RF tones [50]. The obtained value of SFDR provides sufficient margin in terms of nonlinearity and sets the limit on system's scalability for a range of RF powers to be transmitted through the optical fiber.

We have reported on SFDR of the system for increased shot noise (by setting the optical power into the PD to +5 dBm) and included EDFA. EDFA deployment is reported to decrease the SFDR value of the system [49], but it is a necessity in order to improve the power budget for fiber-wireless reach extension. By setting maximum constraints to SFDR, we present the limit on the system performance.

6. Results and Discussion

In this section, we describe the setup performance under a constraint of decreasing optical power on the output of the second span of optical fiber transmission; at the same time, optical power impinging the PD₁ is kept constant at -7 dBm. The curve depicting the generated 60 GHz RF power as a function of carrier suppression is measured to support the link budget discussion. The phase noise performance of the photonically generated RF carrier is also analyzed including

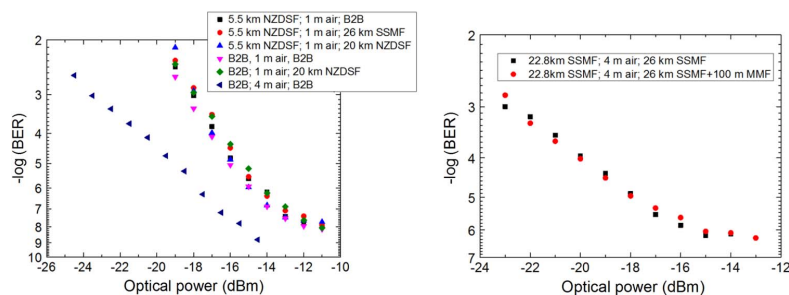


Fig. 8. BER as a function of optical power measured at the PD₂ for B2B/5.5 km NZDSF (left) and 22.8 km SSMF (right) of fiber distance in the first span.

measurements for different types of optical fiber in the first fiber transmission span. BER has been used as a main criterion of system performance constrained by the values of optical power impinging the PD₂, the length of fiber and the wireless transmission distance.

First, we present the results with relaxed requirements for the first span of fiber transmission in terms of dispersion in Fig. 8 (left). We transmit the signal back-to-back (B2B) or employ 5.5 km NZDSF in the first fiber span of the setup and fiber of different lengths and types in the second span. Fig. 8 (left) shows that deployment of SSMF and NZDSF in the second span of transmission introduces no penalty compared to B2B case; however, in all three cases of fiber deployment (B2B, SSMF, NZDSF) in the second span, we observed an error floor on BER performance at approximately 10^{-8} level for 1 m of wireless distance. We suggest that the error floor is not related to chromatic dispersion (CD) given that the distortion of 60 GHz RoF 1.25 Gbps data signal due to CD can be considered negligible in 5.5 km NZDSF and absent in B2B transmission case. We suggest that the error floor is therefore related to degradation of the SNR in the system and to the modulation efficiency of the DFB-EAM₂ which depends on the peak-to-peak voltage level of the baseband electrical signal recovered with ED. Optical B2B curve for 4 m wireless distance in Fig. 8 (left) indicates that, by extending the wireless distance, we are improving the DFB-EAM₂ modulation performance, and the error floor is avoided for extended wireless distances for the same SNR before remodulation on the lightwave. We therefore conclude that presence of the error floor is not related to performance of the wireless channel, i.e. only extension of the wireless distance, and can be mitigated by installing an automatic level control circuit before remodulation on the DFB-EAM₂ to preserve high modulation efficiency and avoid overmodulation.

We then proceeded to emulate deployment of larger distances of fiber in the first span of transmission. Fig. 8 (right) indicates that, when we deploy about 20 km of fiber in both spans, an error floor is present at about a 10^{-6} level. Presence of an error floor is now related to CD impairing the signal in the first span of transmission. When two sidebands are photomixed at the PD, the signal suffers from intersymbol interference caused by a delay between the pulses transmitted on upper and lower sidebands which is reported as a 'bit walk-off' in [51]. However, the periodic dispersion-induced RF power fading is eliminated when the optical carrier is suppressed [51]. For both 1 m and 4 m wireless transmission cases employing fibers with different values of dispersion (NZDSF, SSMF), we demonstrate BER performance well below the 2×10^{-3} limit corresponding to a 7% FEC overhead. BER degradation due to the time shifting of the pulses in the upper and lower sidebands in the first fiber span can be overcome by using a single sideband modulation or diverse CD compensation techniques, however this would increase the setup complexity. Overall, considering the original goal of building a simplified setup, the fact that the penalty is also related to multiple noise sources, and the fact that the FEC is typically implemented in the 60 GHz links [4], [6], we believe that our setup will be a suitable solution for simplified fiber-supported 60 GHz picocell mobile backhaul links.

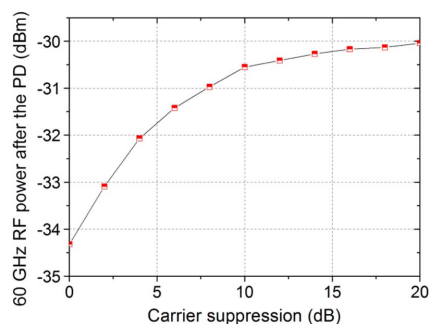


Fig. 9. 60 GHz RF power on the PD output as a function of carrier suppression of the DSB-SC signal.

We have investigated SSMF deployment interfaced with MMF (Fig. 8, right), an appropriate scenario for this combination will be the interface between the access network deployed using SSMF and LAN using MMF. Lightwave was centrally launched from SSMF into MMF which enables mode filtering by exciting only a limited number of lower order modes in the MMF [52]. Intermodal dispersion is thus mitigated because in this case coupling between high and low order modes is reduced significantly. On the receiving side, MMF has been interfaced to the PD by a short patchcord of SSMF (used 75 GHz bandwidth PD only had the SSMF interface) by using which we recover the lowest-order mode (LP_{01}) which implies higher power loss on coupling from MMF to SSMF.

RoF systems in general suffer from the high loss on O/E and E/O conversion due to the resistive impedance matching being an issue at both the transmitter and the receiver. In Fig. 9, we depict power of the 60 GHz RF signal as a function of the sideband-to-carrier suppression ratio which was varied by applying a changing bias voltage. As depicted in Fig. 9, in our system, high power 30 GHz RF signal (+18 dBm) applied at the E/O conversion point is subsequently recovered after photomixing as a -30 dBm 60 GHz RF signal for optimized value of 20 dB carrier suppression and a fixed PD₁ input optical power of 0 dBm. 1 dB reduction in optical power entering the PD will result in 2 dB reduction in the 60 GHz RF power. Thus, at -7 dBm optical power entering the PD, RF at the PD output will be equal to -44 dBm.

In order to extend the wireless link length from 4 m to 300 m of wireless distance, we have to address the necessary provision of 42 dB power margin compared to the link budget of 4 m wireless distance as calculated in Section 3. There are few generally applied techniques to improve the electrical link budget and increase the wireless transmission distance. First, a common technique is to use antennas of higher gain. For V-band, antennas of 42 dBi gain are commercially available which may simultaneously add 34 dB to a power budget of the link. Second, the link distance can be extended through amplification. VEA-PA combination that we employ at the BS₂ may be adjusted to bring the additional 18 dB power without introduction of noise by setting the VEA attenuation to 0. The noise figure of the PA is already a part of the link impairments. Depending on link design, PA might be also offset to the transmitting side. These two methods combined bring a gain of 52 dB to the link that surpasses the required margin of 42 dB. However, it must be taken into account for the link design that, when employing a higher gain antenna, the Fraunhofer distance will increase. For a commercially available lens horn antenna of 42 dBi gain with a diameter of 0.25 m, the Fraunhofer distance is equal to 25 m.

In this work, we study transmission of the OOK signals. However, transparency for higher order modulation formats is an important design criterion for RoF links. High performance of the RF oscillator in terms of phase noise is required to enable such transparency. DSB-SC RoF setups are known to have an excellent performance in terms of phase noise because the sidebands are produced by the same laser source and thus are correlated with each other. We depict the phase

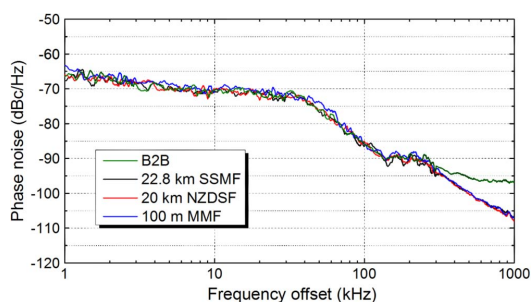


Fig. 10. Phase noise of photonically generated 60 GHz RF signals.

noise performance of the 60 GHz signal before radiation in Fig. 10. We observe a negligible difference in the RF phase noise for generation of the signals that employ different types of fiber benchmarked against B2B optical transmission with the phase noise approximately equal to -85 dBc/Hz at a 100 kHz offset. We conclude that fiber transmission in our setup does not deteriorate the RF phase noise performance. The setup performance is therefore constrained with the phase noise degradation due to multiplication only [53]. In order to enable the higher spectral and power efficiency modulation formats, synchronous downconversion of the RF-modulated signal has to be performed such as in [20] and [54].

7. Conclusion

We experimentally demonstrate the 60 GHz fiber-wireless-fiber communication system enabling the Gigabit picocell mobile backhaul links. Suitability of the proposed approach to diverse fiber deployment scenarios has been assessed. BER performance below the 7% overhead FEC limit is reached for 1.25 Gbps data signals transmission through up to 4 m wireless distance and up to 20 km of SSMF interfacing transmitting and receiving 60 GHz BSs. We simplify the system through the use of the integrated DFB-EAM module in both fiber spans of transmission. The system is further simplified through the use of the ED RF detection technique achieving passive downconversion and eliminating the need for the design of synchronization hardware. 73 dB-Hz^{2/3} SFDR is reported when the EDFA is included as a part of an optical transmitter. Phase noise performance indicates high potential of the system for transmission of advanced modulation formats. Future work is directed towards combating the error floor in the system which will include the fiber-wireless-fiber transmission when RF is generated through photomixing of lightwaves produced by two free running lasers. We suggest that the work can be extended by direct comparison of experimental performance of V- and E-band systems and the SFDR measurement for the link including fiber transmission.

Acknowledgment

The authors would like to acknowledge the support from Radiometer Physics GmbH for loan of V-band amplifiers.

References

- [1] Cisco white paper, "Cisco visual networking index: Global mobile data traffic forecast update, 2012–2017" 2012. [Online]. Available: http://www.cisco.com/en/US/solutions/collateral/ns341/ns525/ns537/ns705/ns827/white_paper_c11-520862.pdf
- [2] Traffic and market data report, Ericsson, Stockholm, Sweden, 2011, Ericsson white paper.
- [3] J. Wells, *Multi-Gigabit Microwave and Millimeter-Wave Wireless Communications*. Norwood, MA, USA: Artech House, 2010.
- [4] Gigabit wireless applications using 60 GHz radios, Bridgewater, Santa Clara, CA, USA, 2006, Bridgewater whitepaper.

- [5] A. Mathew, *Local Area Networking Using MillimetreWaves*. Acton, MA, USA: NewLANs, Inc., 2005.
- [6] AIRLINX Communications, Inc. specification datasheet, "GigaLink 6221/6421/6451" 2013, (AIRLINX Communications, Inc.).
- [7] *WirelessHD Specification Version 1.1 Overview*, WirelessHD, Morgan Hill, CA, USA, 2010, WirelessHD white paper.
- [8] WiGig white paper, Defining the future of multi-gigabit wireless communication, Jul. 2010, (WiGig alliance).
- [9] K. Ramachandran, R. Kokku, R. Mahindra, and S. Rangarajan, "60 GHz data-center networking: Wireless worry less?" NEC, Princeton, NJ, USA, Tech. Rep., 2008.
- [10] S. Kandula, J. Padhye, and P. Bahi, "Flyways to de-congest data center networks," in *Proc. 8th ACM Workshop Hot Topics Netw.*, 2009, pp. 1–6.
- [11] K. Kawasaki, Y. Akiyama, K. Komori, M. Uno, H. Takeuchi, T. Itagaki, Y. Hino, Y. Kawasaki, K. Ito, and A. Hajimiri, "A millimeter-wave intra-connect solution," in *Proc. IEEE Int. Solid-State Circuits Conf.*, 2010, pp. 414–415.
- [12] Ceragon application note, Wireless backhaul solutions for small cells, (Ceragon).
- [13] Sub10 Systems Limited White Paper, "60GHz metro cell and small cell backhauling for service providers," 2011, (Sub10 Systems Limited).
- [14] H. Singh, J. Oh, C. Kweon, X. Qin, H. Shao, and C. Ngo, "A 60 GHz wireless network for enabling uncompressed video communication," *IEEE Commun. Mag.*, vol. 46, no. 12, pp. 71–78, Dec. 2008.
- [15] Z. Lan, J. Wang, C.-S. Sum, T. Baykas, C. Pyo, F. Kojima, H. Harada, and S. Kato, "Unequal error protection for compressed video streaming on 60 GHz WPAN system," in *Proc. Int. Wireless Commun. Mobile Comput. Conf.*, 2008, pp. 689–693.
- [16] H. Singh, X. Qin, H. Shao, C. Ngo, C. Kwon, and S. S. Kim, "Support of uncompressed video streaming over 60 GHz wireless networks," in *Proc. 5th IEEE Consum. Commun. Netw. Conf.*, 2008, pp. 243–248.
- [17] A. Chowdhury, H.-C. Chien, Y.-T. Hsueh, and G.-K. Chang, "Advanced system technologies and field demonstration for in-building optical-wireless network with integrated broadband services," *J. Lightw. Technol.*, vol. 27, no. 12, pp. 1920–1927, Jun. 2009.
- [18] A. Lebedev, T. T. Pham, M. Beltrán, X. Yu, A. Ukhanova, R. Llorente, and I. Taur Monroy, "Optimization of high-definition video coding and hybrid fiber-wireless transmission in the 60 GHz band," *Opt. Exp.*, vol. 19, no. 26, pp. 895–904, Dec. 2011.
- [19] A. Lebedev, J. J. Vegas Olmos, X. Pang, S. Forchhammer, and I. Taur Monroy, "Demonstration and comparison study for V- and W-band real-time high-definition video delivery in diverse fiber-wireless infrastructure," *Fiber Integr. Opt.*, vol. 32, no. 2, pp. 93–104, 2013.
- [20] A. Lebedev, J. J. Vegas Olmos, M. Iglesias, S. Forchhammer, and I. T. Monroy, "Enabling uncompressed video transmission in double-sideband 60 GHz radio-over-fiber links," in *Proc. IEEE IPC*, 2012, pp. 578–579, Paper WS2.
- [21] Z. Tang and S. Pan, "Transmission of 3-Gb/s uncompressed HD video in a optoelectronic-oscillator-based radio over fiber link," in *Proc. IEEE 13th Topical Meet. SiRF*, 2013, pp. 219–221.
- [22] J. Guillery, A. Pizzinat, P. Guignard, F. Richard, B. Charbonnier, P. Chanclou, and C. Algani, "Simultaneous implementation of gigabit Ethernet, RF TV and radio mm-wave in a multifunction home area network," presented at the 37th Eur. Conf. Exhibition Optical Communication (ECOC), Geneva, Switzerland, 2011, Paper We.7.C.3.
- [23] S.-K. Yong, *60 GHz Technology for Gbps WLAN and WPAN: From Theory to Practice*. Hoboken, NJ, USA: Wiley, 2011.
- [24] Siversima application note, "58–63 GHz V-band converter," 2013, (Siversima).
- [25] C. Lim, A. Nirmalathas, M. Bakaul, P. Gamage, K.-L. Lee, Y. Yang, D. Novak, and R. Waterhouse, "Fiber-wireless networks and subsystem technologies," *J. Lightwave Technol.*, vol. 28, no. 4, pp. 390–405, Feb. 2010.
- [26] S. Feddenwitz, C. Leonhardt, J. Honecker, P. Muller, and A. Steffan, "A high linear and high power photoreceiver suitable for analog applications," in *Proc. IEEE IPC*, 2012, pp. 308–309, Paper TuL3.
- [27] K. Xu, X. Sun, J. Yin, H. Huang, J. Wu, X. Hong, and J. Lin, "Enabling ROF technologies and integration architectures for in-building optical-wireless access networks," *IEEE Photon. J.*, vol. 2, no. 2, pp. 102–112, Apr. 2010.
- [28] A. Kanno, P. T. Dat, T. Kuri, I. Hosako, T. Kawanishi, Y. Yoshida, Y. Yasumura, and K. Kitayama, "Coherent radio-over-fiber and millimeter-wave radio seamless transmission system for resilient access networks," *IEEE Photon. J.*, vol. 4, no. 6, pp. 2196–2204, Dec. 2012.
- [29] X. Zhang, B. Hraimel, and K. Wu, "Breakthroughs in optical wireless broadband access networks," *IEEE Photon. J.*, vol. 3, no. 2, pp. 331–336, Apr. 2011.
- [30] X. Li, J. Yu, Z. Dong, and N. Chi, "Photonics millimeter-wave generation in the E-band and bidirectional transmission," *IEEE Photon. J.*, vol. 5, no. 1, p. 7 900 107, Feb. 2013.
- [31] A. M. Zin, M. S. Bongsu, S. M. Idrus, and N. Zulkifli, "An overview of radio-over-fiber network technology," in *Proc. IEEE Int. Conf. Photon.*, 2010, pp. 1–3, Paper ICP2010-85.
- [32] M. C. Parker, S. D. Walker, R. Llorente, M. Morant, M. Beltran, I. Möllers, D. Jäger, C. Vazquez, D. Montero, I. Libran, S. Mikroulis, S. Karabetos, and A. Bogris, "Radio-over-fibre technologies arising from the building the future optical network in Europe (BONE) project," *IET Optoelectron.*, vol. 4, no. 6, pp. 247–259, Dec. 2010.
- [33] M. Beltrán, J. B. Jensen, R. Llorente, and I. Taur Monroy, "Experimental analysis of 60-GHz VCSEL and ECL photonic generation and transmission of impulse-radio ultra-wideband signals," *IEEE Photon. Technol. Lett.*, vol. 23, no. 15, pp. 1055–1057, Aug. 2011.
- [34] X. Pang, M. Beltrán, J. Sánchez, E. Pellicer, J. J. Vegas Olmos, R. Llorente, and I. Taur Monroy, "DWDM fiber-wireless access system with centralized optical frequency comb-based RF carrier generation," presented at the Conf. Optical Fiber Communication, Nat. Fiber Optic Engineers Conf., Anaheim, CA, USA, 2013, Paper JTh2A.56.
- [35] X. Pang, A. Caballero, A. Dogadaev, V. Arlunno, L. Deng, R. Borkowski, J. S. Pedersen, D. Zibar, X. Yu, and I. Taur Monroy, "25 Gbit/s QPSK hybrid fiber-wireless transmission in the W-band (75–110 GHz) with remote antenna unit for in-building wireless networks," *IEEE Photon. J.*, vol. 4, no. 3, pp. 691–698, Jun. 2012.
- [36] X. Pang, X. Yu, Y. Zhao, L. Deng, D. Zibar, and I. Taur Monroy, "Experimental characterization of a hybrid fiber-wireless transmission link in the 75 to 110 GHz band," *Opt. Eng.*, vol. 51, no. 4, pp. 045004-1–045004-5, Apr. 2012.

- [37] A. Caballero, D. Zibar, R. Sambaraju, J. Martí, and I. T. Monroy, "High-capacity 60 GHz and 75–110 GHz band links employing all-optical OFDM generation and digital coherent detection," *J. Lightwave Technol.*, vol. 30, no. 1, pp. 147–155, Jan. 2012.
- [38] T. P. McKenna, J. A. Nanzer, M. L. Dennis, and T. R. Clark, "Fully fiber-remoted 80 GHz wireless communication with multi-subcarrier 16-QAM," in *Proc. IEEE IPC*, 2012, pp. 576–577, Paper WS1.
- [39] G. Shen, R. S. Tucker, and C.-J. Chae, "Fixed mobile convergence architectures for broadband access: Integration of EPON and WiMAX," *IEEE Commun. Mag.*, vol. 45, no. 8, pp. 44–50, Aug. 2007.
- [40] M. Sauer, A. Kobayakov, and A. B. Ruffin, "Radio-over-fiber transmission with mitigated stimulated Brillouin scattering," *IEEE Photon. Technol. Lett.*, vol. 19, no. 19, pp. 1487–1489, Oct. 2007.
- [41] A. Lebedev, X. Pang, J. J. Vegas Olmos, M. Beltran, R. Llorente, S. Forchhammer, and I. Tafur Monroy, "Fiber-supported 60 GHz mobile backhaul links for access/metropolitan deployment," in *Proc. ONDM*, 2013, pp. 190–193.
- [42] SKYFIBER whitepaper, "Breaking the backhaul bottleneck: How to meet your backhaul capacity needs while maximizing revenue," 2012, (SKYFIBER).
- [43] J. Yu, Z. Jia, L. Yi, Y. Su, G.-K. Chang, and T. Wang, "Optical millimeter-wave generation or up-conversion using external modulators," *IEEE Photon. Technol. Lett.*, vol. 18, no. 1, pp. 265–267, Jan. 2006.
- [44] K. Kojucharow, M. Sauer, H. Kaluzni, D. Sommer, F. Poegel, W. Nowak, A. Finger, and D. Ferling, "Simultaneous electrooptical upconversion, remote oscillator generation, and air transmission of multiple optical WDM channels for 60-GHz high-capacity indoor system," *IEEE Trans. Microw. Theory Tech.*, vol. 47, no. 12, pp. 2249–2256, Dec. 1999.
- [45] ITU-R P.676-9 Recommendation (2012) Attenuation by atmospheric gases.
- [46] ITU-R P.838-2 Recommendation (2003) Specific attenuation model for rain for use in prediction methods.
- [47] J. J. O'Reilly, P. M. Lane, R. Heidemann, and R. Hofstetter, "Optical generation of very narrow linewidth millimeter wave signals," *Electron. Lett.*, vol. 28, no. 25, pp. 2309–2311, Dec. 1992.
- [48] Skyworks application note Mixer and detector diodes," 2008, (Skyworks).
- [49] C. H. Cox, *Analog Optical Links*. New York, NY, USA: Cambridge Univ. Press, 2004.
- [50] C. S. Park, Y.-K. Yeo, and L. C. Ong, "Demonstration of the GbE service in the converged radio-over-fiber/optical networks," *J. Lightw. Technol.*, vol. 28, no. 16, pp. 2307–2314, Aug. 2010.
- [51] C. Lim, K.-L. Lee, A. Nirmalathas, D. Novak, and R. Waterhouse, "Impact of chromatic dispersion on 60 GHz radio-over-fiber transmission," in *Proc. 21st Annu. Mee. IEEE Lasers Electro-Optics Soc.*, 2008, pp. 89–90, Paper MJ5.
- [52] I. Gasulla and J. Capmany, "1 Tb/s-km multimode fiber link combining WDM transmission and low-linewidth lasers," *Opt. Exp.*, vol. 16, no. 11, pp. 8033–8038, May 2008.
- [53] G. Qi, J. Yao, J. Seregelyi, and S. Paquet, "Phase-noise analysis of optically generated millimeter-wave signals with external optical modulation techniques," *J. Lightw. Technol.*, vol. 24, no. 12, pp. 4861–4875, Dec. 2006.
- [54] A. Lebedev, J. J. Vegas Olmos, M. Iglesias, S. Forchhammer, and I. Tafur Monroy, "A novel method for combating dispersion induced power fading in dispersion compensating fiber," *Opt. Exp.*, vol. 21, no. 11, pp. 13 617–13 625, Jun. 2013.

[Paper 6]

Alexander Lebedev, Xiaodan Pang, J. J. Vegas Olmos, Søren Forchhammer, Idelfonso Tafur Monroy, "Simultaneous 60 GHz RoF Transmission of Lightwaves Emitted by ECL, DFB, and VCSEL," IEEE Photon. Technol. Lett., submitted.

Simultaneous 60 GHz RoF Transmission of Lightwaves Emitted by ECL, DFB, and VCSEL

Alexander Lebedev, Xiaodan Pang, J.J. Vegas Olmos, Søren Forchhammer,
and Idelfonso Tafur Monroy

Abstract—Simultaneous 60 GHz radio over fiber upconversion and fiber transmission of lightwaves produced by an external cavity laser (ECL), a distributed feedback (DFB) laser, and a C-band vertical cavity surface emitting laser (VCSEL) is demonstrated. 1.25 Gbps data signals are transmitted on each of the lightwaves attaining a bit error rate performance below 10^{-9} level. Carrier suppression of 20 dB is achieved simultaneously for all three lightwaves placed in a wide wavelength range. The 10^{-9} receiver sensitivity level for detection of three lightwaves falls in a <3 dB region. Reported close performance of the investigated techniques enables diversification of options for lightwave generation in mm-wave fiber-wireless networks.

Index Terms—Millimeter wave communication, optical fiber communication.

I. INTRODUCTION

GLOBAL INTERNET traffic is predicted to grow threefold by 2017 [1] driven by high-definition (HD) real-time video streaming, ultrafast data download and teleconferencing [1]. Bandwidth scarcity in the microwave region has led to standardization of new unlicensed bands in the millimeter wave (mm-wave), particularly around the 60 GHz frequency [2]. In mm-wave bands, distributed antenna systems (DAS) architecture is a preferred approach for placement of base stations (BS) and their interconnection to the central office (CO) [3] as the count of BSs is increasing. Radio over fiber (RoF) technology is a physical layer implementation of DAS for hybrid fiber-wireless systems.

In this work, we study the 60 GHz RoF upconversion and delivery of diverse multiple lightwaves by using a single local oscillator (LO) at the CO in order to decrease the quantity of costly mm-wave RF electronic components at the CO. Furthermore, it is beneficial to test low-cost lightwave generation techniques and diversify the set of lightwave generation options in relation to the targeted applications. Numerous schemes have been previously proposed for simultaneous RF upconversion of multiple optical lightwaves in wavelength division multiplexed (WDM) systems [4–6]. Electro-absorption modulators (EAM) [4] and Mach-Zehnder

modulators (MZM) [6] have been used for this purpose in 24 GHz [4], 40 GHz [5] and 60 GHz [6] RoF systems. In this Letter, we investigate simultaneous 60 GHz RoF generation and fiber transmission of three lightwaves produced by an external cavity laser (ECL), a distributed feedback laser integrated with an electro-absorption modulator (DFB-EAM) and a vertical cavity surface emitting laser (VCSEL).

We have previously reported on the hybrid fiber-wireless systems for indoor wireless signal distribution including air propagation of the RF signal [7]. 60 GHz RoF outdoors setups have also recently been demonstrated reaching 78 m wireless distance [8, 9]. The novelty of the present paper is in studying the simultaneous upconversion of lightwaves with diverse performance that might potentially serve in both indoor and outdoor cases.

The proposed network scenario is presented in Fig. 1. WDM lightwaves are modulated by the RF signal and launched into a single fiber by means of wavelength filtering at the CO. The low-cost lightwave generation techniques (DFB, VCSEL) can be assigned for the RF signal delivery to the in-building wireless personal area networks when the air propagation distance does not exceed several meters. Conversely, higher performance techniques (ECL) may be used for scenarios with a higher constraint on power budget such as outdoors connections.

This Letter is organized as follows: in Section 2, the experimental setup is described and analyzed, in Section 3, the results are presented and discussed, and a summary of the paper is given in Section 4.

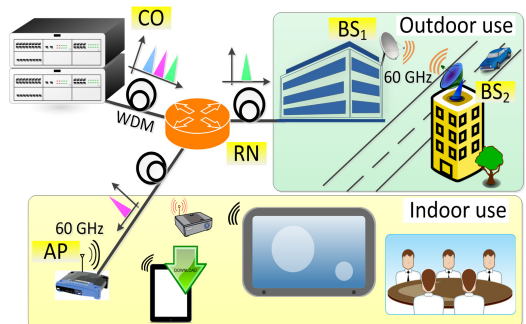


Figure 1. Network scenario for simultaneous photonic RF upconversion of multiple lightwaves for indoor and outdoor use.

This paragraph of the first footnote will contain the date on which you submitted your paper for review.

Authors are with DTU Fotonik – Department of Photonics Engineering, Technical University of Denmark, 2800 Kgs Lyngby, Denmark (e-mail: exrell3@gmail.com).

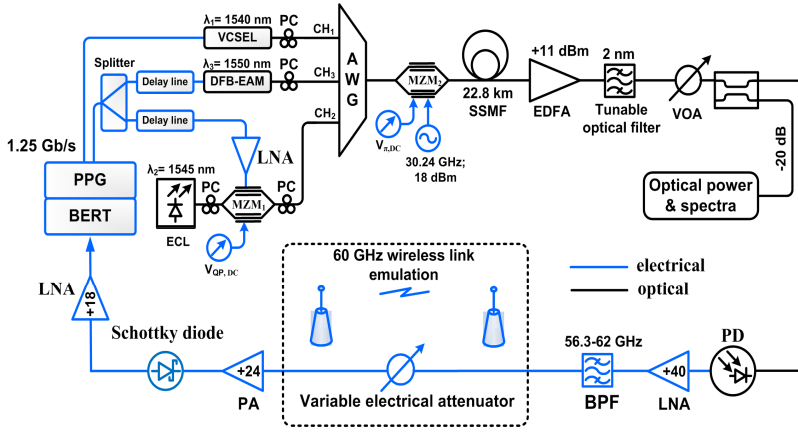


Figure 2. Experimental setup of the 60 GHz RoF system with simultaneous RF upconversion of multiple lightwaves.

II. EXPERIMENTAL SETUP DESCRIPTION

The experimental setup is presented in Fig. 2. Three lasers were used for lightwave generation: the C-band VCSEL ($\lambda_1 \approx 1540$ nm, $P_{opt1} = 0$ dBm), the ECL ($\lambda_2 \approx 1545$ nm, $P_{opt2} = 4$ dBm), and the DFB-EAM module ($\lambda_3 \approx 1550$ nm, $P_{opt3} = 4$ dBm).

A non-return-to-zero pseudorandom binary sequence with a word length of $2^{15}-1$ was produced by a pulse pattern generator (PPG) at a 1.25 Gbps bitrate. It was then directly modulated onto the lightwave at the VCSEL. The inverse data output of the PPG was fed into the electrical signal splitter where two identical 1.25 Gbps data streams were produced and subsequently delayed by 160 ps. A 10 GHz-bandwidth EAM and a 10 GHz-bandwidth MZM₁ were used for data modulation in case of the DFB and the ECL respectively. The DFB-EAM used in this work is an integrated module and we further refer to it for both lightwave generation and data modulation.

The use of the DFB-EAM or the VCSEL for lightwave generation and data modulation relaxes requirements for the peak-to-peak voltage of the driving electrical data signal and simplifies the overall system installation, but at the same time constraints the achievable extinction ratio and introduces chirp.

In case of VCSEL, the system performance will be additionally constrained due to existing trade-off between the extinction ratio and overshoot defining the optimized eye-diagram. In case of external modulation with the use of MZM or EAM, larger extinction ratio can potentially be obtained with MZM, however EAM requires lower driving voltage. The setup has been optimized experimentally by monitoring of the eye-diagram and BER of the system.

Three data-modulated lightwaves were then combined by a 100 GHz-grid arrayed waveguide grating (AWG). Polarization controllers (PCs) were placed before the AWG to adjust the polarization state of incoming lightwaves to achieve maximum carrier suppression in the MZM₂. RF modulation of the lightwaves was performed by a single-drive MZM₂ biased at a null transmission point and driven by the 30.24 GHz

sinusoidal electrical local oscillator (LO) RF of 18 dBm power, resulting in a suppression of the original optical carrier and increase of optical power in the upper and the lower sidebands separated by twice the original RF frequency $2f_{LO}$. The simultaneous RF modulation of several lightwaves will be constrained by slight wavelength-dependence of bias necessary for maximum carrier suppression. We therefore separated the lightwaves by 5 nm to test the system performance in a wide wavelength range.

When two sidebands are photomixed at the PD after fiber transmission, data pulses transmitted on lower and upper sidebands of the RoF signal are shifted in relation to each other in time domain leading to intersymbol interference, the bit walk-off evolution is governed according to Eq. 1:

$$\Delta\tau = \frac{DL\lambda_c^2}{\Delta\lambda_{RF}}, \quad (1)$$

where $D=18$ ps/(nm×km) is the dispersion parameter in standard single mode fiber (SSMF), L is the fiber length, λ_c is the wavelength of the optical carrier, and $\Delta\lambda$ is the wavelength difference between sidebands. By assuming a walk-off equal to 70 % of the pulse width as a maximum tolerable value [10-12], the maximum fiber length is calculated equal to 69 km. We use a shorter fiber span (22.8 km SSMF) for fiber access deployment scenario. If the chromatic dispersion penalty is required to be completely avoided, alternative techniques need to be employed [13]. We use carrier suppression technique owing to its simplicity.

The optical spectra of the generated double-sideband with a suppressed carrier (DSB-SC) signals are presented in Fig. 3 (a, b, c) for the VCSEL, the ECL and the DFB-EAM lightwaves respectively and in Fig. 3 (d) for all lightwaves combined. Carrier suppression of approximately 20 dB was achieved for all lightwaves. The DFB-EAM spectrum (Fig. 3 (c)) indicates the presence of the positive frequency chirp.

60 GHz DSB-SC RoF signals were then transmitted through a 22.8 km SSMF span. Subsequently, the signal was amplified by an erbium-doped fiber amplifier (EDFA) performing a pre-amplifier function in order to compensate for attenuation by fiber transmission and multiplexing.

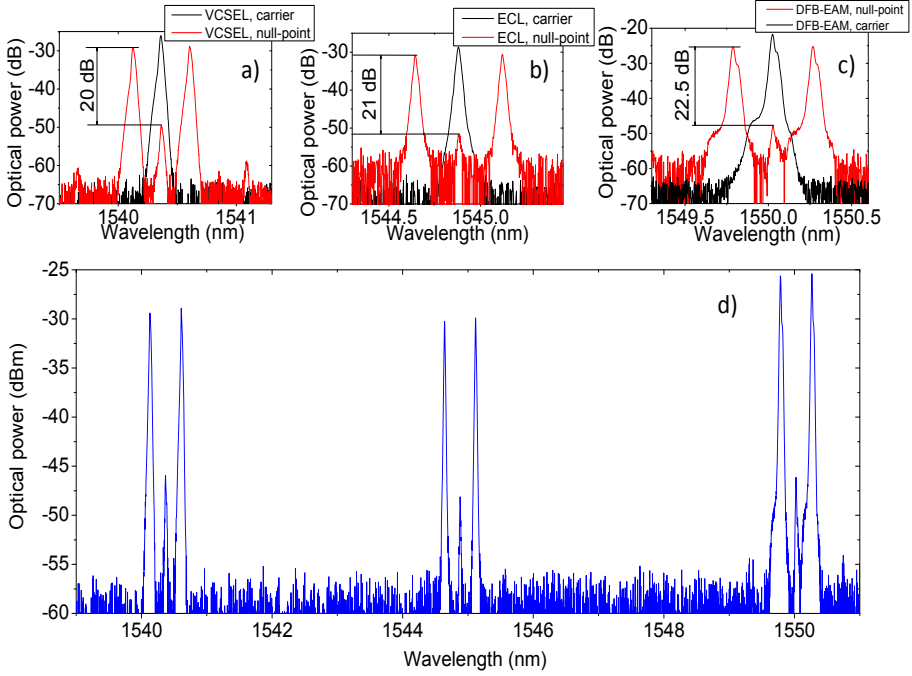


Figure 3. Optical spectra of (a) VCSEL 60 GHz RoF generation, (b) ECL 60 GHz RoF generation, (c) DFB-EAM 60 GHz RoF generation, (d) WDM mix of the 60 GHz RoF DSB-SC lightwaves.

A 2 nm tunable optical bandpass filter was then used to select a single RF-modulated lightwave for subsequent O/E conversion and BER evaluation. A variable optical attenuator (VOA) was employed next to control the power impinging the photodiode (PD). A 20 dB coupler and an optical spectrum analyzer were subsequently used to monitor the optical power and spectra

60 GHz-separated optical sidebands were photomixed at the 75 GHz bandwidth p-i-n PD. The double-stage 40 dB gain low noise amplifier (LNA) was used afterwards in order to boost the 60 GHz RF power before radiation.

The air propagation path loss was emulated by employing a variable electrical attenuator (VEA). The air attenuation of the signal can be approximated using the Friis free space transmission equation [2]:

$$PL_{FS} = 20 \log_{10} \left(\frac{4\pi d}{\lambda} \right) - G_{tx} - G_{rx} \quad (2)$$

where $\lambda = 0.005$ m is a wavelength of the signal, d is the distance between the transmitting and receiving antennas, $G_{tx}=G_{rx}=25$ dBi are the gains of transmitting and receiving antennas respectively. VEA was set to attenuate by 18 dB, which is equivalent to attenuation by 1 meter of wireless transmission when the combined antenna gain (25+25 dBi) is taken into account; the equivalent omnidirectional path loss is equal to 68 dB.

Afterwards, a 24 dB gain power amplifier (PA) was used. The baseband data signal was detected incoherently by using a Schottky diode working as an envelope detector (ED). Main advantage of the envelope detection technique is that it allows circumventing the use of local oscillator RF and a phase locked loop circuitry required for the synchronous mixing

downconversion technique. Additionally, the use of envelope detection has been reported to exhibit higher tolerance to impairments arising from laser linewidth [17]. Finally, the recovered digital baseband signal was then amplified and passed on for further quality evaluation with a bit error rate tester (BERT).

III. RESULTS AND DISCUSSION

Figure 4 (left) shows the RF spectrum after O/E conversion and amplification. The RF has been placed at 60.48 GHz to comply with a grid proposed by Wireless HD standard [14]. The electrical signal power is also set inside of the limits established in the United States (27 dBm) and Europe (10 dBm) [2].

The BER performance of the transmission link as a function of decreasing optical power into the PD is presented in Fig. 4 (right). The ECL-MZM₁ branch represents an example of high-performance schematics as higher power budget is potentially available which can then be used either for extension of fiber transmission distance or transferred into RF power by means of photomixing O/E conversion. As depicted in Fig. 4 (right), about 1.5 dB penalty is observed after fiber transmission compared with B2B at the sensitivity level (BER=10⁻⁹). For fiber transmission of the DFB-EAM produced lightwave, about 2 dB power penalty is observed at the 10⁻⁹ sensitivity level compared to B2B, however as the performance becomes noise-limited in the area of lower optical powers, the two curves cross. The slope of B2B BER curves is identical for the ECL-MZM₁ and the DFB-EAM in our setup.

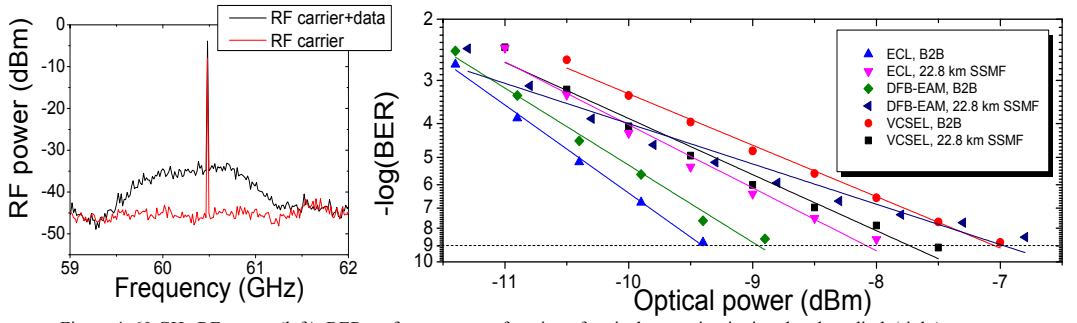


Figure 4. 60 GHz RF spectra(left), BER performance as a function of optical power impinging the photodiode(right).

The B2B performance of the ECL-MZM₁ and the DFB-EAM is different by less than 0.5 dB owing to different driving voltages required for the EAM and the MZM₁. DFB-EAM scheme suffers larger penalty, which, we believe, is related to the presence of the positive chirp as visible in Fig. 3 (c).

In the case of VCSEL, the BER curves' slope is identical for B2B and after fiber transmission, but 22.8 km SSF transmission shows performance superior to B2B with about 0.5 dB margin related to an interaction between negative chirp and dispersion. Negative chirp has been already reported previously to improve the link performance [15-16]. In particular, negative chirp in VCSELs has been shown to bring beneficial effects for fiber transmission distances reaching 40 km [15]. Given that only 0.5 dB difference is observed, and the fact that we limit our discussion in this paper to the access fiber deployment segment, we have restricted the scope of investigation of VCSEL performance to measuring the BER curves.

B2B VCSEL transmission shows less than 2.5 dB penalty compared to both ECL-MZM₁ and DFB-EAM schemes due to lower extinction ratio used with the directly modulated VCSEL.

The VCSEL and the DFB-EAM lightwave generation techniques show performance comparable to the ECL bringing the promise of using low-cost lightwave generation / baseband data modulation techniques for access 60 GHz RoF systems. Additionally, the results could be used to separate the delivery techniques assigned for indoor/outdoor transmission according to our originally proposed network scenario, VCSEL and DFB-EAM techniques may be assigned for short-distance indoor wireless links with lower power-budget constraints, and the ECL laser may be assigned for outdoor wireless transmission as it was successfully investigated in [8-9].

IV. SUMMARY

We have demonstrated the scalability of the simultaneous 60 GHz RoF upconversion technique using a single MZM for the ECL, the DFB, and the VCSEL laser devices. The sensitivity level for detection of three lightwaves falls in a <3 dB region. We suggest that the difference in optical power budget available for ECLs, DFBs and VCSELs is utilized for separating the service quality depending on application scenario. Using the simple carrier suppression technique is optimal for access networks, further investigation

regarding the chirp influence needs to be conducted for the use of the scheme in metro and core infrastructure. We note that the present system is optimal for transmission of OOK signals, however advanced modulation formats are better suited for single sideband RoF systems and synchronous RF downconversion.

REFERENCES

- [1] Cisco white paper, "Cisco visual networking index: Forecast and Methodology, 2012-2017," (Cisco, 2013).
- [2] S.-K. Yong, *60 GHz technology for Gbps WLAN and WPAN: from theory to practice*, Wiley, 2011.
- [3] M. C. Parker, et al., "Radio-over-fibre technologies arising from the building the future optical network in Europe (BONE) project," *IET Optoelectron.*, vol. 4, no. 6, pp. 247-259, 2010.
- [4] H.-J. Kim, J.-I. Song, "Multi-channel photonic frequency upconverter using a single electro-absorption modulator for generating WDM RoF signals," in *Proc. IMS*, 2011, paper WEPL-2.
- [5] J. Yu, et al., "Optical millimeter-wave generation or up-conversion using external modulators," *IEEE Photon. Technol. Lett.*, vol. 18, no. 1, pp. 265-267, 2006.
- [6] K. Kojucharow, et al., "Simultaneous Electrooptical Upconversion, Remote Oscillator Generation, and Air Transmission of Multiple Optical WDM Channels for a 60-GHz High-Capacity Indoor System," *IEEE Trans. Microwave Theor. Tech.*, vol. 47, no. 12, pp. 2249-2256, 1999.
- [7] A. Lebedev, et al., "Optimization of high-definition video coding and hybrid fiber-wireless transmission in the 60 GHz band," *Opt. Express*, vol. 19, no. 26, pp. 895-904, 2011.
- [8] A. Stöhr, et al., "Millimeter-wave photonic components for broadband wireless systems," *IEEE Trans. Microw. Theory Tech.*, vol. 58, no. 11, pp. 3071-3082, 2010.
- [9] J. A. Nanzer, et al., "Millimeter-Wave Wireless Communication Using Dual-Wavelength Photonic Signal Generation and Photonic Upconversion," *IEEE Trans. Microwave Theor. Tech.*, vol. 59, no. 12, pp. 3522-3530, 2011.
- [10] C. Lim, et al., "Impact of Chromatic Dispersion on 60 GHz Radio-over-Fiber Transmission," in *Proc. LEOS*, (IEEE, 2008), paper MJ5.
- [11] J. Ma, J. Yu, C. Yu, X. Xin, J. Zeng, and L. Chen, "Fiber Dispersion Influence on Transmission of the Optical Millimeter-Waves Generated Using LN-MZM Intensity Modulation," *J. Lightwave Technol.*, vol. 25, no. 11, pp. 3244-3256, 2007.
- [12] M. Zhou, et al., "Transmission performance of quadruple frequency optical millimeter-wave with single and dual carrier data modulations," in *Proc. of 2011 IEEE 13th International Conference on Communication Technology (ICCT)*, pp. 538-543, 2011.
- [13] M. Zhu, et al., "Efficient Delivery of Integrated Wired and Wireless Services in UDWDM-RoF-PON Coherent Access Network," *IEEE Photon. Technol. Lett.*, vol. 24, no. 13, pp. 265-267, 2006.
- [14] WirelessHD white paper, "WirelessHD Specification Version 1.1 Overview," (WirelessHD, 2010).
- [15] A. Gatto, et al., "Adjustable-chirp VCSEL-to-VCSEL injection locking for 10-Gb/s transmission at 1.55 μm ," *Opt. Express*, vol. 17, no. 24, pp. 21748-21753, 2009.
- [16] B. Zhang, et al., "Adjustable Chirp Injection-Locked 1.55- μm VCSELs for Enhanced Chromatic Dispersion Compensation at 10-Gbit/s," in *Proc. OFC/NFOEC, 2008*, paper OTW7.
- [17] G. Foschini, et al., "Noncoherent Detection of Coherent Lightwave Signals Corrupted by Phase Noise," *IEEE Transactions on Communications*, vol. 36, no. 3, pp. 306-314, 1988.

[Paper 7]

Alexander Lebedev, Xiaodan Pang, J. J. Vegas Olmos, Søren Forchhammer, Idelfonso Tafur Monroy, "Gigabit close-proximity wireless connections supported by 60 GHz RoF links with low carrier suppression," *Opt. Express*, vol. 21, no. 21, pp. 24574-24581.

Gigabit close-proximity wireless connections supported by 60 GHz RoF links with low carrier suppression

Alexander Lebedev,^{*} Xiaodan Pang, J. J. Vegas Olmos, Søren Forchhammer, and Idelfonso Tafur Monroy

DTU Fotonik, Dept. of Photonics Engineering, DTU, Technical University of Denmark, Kgs. Lyngby, Denmark
^{*}alele@fotonik.dtu.dk

Abstract: We present an experimental investigation of the 60 GHz optical carrier suppressed radio over fiber systems with less than 5 dB carrier suppression. As a case study, the 60 GHz RoF signal is generated using a 12.5 Gb/s commercially available Mach-Zehnder modulator biased at its minimum point. We report on error free transmission over 20 km of standard single mode fiber and 1 m of wireless distance. Furthermore, the efficiency of photonic RF generation depending on the value of carrier suppression is reported. We argue that transport of RoF signals with low carrier suppression assisted with simplified techniques of lightwave generation, baseband data modulation, and RF downconversion might be a promising enabling technology for fiber support of close-proximity wireless terminals.

©2013 Optical Society of America

OCIS codes: (060.2330) Fiber optics communications; (060.5625) Radio frequency photonics.

References and links

1. WirelessHD white paper, "WirelessHD Specification Version 1.1 Overview," (WirelessHD, 2010). <http://www.wirelesshd.org/pdfs/WirelessHD-Specification-Overview-v1.1May2010.pdf>.
2. Wi-Fi alliance press-release, "Wi-Fi Alliance® and Wireless Gigabit Alliance to unify," (Wi-Fi Alliance, 2013). <http://www.wi-fi.org/media/press-releases/wi-fi-alliance®-and-wireless-gigabit-alliance-unify>.
3. A. Stöhr, S. Babel, P. J. Cannard, B. Charbonnier, F. van Dijk, S. Fedderwitz, D. Moodie, L. Pavlovic, L. Ponnampalam, C. C. Renaud, D. Rogers, V. Rymanov, A. J. Seeds, A. G. Steffan, A. Umbach, and M. Weiß, "Millimeter-wave photonic components for broadband wireless systems," *IEEE Trans. Microw. Theory Tech.* **58**(11), 3071–3082 (2010).
4. ITU-R P.676–9 Recommendation (2012) Attenuation by atmospheric gases. ITU, Geneva, Switzerland.
5. Y. Shi, M. Morant, C. Okonkwo, R. Llorente, E. Tangdiongga, and A. M. J. Koonen, "Multistandard Wireless Transmission Over SSMF and Large-Core POF for Access and In-Home Networks," *IEEE Photon. Technol. Lett.* **24**(9), 736–738 (2012).
6. F. Paresys, T. Shao, G. Maury, Y. Le Guennec, and B. Cabon, "Bidirectional Millimeter-Wave Radio-Over-Fiber System Based on Photodiode Mixing and Optical Heterodyning," *J. Opt. Commun. Netw.* **5**(1), 74–80 (2013).
7. T. Shao, F. Paresys, Y. Le Guennec, G. Maury, N. Corrao, and B. Cabon, "Simultaneous Transmission of Gigabit Wireline Signal and ECMA 387 mmW over Fiber Using a Single MZM in Multi-Band Modulation," in *Proceedings of Microwave Photonics Conference*, pp.149–152, 2011.
8. S. Fedderwitz, C. Leonhardt, J. Honecker, P. Muller, and A. Steffan, "A high linear and high power photoreceiver suitable for analog applications," *IEEE Photonics Conference (IPC)*, paper TuL3, pp. 308–309, 2012.
9. S. Babel, I. Flammia, A. Stohr, J. Montero-de-Paz, L. E. Garcia-Munoz, D. Segovia-Vargas, G. Carpintero, A. Lissauskas, and O. Cojocari, "Compact transmitter and receiver modules for E-band wireless links," in *Proceedings of Optical Fiber Communication Conference and Exposition*, paper OW3D.7, 2013.
10. C. Lim, A. Nirmalathas, M. Bakaul, P. Gamage, K.-L. Lee, Y. Yang, D. Novak, and R. Waterhouse, "Fiber-Wireless Networks and Subsystem Technologies," *J. Lightwave Technol.* **28**(4), 390–405 (2010).
11. J. J. O'Reilly, P. M. Lane, R. Heidemann, and R. Hofstetter, "Optical generation of very narrow linewidth millimeter wave signals," *Electron. Lett.* **8**, 2309–2311 (1992).

12. G. Qi, J. Yao, J. Seregelyi, S. Paquet, C. Belisle, X. Zhang, K. Wu, and R. Kashyap, "Phase-Noise Analysis of Optically Generated Millimeter-Wave Signals With External Optical Modulation Techniques," *J. Lightwave Technol.* **24**(12), 4861–4875 (2006).
13. A. Ng'oma, M. Sauer, D. Thelen, and J. George, "Data throughput tripling by Feed-Forward Equalization and photonic QPSK in a 7 Gbps single-carrier RoF link at 60 GHz," in *Proceedings of International Topical Meeting on Microwave Photonics (MWP)*, pp.213–216, Oct. 2008.
14. I. G. Insua, K. Kojucharow, and C. G. Schaeffer, "MultiGbit/s transmission over a fiber optic mm-wave link," in *Proceedings of 2008 IEEE MTT-S International Microwave Symposium*, pp.495–498, June 2008.
15. A. Lebedev, X. Pang, J. J. Vegas Olmos, S. Forchhammer, and I. Tafur Monroy, "Fiber-supported 60 GHz mobile backhaul links for access/metropolitan deployment," in *Proceedings of Optical Networks Design and Modeling*, pp. 189–192, 2013.
16. J. J. Vegas Olmos, X. Pang, A. Lebedev, and I. Tafur Monroy, "VCSEL sources for optical fiber-wireless composite data links at 60GHz," in *Proceedings of OptoElectronics and Communications Conference (OECC 2013)*, paper TuPP-10, 2013, in press.
17. Bridgewave whitepaper, "Gigabit wireless applications using 60 GHz radios," (Bridgewave, 2006).
18. A. Mathew, "Local Area Networking Using MillimetreWaves," (NewLANs, Inc., USA, 2005).
19. AIRLINX Communications, Inc. specification datasheet, "GigaLink® 6221/6421/6451," (AIRLINX Communications, Inc., 2013).
20. Sub10 Systems Limited white paper, "60GHz Metro Cell and Small Cell Backhauling for Service Providers," (Sub10 Systems Limited, 2011).
21. K. Ramachadran, R. Kokku, R. Mahindra, and S. Rangarajan, "60 GHz data-center networking: wireless worry less?" NEC Technical Report, 2008.
22. S. Kandula, J. Padhye, and P. Bahi, "Flyways to de-congest data center networks," in *Proceeding of Eighth ACM Workshop on Hot Topics in Networks*, 2009.
23. K. Kawasaki, Y. Akiyama, K. Komori, M. Uno, H. Takeuchi, T. Itagaki, Y. Hino, Y. Kawasaki, K. Ito, and A. Hajimiri, "A millimeter-wave intra-connect solution," in *Proceedings of IEEE International Solid-State Circuits Conference*, (Institute of Electrical and Electronics Engineers, San Francisco, 2010), pp. 414–415.
24. TransferJet Overview, (TransferJet, 2010). www.transferjet.org/tj/transferjet_overview.pdf.
25. I. G. Insua, "Optical generation of mm-wave signals for use in broadband radio over fiber systems," Ph.D. dissertation, Dresden University of Technology, (2010), pp. 69–75.
26. A. Lebedev, X. Pang, J. J. Vegas Olmos, M. Beltran, R. Llorente, S. Forchhammer, and I. Tafur Monroy, "Feasibility study and experimental verification of simplified fiber-supported 60 GHz picocell mobile backhaul links," *IEEE Photon. J.* **5**(4), 7200913 (2013).
27. I. Garcés, A. Villafranca, and J. Lasobras, "Characterization of the chirp behavior of integrated laser modulators (ILM) by measurements of its optical spectrum," in *Proc. SPIE 699769971S–2*.
28. G. P. Agrawal, *Lightwave technology: communication systems* (Wiley, 2005), Chap. 5.

1. Introduction

Low bandwidth availability within the microwave spectrum of radio communication frequencies may hinder the development of novel services and applications. Hence, it has been proposed to employ the 60 GHz band where up to 9 GHz of unlicensed spectrum [1] has been allocated. Research and development to utilize the 60 GHz band have been conducted by organizations such as the Wireless Gigabit Alliance (WiGig, IEEE 802.11 ad), which proposed a specification to deliver data rates up to 7 Gb/s and enable tri-band networking (2.4-, 5- and 60GHz). ABI Research forecasts that by 2016, annual shipments of devices equipped with both Wi-Fi and WiGig technology will approach 1.8 billion [2].

Radio over fiber (RoF) technologies are providing methods to generate, transport and detect wireless signals at high bitrates in diverse fiber-optic systems [3]. RoF technologies aim at simplification of base station (BS) and access point (AP) units which is crucial in case of the 60 GHz millimeter wave (mm-wave) transmission where coverage is limited by high attenuation due to the free space path loss and absorption on molecules of oxygen and water vapour, and therefore higher density of BSs/APs is required [4].

Recent research on the RoF technology includes studies of the diversified fiber infrastructure for multiband wireless services [5], bidirectional 60 GHz RoF [6] and systems combining RoF and fiber-to-the-home delivery [7]. The development of highly linear high power 60 GHz analog photoreceivers [8] and compact E-band (60-90 GHz) wireless transmitters [9] combining progress in optoelectronic and mm-wave components further strengthens the potential for commercial deployment of mm-wave RoF links. However, a major impediment for widespread adoption of RoF technology is the utilization of costly high

bandwidth optical components to perform the electro-optical (E/O) conversion, especially when dealing with mm-wave signals [10].

In order to alleviate the requirements for high frequency RF generation, optical carrier suppressed (OCS) RoF transmission is used [11] yielding the desired RF after photomixing by doubling the original RF frequency applied at the E/O conversion point. OCS RoF technique generates RF signals with an excellent phase noise performance, which is crucial for support of advanced spectrally efficient modulation formats [12].

Previous experimental demonstrations for generation of 60 GHz electrical signals using the frequency doubling technique rely on optical components with bandwidths in excess of 20 GHz [13]. Such large bandwidth is necessary to yield high carrier-to-sideband suppression ratio. Complementarily, filters and optical interleavers are often used to maximize a suppression ratio [14]. However, additional filters and interleavers have very high performance requirements and naturally increase the cost and complexity of the system.

We have previously reported on transmission of Gigabit data in 60 GHz RoF systems with high carrier suppression using a distributed feedback laser integrated with an electroabsorption modulator (DFB-EAM) and a vertical cavity surface emitting laser (VCSEL) for lightwave generation and data modulation [15, 16].

In this paper, we present novel results demonstrating generation and delivery of 60 GHz OCS RoF signals with low carrier suppression for Gigabit wireless systems. Bit error rate (BER) performance below 10^{-9} level after fiber transmission and 1 m of wireless transmission is reported. We argue that low carrier suppression RoF systems are suitable to enable wireless applications with ultrashort reach.

This paper is organized as follows: in Section 2, potential applications are examined. In Section 3, we present the laboratory setup built to study the performance of low carrier suppressed 60 GHz RoF signals. Discussion of the performance of the low carrier suppression OCS 60 GHz RoF link is conducted in Section 4. Finally, we provide a summary and conclusions in Section 5.

2. 60 GHz links supported by fiber for close proximity wireless communications

60 GHz high-capacity links have been widely adopted by industry to provide private corporate connections reaching 1 km wireless distance [17–19], recently their use has been also proposed for mobile backhaul applications [20].

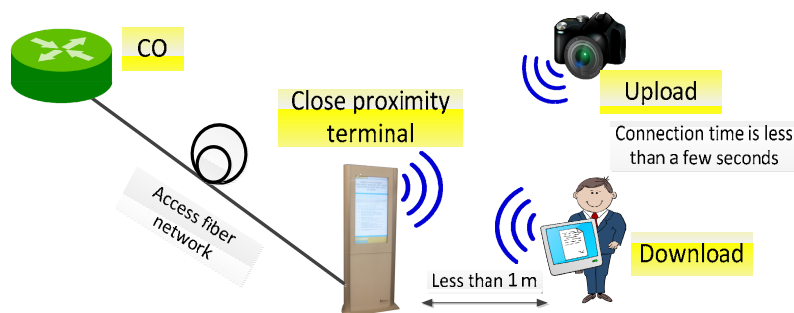


Fig. 1. Network scenario for 60 GHz RoF signals' delivery to close proximity communication terminals. CO: central office.

However, there are a few emerging scenarios for 60 GHz wireless systems that alleviate requirements for wireless transmission distance. First scenario is connectivity in data centers [21–23] where 60 GHz wireless links promise to reduce cabling complexity and related costs of maintenance. Second, we believe that high-capacity 60 GHz links should be considered for close-proximity applications because they naturally fit the close-proximity scenario where

large capacity is required but over a short wireless distance e. g. when digital kiosks are installed in public locations to enable ultrafast upload/download of high-definition video, interactive maps etc. [24]. Furthermore, close-proximity applications may benefit from integration with optical fiber networks if they utilize cost-effective transceivers for fiber-wireless distribution.

We depict the proposed hybrid fiber-wireless architecture to enable close proximity applications in Fig. 1. In this paper, a low complexity RoF system for fiber support of close proximity wireless applications is proposed and experimentally demonstrated.

3. Experimental setup description

In order to confirm the suitability of the 60 GHz RoF transmitter with low carrier suppression, we built an experimental setup and performed quantitative measurements after fiber and wireless transmission. This section describes the experimental setup.

The experimental setup is shown in Fig. 2. We used a single module combining lightwave generation and data modulation composed of a distributed feedback laser integrated with a 12.5 Gb/s electro absorption modulator producing +4 dBm of optical output power. The baseband data signal imposed on the lightwave were generated by a pulse pattern generator (PPG) producing a pseudorandom binary sequence (PRBS) with a word length of $2^{15}-1$. The lightwave was then modulated by a 29.54 GHz RF signal of 18 dBm RF power using a 12.5 Gb/s Mach-Zehnder modulator (MZM, Covega Mach-10) biased at its minimum point. By biasing the MZM at the minimum point, the carrier is suppressed and the double sideband with suppressed carrier RoF signal is generated. The polarization controller (PC) was installed before the MZM to ensure the polarization alignment necessary for maximum achievable carrier suppression.

High RF power and subsequently modulation indices not following small signal modulation criteria have been shown to be beneficial when the bias is set at V_{π} where a modulation index equal to 0.97 has been shown as optimal [25]. We also note that higher order harmonics appearing when higher modulation index is used are later mitigated by the frequency response of the O/E conversion device and the use of mm-wave bandpass filters and amplifiers.

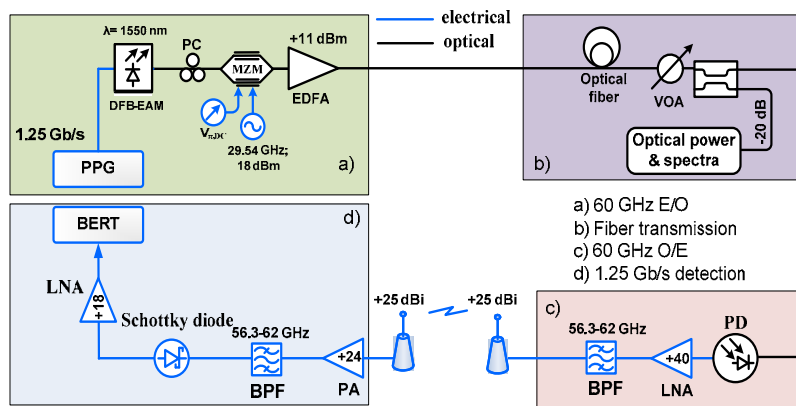


Fig. 2. Experimental setup demonstrating 60 GHz RoF generation, fiber and wireless transmission and baseband data recovery with low carrier suppression. PPG: pulse pattern generator, DFB-EAM: distributed feedback laser integrated with electro absorption modulator, PC: polarization controller, MZM: Mach-Zehnder modulator, EDFA: Erbium doped fiber amplifier, VOA: variable optical attenuator, PD: photodiode, LNA: low noise amplifier, BPF: bandpass filter, PA: power amplifier, BERT: bit error rate tester, E/O: electrical-to-optical conversion, O/E-optical-to-electrical conversion.

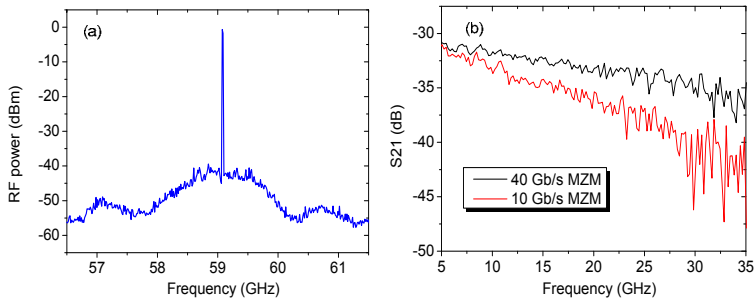


Fig. 3. RF spectrum of the signal (a) and S21 performance of 12.5 Gb/s and 40 Gb/s MZMs (b).

The optical signal was then boosted to + 11 dBm power with an erbium doped fiber amplifier (EDFA). To test the diverse fiber infrastructure, we employed links of dispersion shifted fiber (DSF), nonzero DSF (NZDSF), and standard single-mode fiber (SSMF). After the fiber transmission, the signal was detected with a 75 GHz bandwidth photodiode (PD), and subsequently amplified and filtered (+ 40 dB gain and 56.3-62 GHz passband). The signal was then fed into an antenna for radiation. High directivity horn antennas of 25 dBi gain were used at the wireless transmitter and receiver side. On the receiver end, the signal was amplified (24 dB) and filtered (56.3-62 GHz passband). Downconversion was subsequently performed by a Schottky diode working as an envelope detector (ED). Recovered baseband data were passed on for further detection of bit errors at the bit error rate tester (BERT).

In Fig. 3(a), we depict the RF spectrum of the signal at the output of the 60 GHz low noise amplifier (LNA) on the transmitting side when the 0.4 V peak-to-peak data signal is applied to the DFB-EAM. In Fig. 3(b), we depict the S21 performance of the system employing 12.5 Gb/s MZM (Covega Mach-10) in comparison to a 40 Gb/s MZM that was used in [15, 16]. The S21 performance was measured excluding EDFA from the link, where port 2 was the output of the PD, and port 1 – the MZM RF input. Given the lower E/O conversion performance of the 12.5 Gb/s modulator, higher power RF has been applied to the MZM.

4. Results and discussion

In this section, performance of the setup in terms of BER and RF O/E conversion efficiency is presented and the sources of impairments are reported and analyzed. First, we characterized the conversion efficiency of optical power to 60 GHz RF power depending on the suppression of the optical carrier. Power of the generated 60 GHz RF signal as a function of carrier suppression is depicted in Fig. 4. The carrier suppression was changed by varying a bias voltage of the MZM, and measured as observed in optical spectrum analyzer. As it can be seen from Fig. 4 the slope of the curve flattens at about 0 dBm suppression value. These results are consistent with the results that we previously reported in the case of 40 Gb/s MZM when the carrier suppression was varied from 0 to 20 dB [26]. Reported degradation in RF power after E/O, fiber transmission, and O/E conversion is overcome by using a double-stage LNA. For example, 0 dBm optical signal at the PD is converted to -32 dBm 60 GHz RF signal for 4 dB carrier suppression value, and boosted to + 8 dBm RF power for radiation.

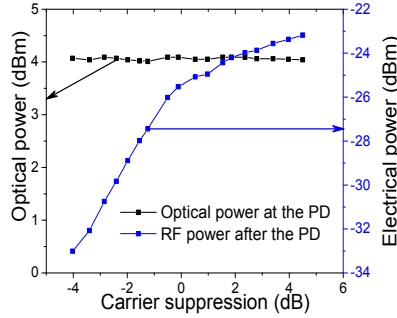


Fig. 4. 60 GHz RF power after the PD as a function of carrier suppression for a constant level of optical power.

From optical spectra depicted in Fig. 5, we can observe the presence of positive frequency chirp and four-wave mixing (FWM). In Fig. 5(a), optical spectra before fiber transmission are presented. Splitting of the carrier at low bitrates indicates the presence of frequency chirp that is caused by the electrical crosstalk due to the integration of laser and modulator sections in the same chip of the DFB-EAM module [27]. However, given the low bitrate and the fact that we model access fiber deployment, chirp does not impose a power penalty. As defined in [28], chirp-induced power penalty at the receiver is measured as a function of $|\beta_2|B^2L$, where $\beta_2 \approx -20$ ps²/km is a group velocity dispersion parameter for SSMF, $B = 1.25$ Gb/s is a bitrate of the system, and $L = 20$ km is a fiber link length. For our system, $|\beta_2|B^2L$ is equal to 0.625×10^{-3} , which according to [28] brings a negligible receiver sensitivity penalty across possible chirp values.

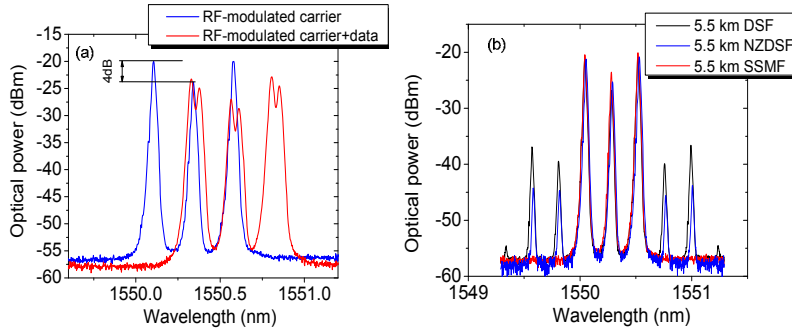


Fig. 5. Optical spectra of the RF- and data-modulated lightwave before fiber propagation (a) and after fiber propagation at 16 dBm optical power into the fiber (b).

It can be observed from Fig. 5(b) that FWM-produced lightwaves start to be noticeable in case of fibers with a low dispersion parameter at 1550 nm. FWM is independent of channel bitrate, but depends critically on the spacing between lightwaves [28]. Power of the signal at new frequencies can be calculated analytically as a function of the effective cross-sectional area of the fiber, the nonlinear refractive index and the fiber length [28]. In our experiment, to confirm that FWM does not influence the performance of the system, we tested that increase in optical power at the EDFA output from 11 to 16 dBm increases power of FWM-generated lightwaves, but does not reduce the BER of the transmitted data signal. It should be noted that

FWM brings a receiver sensitivity penalty for wavelength division multiplexed systems in the case of equally spaced channels through introduction of the inter-channel crosstalk, however it is not an obstacle for a single-channel system under study.

We then evaluated the performance of the system in terms of BER. In Fig. 6(a), we depict the performance of the setup without wireless transmission, when only fiber transmission is considered. BER is measured for different distances and types of fibers in order to account for the effects of dispersion and nonlinearities. Fiber transmission results show a negligible power penalty when compared to the back-to-back transmission, clustering BER performance equal to 10^{-9} around -9.5 dBm region.

Finally, we added wireless transmission to the system. We measured the performance for two wireless distances, 50 cm and 1 m, and with or without 20 km fiber transmission. Figure 6(b) depicts the BER performance of the signal including air transmission. BER below 10^{-9} level is achieved in all cases, being the case of 20 km and 1 m transmission the cases sustaining the highest power penalty, less than 2.5 dB compared to the best case. Higher value of optical power into the PD is necessary to yield the performance below 10^{-9} level due to the fact that wireless channel loss is compensated by increasing optical power impinging the photodiode.

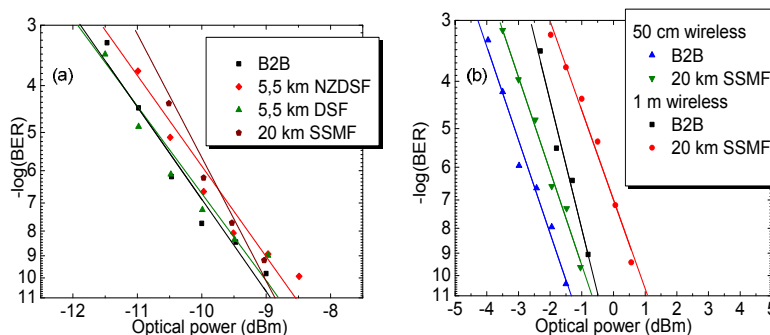


Fig. 6. BER performance back-to-back and after fiber transmission for 2 cases: (a) wireless transmission distance is omitted and (b) up to 1 m wireless transmission is performed. NZDSF: non-zero dispersion shifted fiber, DSF: dispersion shifted fiber, SSMF: standard single mode fiber.

Utilizing E/O components with -3 dB bandwidth lower than a value of the RF frequency used for mm-wave OCS RoF technique leads to certain trade-offs in performance. For given RF signal power at the E/O point and given -3 dB bandwidth of the E/O module, carrier-to-sideband suppression ratio is decreasing with an increase in applied frequency, and, in turn, the amount of the RF power detected after photomixing at the PD is reduced. In this paper, the case study for modulation of 12.5 Gb/s MZM with a 30 GHz RF signal is presented showing that, even when the carrier suppression is decreased to less than 5 dB, excellent transmission performance may still be obtained allowing us to simplify the fiber transport of mm-wave frequencies by utilization of low bandwidth E/O conversion devices. We generalize the presented case by studying the relation between the carrier suppression and the photonically generated RF power for low values of carrier suppression (less than 5 dB).

The choice of lightwave generation, baseband data modulation, and RF downconversion techniques is done in order to further simplify the system. By utilizing the DFB-EAM, we simplify the installation of the system and allow lower driving voltages for baseband lightwave modulation. Performance is constrained by the chirp of the DFB-EAM however the sensitivity penalty is not imposed in our system. The envelope detection technique provides RF downconversion avoiding the use of LO at the wireless receiver.

5. Conclusion

This paper presents an experimental demonstration of 60GHz signals transmission in OCS RoF links with less than 5 dB carrier suppression. The BER of the transmitted data below 10^{-9} level for transmission of 1.25 Gb/s data signal through 20 km of SSMF complemented with 1 m of the 60 GHz wireless link is reported. Presence of the optical carrier and low separation between the carrier and sidebands leads to FWM, however no error floor due to nonlinearities at 16 dBm optical power into the fiber was observed. Furthermore, the system was simplified by utilizing the integrated module for data modulation and lightwave generation and passive RF downconversion with an ED. Results indicate that the simplified OCS RoF systems with low carrier suppression are an effective solution for close-proximity wireless applications.

Acknowledgment

J. J. Vegas Olmos acknowledges the Marie Curie program for partly funding this research through the WISCON project.

[Paper 8]

Alexander Lebedev, J. J. Vegas Olmos, Xiaodan Pang, Søren Forchhammer, Idelfonso Tafur Monroy, "Low-complexity source and channel coding for mm-wave hybrid fiber-wireless links," *Opt. Commun.*, submitted.

Low complexity source and channel coding for mm-wave hybrid fiber-wireless links

Alexander Lebedev, * J. J. Vegas Olmos, Xiaodan Pang, Idelfonso Tafur Monroy, Knud J. Larsen and Søren Forchhammer

DTU Fotonik, Department of Photonics Engineering, Technical University of Denmark, Kongens Lyngby, Denmark

*exrell3@gmail.com

Abstract— We report on the performance of channel and source coding applied for an experimentally realized hybrid fiber-wireless W-band link. BCH and RS pre- and post-coding bit error rate (BER) performance is presented for a wireless propagation distance of 3 meters and 20 km fiber transmission. We report on peak signal-to-noise ratio (PSNR) performance of several encoded video sequences constrained by the channel bitrate and the packet size. We argue that light video compression and low complexity channel coding for the W-band fiber-wireless link enable low-delay multiple channel 1080p wireless HD video transmission.

Keywords: fiber optics, H.264/AVC, millimeter wave transmission, optical communication, Radio over Fiber, W-band wireless.

1. INTRODUCTION

The continuously growing demand for high-bitrate wireless services is now generated through the introduction of diverse real-time high definition (HD) video services including demanding services as delivery of 3DTV, multiview video and HD teleconferencing. This leads to an increasing interest in ultra high frequency unlicensed wireless spectrum in V (50-75 GHz) and W (75-110 GHz) bands [1]. W-band contains two subbands (81-86 GHz and 92-95 GHz) allocated for mm-wave wireless communication that will potentially enable delivery of multigigabit data [1].

Propagation distance for W-band wireless links is severely limited by the free space path loss of the signal according to the Friis transmission equation [2]. We believe that development of W-band systems is likely to follow the V-band development, which already has led to commercial production of multiGbps in-home miniature real-time uncompressed HD video transceivers [3].

W-band systems require deployment of more remote antenna units (RAU) to cover the given area compared to lower frequency microwave links for the same gain of an antenna. With increased density of RAUs, distributed antenna systems (DAS) architecture becomes advantageous [4]. In the DAS scenario, a central base station (CBS) has most of the functionalities, and a RAU should be simplified. We study radio over fiber (RoF) architecture where the optical fiber provides a connection between the CBS and the RAU providing benefit of increased bandwidth and lower loss compared to e.g. a coaxial cable [5]. In the RoF scenario, CBS performs data modulation, RF generation, electrical-to-optical conversion, and the RAU is simplified to perform only RF optical-to-electrical conversion, amplification, filtering and beam formation [6-8]. In this work, we consider both standard single mode fiber (SSMF) and multimode fiber (MMF) media for data delivery between the CBS and the RAU in order to ensure that the diverse preexisting fiber network infrastructure is optimally utilized.

Channel and source coding are essential tools to mitigate the channel impairments under constraints of the available power budget, wireless propagation distance, allocated wireless bandwidth and complexity of the system. In this work, we study Bose-Chaudhuri-Hocquenghem (BCH) and Reed-Solomon (RS) error correction coding (ECC) and H.264/ Advanced Video Codec (AVC) source coding.

This paper extends the list of ECC solutions proposed for mm-wave wireless systems in [9-11] and standard specifications [2, 12, 13]. The references [2, 9-13] report on low-density parity check (LDPC) codes, RS codes, TURBO codes and convolutional codes (CC). The channel coding study for both omnidirectional antennas and antennas with high directivity is presented in [9] where in both cases a line-of-sight (LOS) condition is given, in paper [10] the study for non-line-of-sight (NLOS) mm-wave transmission is presented. Gao et al. [10] reports on channel coding for a model that includes phase noise and nonlinear effects

Novelty of this work is twofold. First, we assess the performance of the channel coding for the experimentally reported mm-wave wireless transmission assisted with a fiber distribution infrastructure. Second,

we present the performance analysis for HD video compression for the W-band provided the joint source-channel optimization framework.

This report complements our previous work on uncompressed real-time HD video transmission in W-band [14] and compressed HD video transmission in V-band [15], now providing the estimate on the channel coding performance.

This paper is organized as follows: the experimental setup is presented in Section 2, major parameters of source and channel coding are reported in Section 3 together with a simple analytical method for ECC performance assessment. Results for uncoded physical layer transmission, post-decoding BCH- and RS-protected transmission and peak signal-to-noise ratio (PSNR) metric for 150 Mbps full bandwidth utilization coded video are discussed in Section 4. In Section 5, we conclude the paper and suggest the future work.

2. EXPERIMENTAL SETUP DESCRIPTION

In this section, we present the experimental setup of a hybrid fiber-wireless W-band link for delivery of 150 Mb/s data signal. As depicted in Fig. 1, main building blocks of the system are a signal generation part, combined SSMF and MMF fiber distribution, RAU, and an end-user terminal.

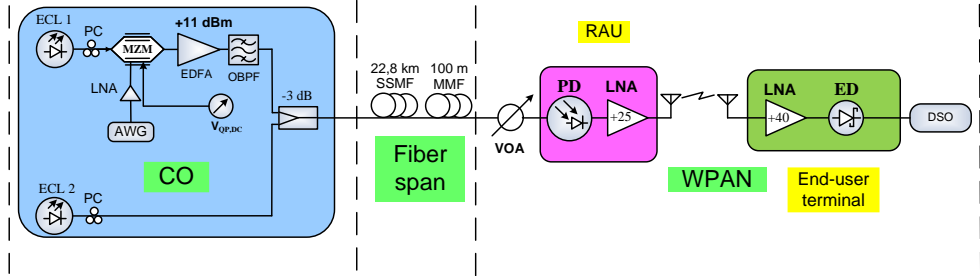


Fig.1 Experimental W-band RoF system with envelope detection, RAU: remote antenna unit, LD: laser diode, AWG: arbitrary waveform generator, PC: polarization controller, MZM: Mach-Zehnder modulator, LNA: low noise amplifier, EDFA: Erbium doped fiber amplifier, OBPF: optical band pass filter, VOA: variable optical attenuator, BPF: band pass filter, ED: envelope detector, LPF: low pass filter, DSO: digital sampling oscilloscope, CO: central office, RAU: remote antenna unit, WPAN: wireless personal area network.

In the signal generation part, two identical 100-kHz linewidth external cavity lasers (ECL) were used for generating two lightwaves in a 1550 nm wavelength region with a frequency offset of 84 GHz with optical power of each lightwave equal to 15 dBm. Baseband data were imposed onto one of the optical carriers by using an optical Mach-Zehnder modulator (MZM) biased at its quadrature point and driven by an arbitrary waveform generator (AWG). Subsequently, an Erbium doped fiber amplifier (EDFA) was employed followed by an optical bandpass filter (OBPF) used to mitigate out of band amplified spontaneous emission (ASE) noise from EDFA. A 3 dB coupler was used to combine the two lightwaves before the single fiber transmission.

The fiber link was composed of a 22.8 km span of SSMF and a 100 m span of MMF. Following fiber transmission, a variable optical attenuator was employed to control the optical power entering the 75 GHz bandwidth photodiode (PD) in order to evaluate the BER performance of the system.

At the RAU, upconversion to 84 GHz RF took place through photomixing of the two lightwaves in the photodiode. Subsequently, a 25 dB gain W-band amplifier was used before feeding the 84 GHz RF signal to an antenna for wireless transmission.

In this work, we report the transmission performance including a 3 m W-band wireless link. The transmitting and receiving antennas used in the experiment are commercially available 25 dBi gain horn antennas. After receiving the signal with the antenna and following double-stage W-band amplification (40 dB gain), envelope detection (ED) with the Schottky barrier diode was used for down-conversion of the data signal from the RF carrier to baseband. Finally, a digital sampling oscilloscope (DSO) was employed to store the waveform containing the transmitted data.

3. BCH, RS AND H.264/AVC CODEC SETTINGS.

In this section we discuss the choice of parameters for channel and source coding. Packetization is required in both channel and source coding, the video packet size for video transmission was chosen to be equal to 20000 bits, and closest packet sizes capable of covering the video packet were chosen for BCH and RS coding.

BCH and RS were used to test the channel coding for the mm-wave fiber-wireless link. The BCH primitive block length was set to 32767 bits. We employ the BCH encoder with the number of overhead bits equal to 150, 450 and 750 bits per block (0.5, 1.4 and 2.3 percents of overhead).

Analytical solution for BCH performance is governed according to Eq. (1) [16]:

$$p_{pd} = \sum_{i=t+1}^n (i/n) \times (n, k) \times p^i \times (1-p)^{n-i}, \quad (1)$$

where k is the message length, n is the block length, t is the error-correction capability of the code, p is the uncoded BER, and p_{pd} is the post-decoding BER.

We compare the performance of BCH codes to the performance of RS codes. In order to cover the video packet with the channel coding packet optimally, we have chosen 11-bits symbols ($m=11$, $n=2047$). By setting the error-correction capability $t=10$ symbols, the code is described as RS (2047, 2027). For analytical estimation of RS codes performance, we have applied approximation for the relation between the symbol-error rate and the bit error rate given by Eq. 2 and Eq. 3:

$$p_s = 1 - (1 - p_b)^m, \quad (2)$$

$$p_b = 1 - (1 - p_s)^{1/m}, \quad (3)$$

where p_s is a symbol error rate and p_b is a bit error rate.

The video encoding was performed using the Joint Model (JM) reference software implementation of the H.264/AVC standard [17]. H.264/AVC is one of the latest and most widely used video coding standards suitable for a wide variety of applications [18, 19].

H.264/AVC defines several mechanisms that allow error concealment at a decoder such as avoiding temporal error propagation with Intra-only (frame-by-frame) coding, intra-frame slicing, flexible macroblock ordering (FMO) inside of the slice, and data-partitioned slicing [18,19]. In this work, we employ an Intra coding mode only and a frame slicing mechanism to increase the error-robustness by limiting spatio-temporal error propagation. Frame slicing leads to decreasing the average length of H.264/AVC network abstraction layer units (video packets); it is reported in [18] to reduce the packet error rate (PER) and in turn improve the PSNR of the impaired video. The encoder is further simplified by using only Universal Variable Length Coding (UVLC) for H.264/AVC entropy coding.

Uncompressed real-time transmission of 1080p 60 frames per second 4:4:4 video signal requires a 3 Gbps channel bitrate [20]. Without compression, it would only be possible to fit a 1080p channel in the allocated bandwidth (81-86 GHz, 92-95 GHz) with multilevel modulation formats in either of the W-bands since the main lobe of uncompressed 1080p video signal will occupy 6 GHz of spectrum in RF domain. However, with a moderate compression ratio of 20, the real-time full-bandwidth of the signal can be reduced to 150 Mbps and thus multichannel transmission can be enabled. Uncompressed 1080p HD test video sequences were used for video coding. The sequences were originally shot in 4:2:0 YUV 1080p format. We upsampled them to 4:4:4 YUV format to model the highest quality and most bitrate demanding case.

We use PSNR as an objective quality metric for video, which is defined in Eq. 4 and Eq. 5:

$$MSE = \frac{1}{N} \sum_{i=1}^N (x_i - y_i)^2, \quad (4)$$

$$PSNR = 10 \log_{10} \left(\frac{L^2}{MSE} \right), \quad (5)$$

where MSE stands for a mean squared error, N is the number of pixels in the image, and x_i and y_i are the i -th pixels in the original and the distorted signals, respectively. L is the dynamic range of pixel values. For an 8 bits/color signal, L is equal to 255. PSNR is evaluated for the luminance (Y) component of the compressed video signal.

4. EXPERIMENTAL AND ANALYTICAL RESULTS AND DISCUSSION

In this section, we analyze the performance of the transmission system in terms of BER with and without BCH and RS coding. The BER performance for combined SSMF and MMF fiber transmission and 3 meters of wireless propagation as a function of the optical power impinging the PD is evaluated. Analysis of statistical distribution of voltage samples of ‘ones’ and ‘zeros’ after the RF downconversion by means of envelope detection is conducted.

Video degradation in commonly used H.264/AVC decoder implementations is related to the loss of packets. The PER depends on the BER, the packet length, and distribution of the bit errors (presence/absence of bursts due to possible multipath fading in the wireless channel or intersymbol interference due to dispersion). BER in turn depends on the signal-to-noise ratio (SNR) of the downconverted baseband signal with relationship being defined by the type of RF detection (coherent/incoherent) [21].

In order to examine the pattern of errors in the mm-wave channel, we have measured the histogram of voltage samples of the received waveform. The original hypothesis for the error distribution in the recovered baseband signal is the case of randomly distributed bit errors with absence of bursts, voltage samples of the waveform representing transmitted ‘ones’ and ‘zeros’ are expected to be approximated by Rician and Rayleigh probability density functions (PDF), respectively [21]. By examining the histogram of voltage samples in Fig. 2 (left), we can clearly see the absence of dispersion-related intersymbol interference which is explained by the low bitrate of the link and the fact that RoF transmission is performed in single sideband (SSB) modulation format which is reported to be robust against dispersion-related impairments that are otherwise common to RoF links [22].

As it is shown in Fig. 2 (left), the standard deviation of voltage samples representing the transmitted ‘zero’ is lower than the standard deviation of ‘ones’ which is characteristic of envelope detection. Envelope detection only allows positive voltages at its output, however the waveform at ‘zero’ is stretching into the region of negative voltages due to the remaining mm-wave RF carrier.

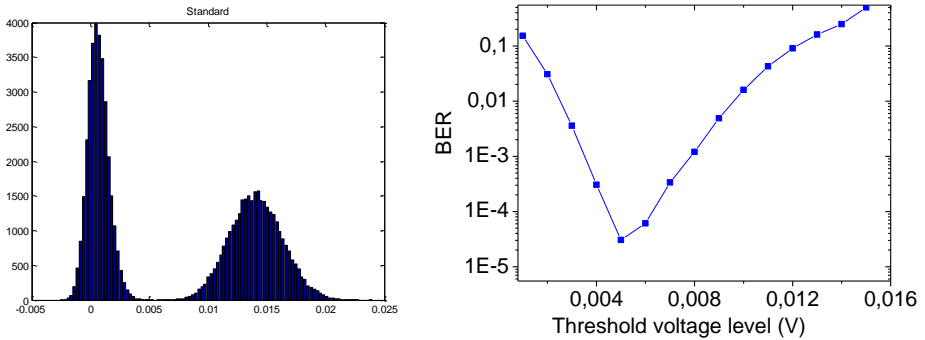


Figure 2. Histogram of the baseband signal after envelope detection (left), BER as a function of the threshold voltage level (right).

In Fig. 2 (right), we depict the search for the optimal threshold over the voltage values of the received waveform. For the detected baseband signal depicted in Fig. 2 (left), the mean value of ‘ones’ is equal to 14.1 mV and the optimal BER value is achieved in the region between 5 and 6 mV according to Fig. 2 (right). This result deviates from the commonly used threshold location at a half of the mean voltage of ‘ones’ for envelope detection [23]. Use of the ED receivers for on-off keying heterodyne systems has been thoroughly analyzed in [24], where the phase noise influence due to laser linewidth was reported. Similarly to [24], we also report that the use of photonic heterodyne systems for the RF generation leads to reducing the optimal threshold value. We show in Fig. 3 that distribution of ‘ones’ can be well matched by a Rician PDF. However, distribution of zeros cannot be equally well matched by a Rayleigh PDF. We suggest that the explanation for this is that there are still residuals of the RF signal present in the electrical waveform after downconversion stretching it into negative voltage polarity which cannot be modeled by Rayleigh distribution.

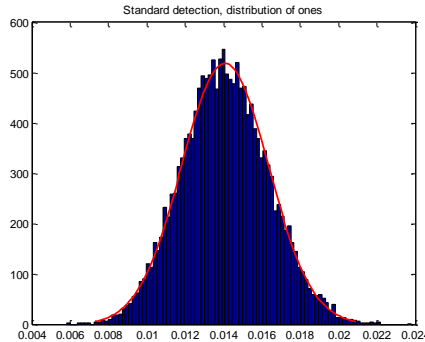


Figure 3. Distribution of ‘ones’ matched by a Rician probability distribution.

As it can be seen in Fig. 4, analytical solution based on Eq. 1 approximates well the results achieved by BCH coding applied to channel error traces. Since the amount of bits stored with the DSO was $\sim 2 \cdot 10^7$, we can

only measure post-decoding BCH BER of up to 10^{-5} - 10^{-6} with the necessary precision. Figure 6 shows the comparison between BCH and RS codes for error correction capability of 10 symbols.

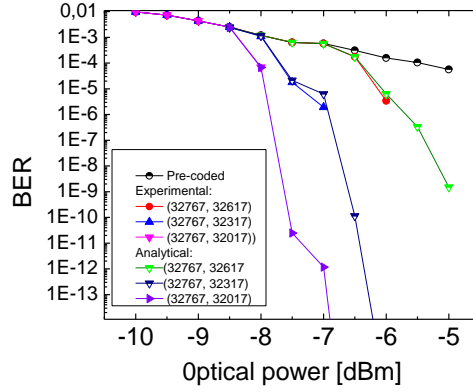


Figure 4. Experimental and analytical BERs as a function of optical power.

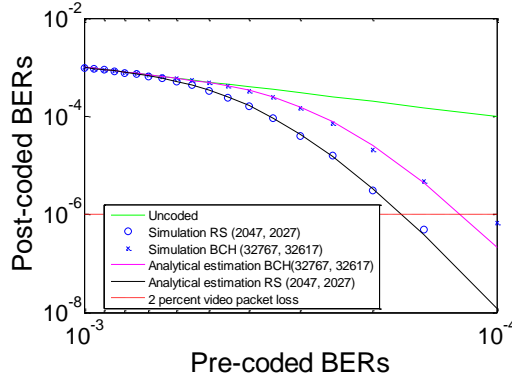


Figure 5. Comparison between RS and BCH for 10 symbols error correction capability.

The acceptable PER and BER for video transmission are usually defined through objective and subjective video quality estimation. For selected RS and BCH codes (Figs. 5 and 6), the BER of the system improves rapidly so most of the uncoded BER values that we present are converted to error-free performance where undistorted quality is guaranteed. As a rough estimate, we plot the probability of 2 percent video packet loss where the packet loss artifacts can still be compensated by H.264 decoder error concealment tools.

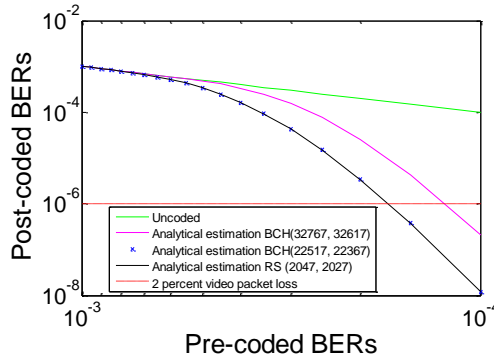


Figure 6. Comparisons between RS and BCH for 10 symbols error correction capability.

In Fig. 6, we also plot the results for BCH and RS sustaining 10 symbols error correction capability including shortened BCH codes. These results show that shortened BCH codes in the setting used for this paper can bring performance almost identical to that of RS codes at a slightly lower redundancy rate. However, we note that discussion on applicability of a particular code is also constrained by the difficulty of hardware implementation which is our planned future work.

The targeted compressed video bitrate yields a required compression ratio of 20, which is considered as a computationally simple task for H.264/AVC. We test the simplified setting described in Section 3 for coding test video sequences including static video and videos with complex motion. PSNR of compressed 1080p 60 frames per second 4:4:4 video clips is presented in the Table 1 for video packet size equal to approximately 20000 bits and varying test video sequences. Encoding is performed in a very close range of QPs.

Table 1. PSNR of 60 fps 1080p 4:4:4 video compressed to <150 Mbps bitrate.

Test sequence title	PSNR, ~20000 bits packet length	Bitrate, kbit/s	QP
Blue sky	42.02	146002.00	25
Sunflower	43.94	127020.34	24
Riverbed	40.19	148171.46	25
Pedestrian area	42.23	93070.27	24

From Table 1, we conclude that, given generous bandwidth provided by hybrid fiber-wireless links, there is no significant difference in terms of PSNR between encoded videos with varying content, however the bitrate shows relatively large variations for a very narrow range of QPs. Compression by about a factor of 20 leaves a large margin to preserve high video quality enabling low-complexity coding solutions.

As the video packets containing slices are large (20000 bits), dropping the video frame when the slice is lost might be an efficient solution to avoid the visible video quality degradation. In our case, no more than 10 slices per frame are generated for video sequences under study, thus the loss of the slice will result in visible deterioration of video quality if the slice is located e. g. in the middle of the frame, and therefore frame dropping might reduce the perceived video quality distortion causing only moderate reduction in the frame rate if 1-2 percents of packet loss are not exceeded. However, depending on the video content and position of the slice in the frame, the lost slice might be approximated by neighboring slices.

Finally, we note that in traditional hybrid wired-wireless systems, transcoding is usually employed, but for the mm-wave fiber-wireless transmission it might be avoided in the absence of significant difference between capacity of wireless and wireline channel.

5. CONCLUSIONS

In this work, we have shown that, in combination with the source coding use, the fiber-wireless link budget can be aided through implementation of the channel coding. The experimental results for BCH-protected transmission match the results of the analytical calculation. We report on noise statistics of the envelope detection of mm-wave RF generated through photomixing of two unlocked lasers. We have shown that due to residuals of RF carrier passed by the ED, 'zero' level cannot be approximated by Rayleigh PDF and, secondly, optimum threshold level is decreased compared to generally used value. Finally, we analyze light compression techniques for 1080p HD video transmission. The experimental results presented and analysis enable multiple channel HD video transmission in W-band through support of source and channel coding. Future work is related to studying the statistics of envelope detection of RF produced by homodyne technique. Furthermore, it is desirable that the packet size is reduced, and therefore error concealment using neighboring slices might be employed efficiently.

REFERENCES:

- 1) Australian communications authority report, "60 GHz Band millimeter wave technology," (2004) http://www.acma.gov.au/webwr/radcomm/frequency_planning/radiofrequency_planning_topics/docs/sp3_04_60%20ghz%20mwt%20-%20discussion%20paper-final.pdf.
- 2) S.-Q. Xiao, M.-T. Zhou, and Y. Zhang, "Millimeter wave technology in wireless Pan, Lan, and Man," (CRC Press, 2007), Chap. 1.
- 3) WirelessHD white paper, "WirelessHD Specification Version 1.1 Overview," (WirelessHD, 2010). <http://www.wirelesshd.org/pdfs/WirelessHD-Specification-Overview-v1.1May2010.pdf>.
- 4) Ericsson white paper, "Heterogeneous networks," (Ericsson, 2012). <http://www.ericsson.com/res/docs/whitepapers/WP-Heterogeneous-Networks.pdf>.
- 5) S. Iezekiel, "Microwave photonics: devices and applications", (Wiley, 2009), Chap. 1.
- 6) M. C. Parker, S. D. Walker, R. Llorente, M. Morant, M. Beltrán, I. Möllers, D. Jäger, C. Vázquez, D. Montero, I. Librán, S. Mikroulis, S. Karabetsos, A. Bogris, "Radio-over-fibre technologies arising from the building the future optical network in Europe (BONE) project," *IET Optoelectronics*, vol.4, no.6, pp. 247-259, December 2010.

- 7) C. Lim, A. Nirmalathas, M. Bakaul, P. Gamage, K.-L. Lee, Y. Yang, D. Novak, R. Waterhouse, "Fiber-Wireless Networks and Subsystem Technologies," *J. Lightw. Technol.*, vol.28, no.4, pp.390-405, February 2010.
- 8) A. M. Zin, M. S. Bongsu, S. M. Idrus, N. Zulkifli, "An overview of radio-over-fiber network technology," in *Proceedings of International Conference on Photonics (ICP)*, paper ICP2010-85, 2010.
- 9) F. Poegel, S. Zeisberg, A. Finger, "Comparison of different coding schemes for high bit rate OFDM in a 60 GHz environment," in *Proceedings of 4th International Symposium on Spread Spectrum Techniques and Applications*, pp.122-125, 1996.
- 10) M. Marinkovic, M. Piz, C.-S. Choi, G. Panic, M. Ehrig, E. Grass, "Performance evaluation of channel coding for Gbps 60-GHz OFDM-based wireless communications," in *Proceedings of IEEE 21st International Symposium on Personal Indoor and Mobile Radio Communications (PIMRC)*, pp.994-998, 2010.
- 11) B. Gao, Z. Xiao, C. Zhang, L. Su, D. Jin, L. Zeng, "Performance comparison of channel coding for 60GHz SC-PHY and a multigigabit Viterbi decoder," in *Proceedings of International Conference on Computational Problem-Solving (ICCP)*, pp.714-718, 21-23 Oct. 2011.
- 12) "IEEE Standard for Information technology - Telecommunications and information exchange between systems - Local and metropolitan area networks - Specific requirements. Part 15.3: Wireless Medium Access Control (MAC) and Physical Layer (PHY) Specifications for High Rate Wireless Personal Area Networks (WPANs) Amendment 2: Millimeter-wave-based Alternative Physical Layer Extension," IEEE Std 802.15.3c-2009 (Amendment to IEEE Std 802.15.3-2003), pp. 1-187, Oct. 12 2009.
- 13) E. Perahia, C. Cordeiro, M. Park, L. L. Yang, "IEEE 802.11ad: Defining the Next Generation Multi-Gbps Wi-Fi," in *Proceedings of 7th IEEE Consumer Communications and Networking Conference (CCNC)*, pp.1-5, 9-12 Jan. 2010.
- 14) A. Lebedev, J. J. Vegas Olmos, X. Pang, S. Forchhammer, and I. Tafur Monroy, "Demonstration and comparison study for V- and W-band real-time high-definition video delivery in diverse fiber-wireless infrastructure," *Fiber Integrated Opt.*, vol. 32, no. 2, pp. 93-104, 2013.
- 15) A. Lebedev, T. T. Pham, M. Beltrán, X. Yu, A. Ukhanova, R. Llorente and I. Tafur Monroy, "Optimization of high-definition video coding and hybrid fiber-wireless transmission in the 60 GHz band," *Opt. Express*, vol. 19, no. 26, pp. 895-904, 2011.
- 16) G. C. Clark and J. B. Cain, Error-correction coding for digital communications. New York: Plenum Press, 1981.
- 17) <http://iphone.hhi.de/suehring/tml/>.
- 18) T. Stockhammer, M. Hannuksela, and T. Wiegand, "H.264/AVC in Wireless Environments," *IEEE Transactions on circuits and systems for video technology*, vol. 13, no. 7, July 2003.
- 19) Iain E. Richardson "The H.264 advanced video compression standard," (Wiley, 2010).
- 20) S. K. Yong and C.-C. Chong, "An Overview of Multigigabit Wireless through Millimeter Wave Technology: Potentials and Technical Challenges," in *EURASIP Journal on Wireless Communications and Networking*, vol. 2007, Article ID 78907.
- 21) J. Proakis, "Digital communications," McGraw-Hill, 4th ed., 2000, Chapter 5.
- 22) J. Yu, Z. Jia, L. Yi, Y. Su, G.-K. Chang, and T. Wang, "Optical Millimeter-Wave Generation or Up-Conversion Using External Modulators," *IEEE Photon. Technol. Lett.*, vol. 18, no. 1, pp. 265-267, 2006.
- 23) S. B. Alexander, "Optical Communication Receiver Design," SPIE, 1997, Chapter 7.
- 24) J. Franz, "Receiver analysis for incoherent optical ASK heterodyne systems," *Journal of Optical Communications*, vol. 8, no. 2, pp. 57-66, 1987.

[Paper 9]

Alexander Lebedev, Xiaodan Pang, Juan Jose Vegas Olmos, Søren Forchhammer, Idelfonso Tafur Monroy, "Tunable photonic RF generator for dynamic allocation and multicast of 1.25 Gbps channels in the 60 GHz unlicensed band," in *Proceedings of International Microwave Symposium (IMS 2013)*, paper THPP-2, 2013.

Tunable Photonic RF Generator for Dynamic Allocation and Multicast of 1.25 Gbps Channels in the 60 GHz Unlicensed Band

Alexander Lebedev, Xiaodan Pang, Juan Jose Vegas Olmos, Idelfonso Tafur Monroy, Søren Forchhammer
DTU Fotonik, Department of Photonics Engineering, Technical University of Denmark, 2800 Kgs. Lyngby, Denmark, alele@fotonik.dtu.dk

Abstract — We propose an approach for dynamic channel allocation and multicast data delivery inside the 60 GHz unlicensed band. Channels, conveying 1.25 Gbps signals, can be allocated on demand by tuning the frequency sweep of an external cavity laser (ECL) either in the optical remote node (RN) or in the central office (CO). At the RN, we perform the replication of the original channel suitable for closely spaced multicast applications such as high definition (HD) video delivery where RN serves as a photonic radio frequency (RF) generator for both channel allocation and multicast. Experimental demonstration is presented with bit error rate (BER) performance below 10^{-9} for original and replicated channels after transmission through 22.8 km of standard single mode fiber (SSMF).

Index Terms — microwave photonics, Radio-over-Fiber (RoF), hybrid fiber wireless transmission, wireless distribution.

I. INTRODUCTION

Radio-over-Fiber (RoF) networks are a promising communication paradigm for delivering broadband services to mobile users in the 60 GHz unlicensed wireless band; optical fiber systems can effectively provide the transport infrastructure to generate and distribute broadband wireless signals while also supporting baseband broadband systems. Several RoF systems providing wireless gigabit connectivity have been demonstrated for 60 GHz radio frequency (RF) delivery achieving 40 Gbps bitrate [1] and wireless transmission in the order of 80 m in line-of-sight outdoors [2]. However, these demonstrations focus on static scenarios, omitting roaming and mobility factors. It is recognized that hand-off mechanisms [3] and network architectures [4] for high mobility users are required features of the future 60 GHz networks. So far, at the physical layer, demonstrations of dynamic bandwidth allocation of 60 GHz have been proposed, relying on optical switches [5]-[7].

In this paper, we present a tunable photonic radio frequency (RF) generator for dynamic allocation of 1.25 Gbps channels inside of the 60 GHz unlicensed band (57-66 GHz in Europe, 57-64 GHz in USA) [8]. Architecture and network scenarios are presented, and then an experimental validation is conducted. The novelty of this paper lies in the dynamism of the system since allocation of the channels to the end-user can be done without impacting overall setup. Bit error rate (BER) measurements confirm that channel allocation can be done without introducing impairments to transmitted data as well. This enables a new degree of freedom in network design, and mobility features can be considered and addressed within the physical layer.

II. ARCHITECTURE AND NETWORK SCENARIO

In a RoF system, a central office (CO) contains the elements in charge of photonicallly generating the 60GHz signals. Then, the signals are transported over fiber to the remote node (RN), which distributes them to the different access points (AP). Allocation of channels can hence be done both at the CO or the RN.

In our concept, we first use modulation of the lightwave with RF signal at the CO to produce the original signal for the AP, which then can be replicated and tuned by means of remote heterodyning with a tunable laser at the RN. Fig. 1 shows the architecture of our concept, and depicts some of the network scenarios that it can serve. Our proposed system can be installed in the scenario where both wireless services and fiber-to-the-home (FTTH) connectivity are provided.

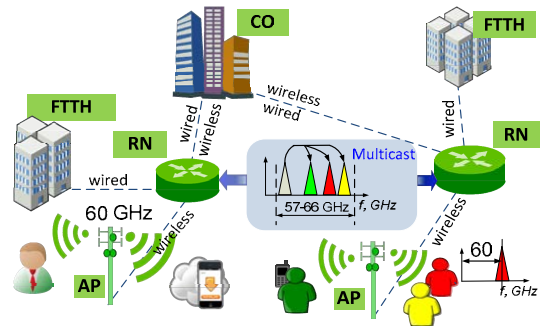


Figure 1. Network scenario for 60 GHz RoF system providing the RF tunability. CO: central office, FTTH: fiber-to-the-home, RN: remote node, AP: access point.

Tunable photonic RF generation and multicast of wireless channels is interesting for several applications in the access segment. For instance, high definition (HD) real time video distribution, which is a main driver for internet connectivity, can be efficiently delivered to several end-users. Furthermore, in wireless networks, one node may need to dynamically assign channels in order to enable multipoint-to-multipoint communication [9]. Proposed tunability complements the regular wireless dynamic channel allocation protocols, which are usually implemented at the control plane of the network.

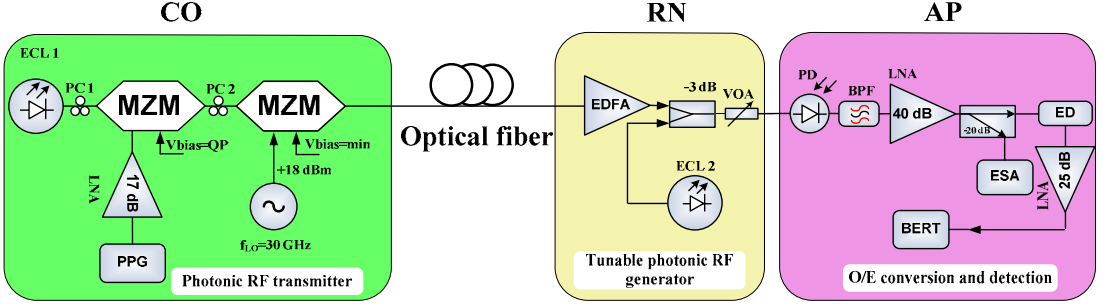


Figure 2. Experimental setup of photonic allocation of channels in the 60 GHz unlicensed band. ECL: external cavity laser, PC: polarization controller, MZM: Mach-Zehnder modulator, LO-local oscillator, EDFA: Erbium doped fiber amplifier, VOA: variable optical attenuator, PD: photodiode, BPF: bandpass filter, LNA: low noise amplifier, ESA: electrical spectrum analyzer, ED: envelope detector, BERT: bit error rate tester, PPG: pulse pattern generator, O/E-optical-to-electrical conversion.

In general, tunability of the RF frequency is important in order to utilize the bandwidth efficiently in dense wireless deployment scenarios, where the channels have to be allocated to unused wireless spectrum slots.

III. EXPERIMENTAL SETUP

The experimental setup employed to demonstrate our concept is depicted in Fig. 2. The main building blocks are the photonic RF transmitter, located at the CO, the tunable photonic RF generator located at the RN and the AP. At the CO, we employed a tunable external cavity laser (ECL₁) to produce a 15.5 dBm optical power lightwave with a less than 100 kHz linewidth. The polarization state of the lightwave was adjusted with a polarization controller (PC). In order to perform the modulation in a photonic RF transmitter block, we employed two cascaded Mach-Zehnder modulators (MZM). MZM₁ has ~10-GHz of -3 dB bandwidth and MZM₂ is a high performance modulator with ~25 GHz of -3dB bandwidth. MZM₁ was biased at a quadrature point of its transfer function for modulation of the baseband data; we use the driving amplifier to increase the peak-to-peak voltage to drive the MZM₁ efficiently. Meanwhile MZM₂ was biased at the minimum point and modulated with ~30 GHz RF sinusoidal signal of +18 dBm power. In this way, we suppress the carrier and can double the RF frequency of modulation which in turn helps us to ease the requirements for high frequency RF components. Furthermore, the doubling technique produces the sidebands that are correlated and thus, following O/E conversion, RF signal with high quality phase noise performance can be obtained. The data employed was a $2^{31}-1$ long pseudorandom bit sequence (PRBS). The signal was subsequently sent through 22.8 km of standard single mode fiber (SSMF).

After optical fiber transmission, the signal was first amplified with an Erbium doped fiber amplifier (EDFA) up to +8 dBm at the RN. The signal was then combined with the local lightwave source, produced by a tunable ECL₂. The combined mix was then passed through a variable optical attenuator (VOA) to control the optical power incident on the photodiode (PD). Because of the limitations in the electrical devices employed during the experiments, we explored

channel allocation for two cases only: 1) the original signal sent from the CO is allocated to the AP, 2) a replica of the original signal produced at the RN is allocated to the AP. Figure 3 shows the optical spectra of the two cases.

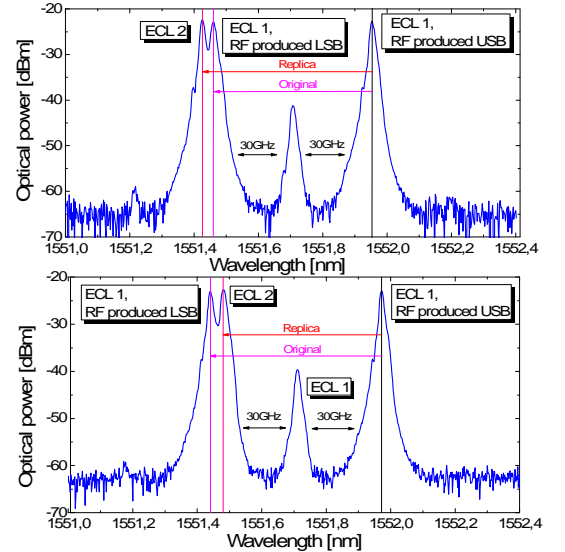


Figure 3. Optical spectra of the generated signals. Two cases were assessed, namely allocation of the original signal from the CO in the passband (top) and allocation of a replica produced at the RN in the passband (bottom). USB: upper sideband, LSB: lower sideband.

To convert the RF-modulated lightwave into electrical domain, we employed a high performance P-I-N photodiode with ~75 GHz of -3 dB bandwidth. A high frequency bandpass filter (58.1-61.9 GHz) was then used to filter out the signal of interest, which was subsequently amplified with a double-stage 40 dB gain low noise amplifier (LNA). Then we passed the signal through a 20dB coupler, which served for monitoring purposes. The signal was then fed to a zero-biased Schottky diode performing a function of an envelope detector (ED) for downconversion from RF into baseband. The signal

is then amplified and passed on to the bit error rate tester (BERT).

IV. RESULTS AND DISCUSSION

The two channel allocation scenario described in the previous sections was assessed in terms of BER performance. We also present electrical spectra to reflect on the allocation of original and replicated channel throughout the BER measurements.

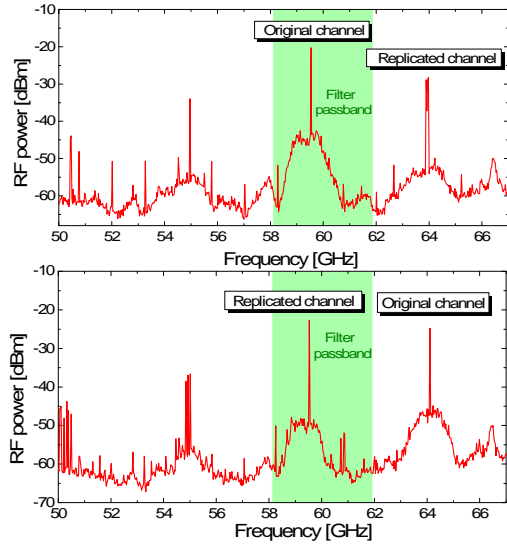


Figure 4. Electrical spectra of the signals: (top) when signal from the CO is allocated for transmission, (bottom) when RN-produced replica is allocated for transmission.

Figure 4 shows the electrical spectra of the multicast signals, both for the allocation of the original signal from the CO and the allocation of the replica from the RN.

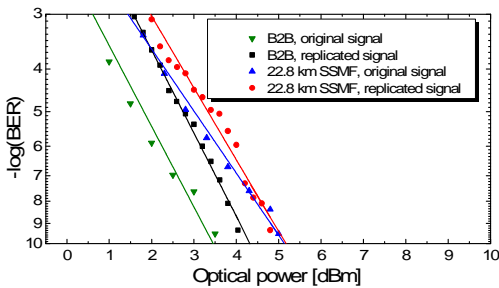


Figure 5. BER as a function of measured optical power.

In Fig. 5, we present the measured BER curves for the two cases. The measurements indicate BER operation below 10^{-9} level for both the original and the replicated channel, including B2B and after optical fiber transmission. The power penalty for generating a replica of the original signal is less than 1dB; transmission over 22.8km induces approximately 1dB of power penalty in both cases. Penalty between B2B and

22.8 km SSF is slightly larger for the original signal since we employ double-sideband modulation for original channel sent from the CO; at the same time, replicated signal is produced through heterodyning of the data-bearing lightwave with a continuous lightwave using the single sideband modulation format.

V. CONCLUSION

In this paper, we proposed an approach to photonically allocate and multicast 1.25 Gbps channels in the 60GHz unlicensed band. Through an experimental demonstration, we show generation and transmission through 22.8 km of SMF, and optical-to-electrical conversion of closely spaced 1.25Gbps allocated channels yielding BER performance below 10^{-9} level. Future work includes assessing the laser linewidth requirements when using advanced modulation formats to convey the data, and comparative study for alternative RF-downconversion methods such as synchronous detection.

REFERENCES

- [1] J. Wen-Jr, Y. Hejie, Y. Yi-Ming, L. Chun-Ting, and A. Ng'oma, "40 Gb/s RoF signal transmission with 10 m wireless distance at 60 GHz," *Optical Fiber Communication Conference and Exposition (OFC/NFOEC)*, 2012 and the *National Fiber Optic Engineers Conference*, pp.1-3, 4-8 March 2012
- [2] J.A. Nanzer, P.T. Callahan, M.L. Dennis, T.R. Clark, D. Novak, R.B. Waterhouse, "Millimeter-Wave Wireless Communication Using Dual-Wavelength Photonic Signal Generation and Photonic Upconversion," *IEEE Transactions on Microwave Theory and Techniques*, vol.59, no.12, pp.3522-3530, Dec. 2011
- [3] A. Tayebi, C. Lim, A. Nirmalathas, and K.L. Lee, "Seamless hand-off mechanism for high mobility broadband wireless access using 60 GHz radio-over-fiber networks," *The 16th Opto-Electronics and Communications Conference, OECC*, pp. 360-361, July 2011
- [4] Q. Bien Van, R.V. Prasad, I. Niemegeers, "A Survey on Handoffs — Lessons for 60 GHz Based Wireless Systems," *IEEE Communications Surveys & Tutorials*, vol.14, no 1, pp. 64-86, 2012
- [5] N. Pleros, K. Vysokinos, K. Tsagkaris, and N. D. Tselikas, "A 60 GHz radio-over-fiber network architecture for seamless communication with high mobility," *IEEE Journal of Lightwave Technology*, vol. 27, no. 12, June 2009
- [6] J.J. Vegas Olmos, T. Kuri, and K. Kitayama, "Reconfigurable radio-over-fiber networks: multiple-access functionality directly over the optical layer," *IEEE Transactions on Microwave Theory and Techniques*, vol. 58, no. 11, pp. 3001-3010, November 2010
- [7] M.J. Crisp, E.T. Aw, A. Wonfor, R.V. Pentty, and I. White, "Demonstration of an SOA efficient 32x32 optical switch for radio over fiber distribution systems," *Optical Fiber Communications conference, OFC*, paper OThP4, Feb. 2008.
- [8] S. K. Yong, C.-C. Chong, "An overview of multigigabit wireless through millimeter wave technology: potentials and technical challenges," *EURASIP J. Wirel. Commun. Netw.*, vol. 2007, no. 1, pp.1 -10, article ID 78907, 2007
- [9] J. Guillory, Y. Ait Yahia, A. Pizzinat, B. Charbonnier, C. Algani, M.D. Rosales, and J.L. Polleux, "Comparison between two 60GHz multipoint RoF architectures for the Home Area Network," *17th European Conference on Networks and Optical Communications (NOC)*, 2012, pp.1-5, June 2012